NORSAR ROYAL NORWEGIAN COUNCIL FOR SCIENTIFIC AND INDUSTRIAL RESEARCH

⑬

Scientific Report No. 2-85/86

SEMIANNUAL TECHNICAL SUMMARY
1 October 1985 – 31 March 1986

L.B. Loughran (ed.)

DTIC
ELECTE
SEP 8 1986

B

Kjeller, May 1986

86 9 8 065

REPORT DOCUMENTATION PAGE

1a. REPORT SECURITY CLASSIFICATION	1b. RESTRICTIVE MARKINGS
UNCLASSIFIED	NOT APPLICABLE

2a. SECURITY CLASSIFICATION AUTHORITY	3. DISTRIBUTION/AVAILABILITY OF REPORT
NOT APPLICABLE	APPROVED FOR PUBLIC RELEASE
2b. DECLASSIFICATION/DOWNGRADING SCHEDULE	DISTRIBUTION UNLIMITED
NOT APPLICABLE	

4. PERFORMING ORGANIZATION REPORT NUMBER(S)	5. MONITORING ORGANIZATION REPORT NUMBER(S)
SCIENTIFIC REPORT 2-85/86	SCIENTIFIC REPORT 2-85/86

6a. NAME OF PERFORMING ORGANIZATION	6b. OFFICE SYMBOL (If applicable)	7a. NAME OF MONITORING ORGANIZATION
NTNF/NORSAR	GSD	HQ AFTAC/TGX

6c. ADDRESS (City, State and ZIP Code)	7b. ADDRESS (City, State and ZIP Code)
POST BOX 51 N-2007 KJELLER, NORWAY	PATRICK AFB, FL 32925-6001

8a. NAME OF FUNDING/SPONSORING ORGANIZATION	8b. OFFICE SYMBOL (If applicable)	9. PROCUREMENT INSTRUMENT IDENTIFICATION NUMBER
DEFENSE ADVANCED RESEARCH PROJECTS AGENCY		CONTRACT NO. F08606-86-C-0004

8c. ADDRESS (City, State and ZIP Code)	10. SOURCE OF FUNDING NOS			
1400 Wilson Blvd Arlington, VA 22209-2308	PROGRAM ELEMENT NO.	PROJECT NO.	TASK NO.	WORK UNIT NO.
	R&D	NORSAR PHASE 3	SOW TASK 5.0	SEQUENCE NUMBER 003A2

11. TITLE (Include Security Classification) SEMIANNUAL TECHNICAL SUMMARY 1 OCT 85-31 MAR 86 (UNCLASSIFIED)

12. PERSONAL AUTHOR(S)
L. B. LOUGHRAN (ED.)

13a. TYPE OF REPORT	13b. TIME COVERED	14. DATE OF REPORT (Yr., Mo., Day)	15. PAGE COUNT
SCIENTIFIC SUMMARY	FROM 1 OCT 85 TO 31 MAR 86	MAY 86	93

16. SUPPLEMENTARY NOTATION

NOT APPLICABLE

17	COSATI CODES		18. SUBJECT TERMS (Continue on reverse if necessary and identify by block number)
FIELD	GROUP	SUB. GR.	
8	11		NORSAR, NORWEGIAN SEISMIC ARRAY

19. ABSTRACT (Continue on reverse if necessary and identify by block number)

This Semiannual Technical Summary describes the operation, maintenance and research activities at the Norwegian Seismic Array (NORSAR) for the period 1 October 1985 – 31 March 1986.

(continued next page)

20. DISTRIBUTION/AVAILABILITY OF ABSTRACT	21. ABSTRACT SECURITY CLASSIFICATION
UNCLASSIFIED/UNLIMITED ☒ SAME AS RPT ☐ DTIC USERS ☐	UNCLASSIFIED

22a. NAME OF RESPONSIBLE INDIVIDUAL	22b. TELEPHONE NUMBER (Include Area Code)	22c. OFFICE SYMBOL
CAPT JAMES A. ROBB	(305) 494-7665	AFTAC/TGX

DD FORM 1473, 83 APR   EDITION OF 1 JAN 73 IS OBSOLETE

19. (cont.)

The NORSAR Detection Processing system has been operated through the reporting period with an average uptime of 98.8 per cent. Most of the downtime has been caused by disk failure and schedule maintenance at the central recording computer. A total of 1931 seismic events have been reported by NORSAR in the period. The performance of the continuous alarm system and the automatic bulletin transfer by telex to AFTAC have been satisfactory. Regular transmission by telex to AFTAC of NORESS detection lists has been initiated. Processing of requests for full NORSAR/NORESS data on magnetic tape has progressed without problems.

A study of NORESS regional detection performance has been conducted, using a data base of 477 events in Finland/Western Russia reported in the University of Helsinki bulletin. The distance range is 500-1500 km from NORESS. The 50 per cent NORESS detection threshold for the data set is $M_L = 1.9$ and the 90 per cent threshold is $M_L = 2.5$, assuming as detection criteria that either P, Sn or Lg is detected. If P-detection only is considered, the respective thresholds are 2.3 and 2.7. The magnitudes are taken from the Helsinki bulletin, and are thought to be reasonably consistent with the m_b scale, although this needs further investigation. At low magnitudes ($M_L < 2$), Lg is by far the most easily detectable phase.

About 100 regional events recorded by the High Frequency Seismic Element (HFSE) at NORSAR have been analyzed with respect to spectral characteristics of recorded phases. For epicentral distances within about 500 km, the Pn and Sn phases consistently show extremely strong high frequency energy. Thus, the SNR shows no drop with increasing frequency within the recorded bandwidth (up to 62.5 Hz). Around 400 km distance, where we have a particularly good data set, the Pg and Lg phases are dominant at low frequencies (1-5 Hz), whereas the Pn and Sn phases dominate the seismograms from 10-62.5 Hz. At distances from 500-1500 km, the signal spectra drop more rapidly than the noise spectra at high frequencies, but signal energy up to 20-30 Hz is still observable for many events of $M_L \sim 3.0$.

In a continuation of an earlier study, a data base of 251 reported (by the University of Bergen) Western Norway/North Sea events at a distance range of 250-700 km have been analyzed. A detection probability of the P phase of 50% is achieved at magnitude 1.8. For detection of P or S, the probability is about 70% at magnitude 1.8. Statistics on actually observed phase arrival times relative to expected ones (from the network reports), show that the Pn detections are typically 2 seconds early and that the onset of the Lg wave train on the average arrives 3 seconds before the predicted arrival time. These results

allow a calibration for this region, which in turn will reduce the
automatic location uncertainty. Statistics on automatically determined
phase velocities shows reasonable separation between Pn and Pg, and
also shows that Sn phase velocities tend to be higher than Lg ones.
Automatic Lg phase velocities are remarkably stable around 4.1 km/s.

An automatic algorithm has been implemented to compute and store noise
spectra from NORESS and the HFSE once every hour. The spectra comprise
individual channels as well as beams based on subgeometries of NORESS.
So far we have obtained initial information on the diurnal noise
variation. During weekends and holidays, the noise level is very
stable at all frequencies, whereas cultural noise during weekdays
causes some significant variations. These are only minor (± 2 dB or
less) below 2 Hz, increasing slightly up to 5 Hz and becoming very
strong around 6 Hz (± 10 dB). At frequencies above 8 Hz, the
variations are again modest (typically ± 3 dB). The problem around
6 Hz is probably caused by a sawmill 15 km away from NORESS.

A method has been developed to obtain phase velocity and azimuth using
broad-band f-k analysis, and the results have been compared to the
monochromatic f-k analysis used in the RONAPP program. Initial results
are very encouraging, e.g., for a set of 5 Western Russia explosions
from one mining area the broad-band azimuth results are consistent
within 2-3 degrees whereas the single-frequency results show a scatter
of 5-10 degrees.

The theoretical framework for the maximum likelihood 3-component
analysis method previously reported upon has now been completed. The
method has been applied in particle motion modelling, scattering stu-
dies and epicenter location estimation. For large earthquakes at tele-
seismic distances, broad-band 3-component analysis has given very
accurate location results. Obtaining reliable locations from short
period 3-component records is more difficult, but good to very good
estimates have been found feasible both at local, regional and tele-
seismic distances.

A study has been undertaken to obtain a 3-D imaging of the upper
mantle velocity structure beneath the southern part of Fennoscandia,
on the basis of P-wave travel time residuals as observed across a
local seismograph network in this region. Results are presented in the
form of a map showing areas of high and low velocities in four layers,
extending to 600 km depth.

AFTAC Project Authorization	:	T/6141/B/PMP
ARPA Order No.	:	4138
Program Code No.	:	0F10
Name of Contractor	:	Royal Norwegian Council for Scientific and Industrial Research
Effective Date of Contract	:	1 October 1985
Contract Expiration Date	:	30 September 1986
Project Manager	:	Frode Ringdal (02) 71 69 15
Title of Work	:	The Norwegian Seismic Array (NORSAR) Phase 3
Amount of Contract	:	$ 686,546.00
Contract Period Covered by the Report	:	1 Oct 1985 - 31 Mar 1986

DTIC
ELECTE
SEP 8 1986
B

TABLE OF CONTENTS

I. SUMMARY

This Semiannual Technical Summary describes the operation, maintenance and research activities at the Norwegian Seismic Array (NORSAR) for the period 1 Oct 1985 – 31 March 1986.

The uptime of the NORSAR online detection processor system has averaged 98.8 per cent during the reporting period, which is slightly higher than for the previous half-year period. Disk problems and scheduled maintenance were the factors contributing most to the downtime of 1.2%. The array communications system has in general shown high reliability. A total of 1931 events were reported in this period, giving a daily average of 10.5 events.

The performance of the continuous alarm system and the automatic bulletin transfer by telex to AFTAC have been satisfactory. Regular transmission by telex to AFTAC of NORESS detection lists has been initiated. Processing of requests for full NORSAR/NORESS data on magnetic tape has progressed without problems.

Field maintenance activity has included regular preventive maintenance at all subarrays and occasional corrective actions as required. No special problems have been noted in the performance of the field installations.

The research activity is summarized in section VII. Section VII.1 discusses regional event detection using the NORESS array. Initial results from the NORESS High Frequency Seismic Element are presented in section VII.2. Section VII.3 contains an evaluation of NORESS real time processing performance for events in western Norway and the North Sea, while Section VII.4 contains a preliminary report on NORESS noise spectral studies. An integrated approach to slowness analysis with arrays and three-component stations is discussed in Section VII.5. In

Section VII.6 some of the principal features of wavefield decom-
position using ML-probabilities in modelling single-site 3-component
records are presented. Section VII.7 addresses event locations using
small arrays and single-site 3-component records, and in section VII.8
3-D ray tracing and structural heterogeneities in Fennoscandia are
discussed.

II.   OPERATION OF ALL SYSTEMS

II.1   Detection Processor (DP) Operation

There have been 75 breaks in the otherwise continuous operation
of the NORSAR online system within the current 6-month reporting
interval. The uptime percentage for the period is 98.8 as com-
pared to 98.2 for the previous half-year period. Almost 2/3 of
the downtime was caused by disk failure and maintenance.

Fig. II.1.1 and the accompanying Table II.1.1 both show the daily
DP downtime for the days between 1 October 1985 and 31 March 1986.
The monthly recording times and percentages are given in Table
II.1.2.

The breaks are grouped as follows:

a)	Hardware failure	13
b)	Stops related to programming work	
	or error	1
c)	Hardware maintenance stops	5
d)	Power jumps and breaks	3
e)	TOD error correction	31
f)	Communication lines	22

The total downtime for the period was 51 hours and 27 minutes.
The mean-time-between-failure (MTBF) was 2.4 days, as compared to
2.0 for the previous period.

J. Torstveit
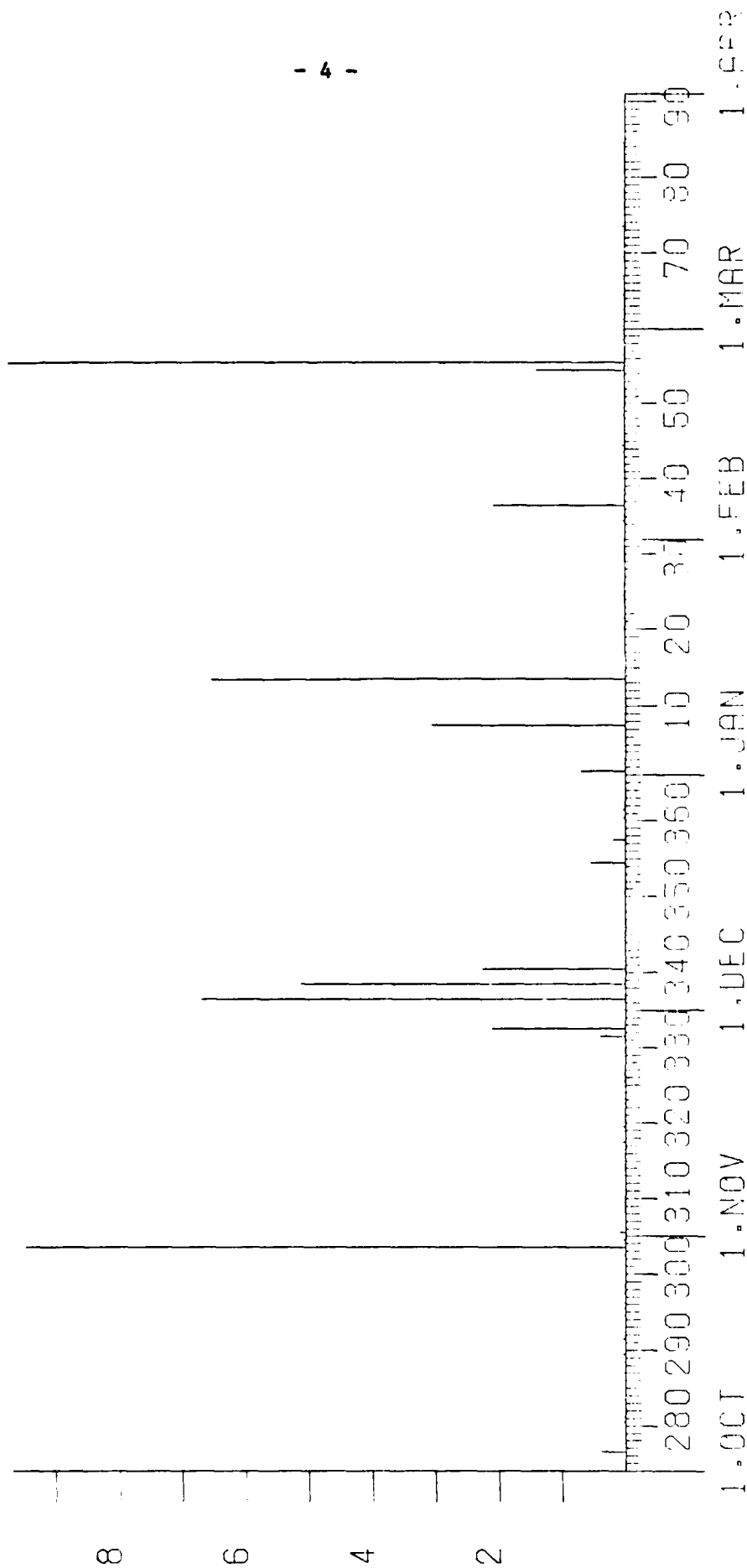
Fig. II.1.1 Detection Processor downtime in the period 1 September 1985 - 31 March 1986.

LIST OF BREAKS IN DP PROCESSING THE LAST HALF-YEAR

DAY	START		STOP		COMMENTS	DAY	START		STOP		COMMENTS
276	11	28	11	50	POWER BREAK	354	12	9	12	26	DISK FAILURE
276	12	15	12	16	LINE FAILURE	354	12	46	13	1	DISK FAILURE
280	7	1	7	2	TOD RETARED 60MS	357	7	33	7	36	TOD RETARED 15MS
283	11	21	11	22	LINE FAILURE	357	10	46	10	55	DISK FAILURE
288	13	18	13	19	LINE FAILURE	360	16	34	16	36	LINE FAILURE
289	13	36	13	38	LINE FAILURE	361	9	30	9	32	TOD RETARED 25MS
291	7	1	7	2	TOD RETARED 30MS	1	13	42	14	24	SYSTEM WORK
291	11	56	11	57	LINE FAILURE	2	8	51	8	52	TOD RETARED 33MS
294	12	46	12	47	LINE FAILURE	7	9	45	10	5	DISK FAILURE
295	11	33	11	34	LINE FAILURE	7	12	7	14	47	DISK FAILURE
297	14	28	14	29	LINE FAILURE	7	15	1	15	2	LINE FAILURE
302	7	1	7	7	TOD RETARED 30MS	7	15	10	15	11	LINE FAILURE
303	14	33	24	0	DISK FAILURE	13	7	2	7	3	TOD RETARED 46MS
304	11	46	11	48	LINE FAILURE	13	9	17	13	30	DISK SERVICE
305	13	55	13	59	MODCOMP FAILURE	13	13	37	13	39	DISK SERVICE
305	14	20	14	21	TOD RETARED 30MS	13	13	44	14	8	DISK SERVICE
308	15	17	15	18	LINE FAILURE	13	17	9	18	59	DISK FAILURE
309	9	51	9	52	TOD RETARED 20MS	21	7	1	7	2	TOD RETARED
316	7	1	7	2	TOD RETARED 25MS	24	14	13	14	14	TOD RETARED 25MS
317	7	3	7	4	LINE FAILURE	29	11	46	11	47	TOD RETARED 25MS
317	7	8	7	9	LINE FAILURE	34	7	7	7	3	TOD RETARED 25MS
317	13	32	13	33	LINE FAILURE	36	7	0	7	41	POWER FAILURE
319	7	1	7	2	TOD RETARED 25MS	36	11	38	13	1	SERVIVE MODCOMP
319	13	26	13	28	LINE FAILURE	38	7	1	7	2	TOD RETARED 43MS
322	8	16	8	17	LINE FAILURE	44	7	0	7	1	TOD RETARED
325	13	40	13	41	LINE FAILURE	44	7	16	7	17	LINE FAILURE
326	7	1	7	2	TOD RETARED 15MS	48	7	0	7	1	TOD RETARED 25MS
329	7	1	7	2	TOD RETARED 25MS	54	13	14	14	30	DISK FAILURE
331	11	38	12	2	INST. 4381	54	15	16	15	23	DISK FAILURE
332	7	1	7	2	TOD RETARED 25MS	55	10	29	20	10	DISK SERVICE
332	19	53	21	58	MACHINE FAILURE 2701	56	7	2	7	3	TOD RETARED 46MS
336	6	24	13	5	2701 FAILURE	58	10	2	10	3	LINE FAILURE
338	3	1	8	8	CPUA FAILURE	62	7	1	7	2	TOD RETARED 46MS
340	9	39	11	53	POWER BREAK	64	7	1	7	2	TOD RETARED 40MS
340	13	14	13	15	TOD RETARED 25MS	69	7	1	7	2	TOD RETARED 40MS
345	7	1	7	2	TOD RETARED 25MS	73	14	11	14	13	TOD RETARED 20MS
350	8	29	8	30	LINE FAILURE	79	7	2	7	4	TOD RETARED 40MS
354	7	3	7	4	TOD RETARED 30MS	84	7	1	7	3	TOD RETARED 25MS

Table 11.1.1   Daily DP downtime in the period 1 October 1985 - 31 March 1986.

Month	DP uptime hours	DP uptime %	No. of DP breaks	No. of days with breaks	DP MTBF* (days)
OCT	733.95	98.6	14	12	2.0
NOV	717.20	99.6	17	12	1.7
DEC	729.10	98.0	12	8	2.3
JAN	733.70	98.6	14	7	2.0
FEB	658.73	98.0	12	9	2.1
MAR	753.85	99.98	6	6	4.4
		98.8	75	54	2.4

* Mean-time-between-failures = total uptime/no. of up intervals.

Table II.1.2 Online system performance, 1 Oct 1985 – 31 March 1986.

II.2   Array communications

Table II.2.1 reflects the performance of the communications system during the reporting period. In general, the data communication has shown high reliability for all subarrays. Occasional line problems have been observed, with main causes being as follows:

- Synchr. problems caused by reduced line quality - 01B,
- lack of power - 02B
- line quality reduced - 02C, 06C,
- broken cable/modem fault and synchr. problem - 04C,
- faulty carrier frequency system between Hamar and Elverum - 03, 04C.

Summary

Oct 85   01B was affected by a deteriorated line week 43, resulted in synchr. problems.

02B was down weeks 40-43 due to a power outage.

04C performance was reduced by a faulty cable 24 September and remained so throughout September and part of week 40.

01B was affected week 43 by a combination of bad line quality and synchr. problems.

Corrective maintenance (03C) required temporary replacement of communications equipment, etc.

Nov 85   03C was visited 1, 4 and 15 Nov, and attempts to replace modem and Loop Control Logic were made, but without improvement. High attenuation on frequencies 390-500 Hz operating the logic via modem supervisory channel was suspected, but measurement (15 Nov) proved normal attenuation. The performance of the data channel was not affected by the failing loop circuit.

04C was visited (12, 14 and 18 Nov) due to low output of the CTV modem (-20.0 dB m), normal -15.0 dB m. Attempts were made to replace the modem, but without success, until 18 Nov when

the output level became correct. In addition synchr. problems contributed to high "down" figure week 46.

Otherwise 06C was affected by reduced line quality by the end of Nov, creating high error figures.

The performance of the remaining communications system in November was most satisfactory.

Dec 85   In spite of 02C and 06C irregularities, average 11.2, 1.4% respectively, December was a satisfactory period with high performance of the systems.

02C was affected week 49 (1.8%), week 50 (33.9%) and week 52 (8.95%).

06C was affected week 49 (5.4%).

Jan 86   The performance of the systems was most reliable in January, with an average 5-week uptime of 99.98%, which is very good, taking the complex systems into consideration.

Feb 86   02C, 03C, 04C and 06C were affected in February. Although 02C communications system did not cause loss of data, a SLEM "hang up" was the possible cause.

A failing "carrier frequency system" between Hamar and Elverum affected 03C and 04C (23 Feb).

A deteriorated line between Hamar and 06C caused synchr. problems weeks 6,7, resulting in data spikes.

Mar 86   Also in March all the communications systems functioned most satisfactorily, including 03C, in spite of a percentage outage of 0.33% week 10 in connection with 03C.

O.A. Hansen

Sub-array	OCT 85 (5) (30.9-3.11)	NOV 85 (4) (4.11-1.12)	DEC 85 (4) (2-29.12)	JAN 86 (5) (30.12-1.2)	FEB 86 (4) (3.2-2.3)	MAR 86 (4) (3-30.3)	Average ½ yr
01A	0.03	0.013	0.013	0.03	0.02	0.08	0.03
01B	*1.85	0.008	0.017	0.013	0.03	0.05	0.23
02B	*46.80	0.025	0.011	0.016	0.015	0.06	7.82
02C	0.03	0.24	*11.17	0.016	*0.92	0.06	2.07
03C	0.42	0.086	0.01	0.023	*4.84	0.14	0.92
04C	*13.39	*7.18	0.01	0.015	*4.85	0.06	4.24
06C	0.03	*10.72	*1.35	0.016	*9.40	0.06	3.60
AVER	8.94	2.61	1.80	0.018	2.87	0.07	2.72
Less	{01B,02B / 04C}	04C,06C	02C		{02C,04C / 06C}		
	0.13	0.07	0.24		0.24		

* see item II.2 regarding figures with asterisks

Table II.2.1   Communications performance. Figures in per cent based on total transmitted frames/week (1 Oct 1985 - 31 Mar 1986). Note that the percentages refer to times when data were recorded at Kjeller; therefore this table must be seen in conjunction with Table II.1.2.

II.3   Data exchange

Automatic telex transmission of NORSAR DPX and EPX to AFTAC has proceeded normally in the period. NORESS bulletins have been transmitted daily (weekdays only, with weekends included in following Monday's bulletin) to the CSS via ARPANET throughout the period.

Starting January 1986 telex transmissions of NORESS detection lists to AFTAC have been implemented automatically in a way similar to what has been done for NORSAR data. The performance of these transmissions has been satisfactory.

Processing of requests by AFTAC for complete NORSAR/NORESS data files covering selected time intervals has progressed normally during the period. Such data are currently copied to magnetic tape in standard formats, and the tapes are mailed through the APO system. NORSAR also regularly handles requests for NORSAR, NORESS and HFSE data from various U.S. Government contractors.

The NORSAR monthly seismic event summary is currently being distri-buted to about 50 recipients in 26 countries.

F. Ringdal

III.   ARRAY PERFORMANCE

III.1   Event Processor Operation

In Table III.1 some monthly statistics of the Event Processor operation are given:

	Teleseismic	Core Phases	Sum	Daily
OCT 85	225	61	286	9.2
NOV 85	255	62	317	10.6
DEC 85	230	79	309	10.0
JAN 86	233	59	292	9.4
FEB 86	238	49	287	9.6
MAR 86	355	85	440	14.2
	1536	395	1931	10.5

Table III.1   Event Processor Statistics, October 1985 - March 1986.

B. Paulsen

IV.   IMPROVEMENTS AND MODIFICATIONS

IV.1   NORSAR on-line system using 4341 and MODCOMP Classic

We refer to section II for detailed information about uptime, com-
munication and processing performance. No modifications in the NORSAR
on-line system have been implemented during the reporting period.
Transmission of NORESS detection lists to AFTAC was initiated in
January 1986.

IV.2   Data quality

The data quality in the NORSAR online processing system depends mainly
on the communication line quality. There is currently no automatic
masking of subarrays or instruments when poor data quality occurs.
Instead, the operator masks instruments or subarrays as soon as
possible after malfunctioning of communications lines is observed.
Before the masking is done several false detections may occur as a
result of spikes, etc., in the data, and this procedure is therefore
not entirely satisfactory.

We are now working on procedures to automatically detect periods of
bad data quality and automatically mask faulty channels. The first
step has been to develop a program called NRSTAT which produces sta-
tistics for communication errors and status information in much
greater detail than provided by the current on-line system. These sta-
tistics will now be correlated with periods of false detections in
order to obtain rules for automatic masking of instruments. An example
of the output from NRSTAT is shown in Fig. IV.2.1, which covers a
24-hour period. Similar statistics will be compiled on an hourly basis.

IV.3   ARPANET

NORSAR is now a host on the ARPANET. Our node name is norsar.arpa and the physical adress is 195.5.46.2. A list of user identifications which may be used for messages and data transfer is given below:

FR   -   Frode Ringdal

SM   -   Svein Mykkeltveit

HB   -   Hilmar Bungum

ESH   -   Eystein Husebye

RUNE -   Rune Paulsen

Rune Paulsen

```
FILE: EOCREC   RECORD   A   PRINTED 05/16/86 09:50:41


INTERVALL START 135/ 1. 0. 0.0 ENDS 136/ 0. 0. 0.0

SUB   ICWSYN   ICWPOL   ODWSYN   ODWPOL   ODWREC   DATREP   DATPRE   ODWRED   NOLINE   ISCAN   ISYNC
01A      1        2        0       63        0        0       66        1        0        0       0
01B      0        1        0        0        1        1       46        1       25       25      25
02B      0        1        0       25        0        0       28        0        0        0       0
02C      2        3        1        1        0        0        3        0        0        0       0
03C      2        5        1       13        1        2       15        2        0        0       0
04C      2        5        1       66        0        1       68        0        0        0       0
06C      1        6        2        1        0        0        4        0        0        0       0
---------------------------------------------------------------------------------------------------------
PRECENT OUTAGE FOR   24 HOURS
SUB   ICWSYN   ICWPOL   ODWSYN   ODWPOL   ODWREC   DATREP   DATPRE   ODWRED   NOLINE   ISCAN   ISYNC

01A   0.000    0.000    0.000    0.007    0.000    0.000    0.008    0.000    0.000    0.000   0.000
01B   0.000    0.000    0.000    0.000    0.000    0.000    0.005    0.000    0.003    0.003   0.003
02B   0.000    0.000    0.000    0.003    0.000    0.000    0.003    0.000    0.000    0.000   0.000
02C   0.000    0.000    0.000    0.000    0.000    0.000    0.000    0.000    0.000    0.000   0.000
03C   0.000    0.001    0.000    0.002    0.000    0.000    0.002    0.000    0.000    0.000   0.000
04C   0.000    0.001    0.000    0.008    0.000    0.000    0.008    0.000    0.000    0.000   0.000
06C   0.000    0.001    0.000    0.000    0.000    0.000    0.000    0.000    0.000    0.000   0.000

                         01A       01B       02B       02C       03C       04C       06C
DOY  135 PERCENT LINE OUT 0.007    0.000    0.003    0.001    0.002    0.008    0.001
DOY  136 PERCENT LINE OUT 0.022    0.000    0.000    0.000    0.000    0.008    0.000
-------------------------------------------------------------------------------------------
TOTALS  FOR   24 HOURS    0.029    0.000    0.003    0.001    0.002    0.017    0.001
-------------------------------------------------------------------------------------------
AVERAGE FOR   24 HOURS    0.008    0.000    0.003    0.001    0.002    0.008    0.001
```

Fig. IV.2.1 Output from NRSTAT.

ICWSYN	–	Input Command Word SYNc error.
ICWPOL	–	Input Command Word POLy error.
ODWSYN	–	Output Data Word SYNc error.
ODWPOL	–	Output Data Word POLy error.
ODWREC	–	Output Data Word RECeived late in previous sample period and is being treated as early for current sample.
DATREP	–	DATa REPeted, this data sample is repeated from previous sample period.
DATPRE	–	DATa not PREsent this sample period.
ODWRED	–	Output Data Word REDundant ODW received.
NOLINE	–	NOLINE, line decommissioned
ISCAN	–	Subarray in total ICW scan
ISYNC	–	Subarray being synchronized.

V. MAINTENANCE ACTIVITIES

V.1   Activities in the field and at the maintenance center

Activities in October, November and December involved modem replacement (02B, 04C), line check/measurements (02B, 03C, 04C), and fault-finding Loop Control Logic in connection with failing B/C-loop (03C).

Other activities the same months involved RA-5 fault-finding and/or repair (02B), SP seismometer replacement (02B), SP cable replacement (06C), LP seisometer check and adjustment (01B, 03C), Remote Centering Device replacement (03C), CTV dryout and inspection (01B, 06C) and battery checks (all subarrays).

In the same period 8 modems were repaired (NMC) and re-establishment of the new maintenance center in Hamar continued.

Also during the remaining period, January - March, a wide range of activities was covered, such as design of a prototype broadband filter for SP LTA cards, tested on SP channel 05, 06C. At the NMC a number of cards have been repaired: SP/LTA cards, ADC MUX and SLEM test generator cards. Besides, modifications of SP/LTA cards in connection with the new filters have been made.

All the subarrays were visited in March in connection with inspection and preventive maintenance. SP/LP seismometers were checked and adjusted when necessary, and the CTV (01B) was dried out.

The NORESS area has been visited and the HUB TWT Amplifier checked and cleaned. Besides cards have been replaced at the stations C4 and D7.

Subarray/ area	Task	Date
		1985
02B (Tel)	Vital elements of the array prepared to meet winter conditions	1,2,3 Oct
02B	Line check and modem replaced	15,16 Oct
04C	Line was checked. SP protection cards SP01,03 04 and 00 replaced	16 Oct
01B	CTV water leakage tested and LP instruments checked	17,18 Oct
NORESS	Participation in connection with finishing the installatin of a water closet (central station).	23,24,25 29 Oct

From NDPC NORSAR channels have been remotely   Oct
monitored and LP instruments adjusted as
follows:

3 Vertical	seism.	MP adj		4	times
4 NS	"	"	"	5	"
5 EW	"	"	"	7	"
3 Vertical	"	FP adj		3	"
4 NS	"	"	"	7	"
3 EW	"	"	"	6	"

03C	Attempts to solve B/C-loop problem by replacing the modem and Loop Control Logic	1 Nov
02B	RA-5 fault SP01 (02B LPV) located	4 Nov
03C	Both Remote Centering Devices (RCDs) NS LP seismometers replaced	4 Nov
04C	Modem replaced in order to raise output to correct level, -15 dB m. New modem probably also faulty, as the level did not increase	12 Nov
04C	Fault tracing in conection with low frequency component superimposed the data from the vertical LP seismometers	14 Nov
04C	Second attempt with a new modem succeeded. Level correct, -15 dB m	18 Nov

Subarray/ area	Task	Date
02B	Faulty RA-5 amplifier repaired SPO 1 (LPV)	15 Nov
03C	Frequency attenuation measurements performed in both directions on the communications line. Low frequency 390-500 Hz not specially affected or attenuated	15 Nov
	P.W. Larsen to Finland in connection with faulty DDS 1105 equipment	13,14 Nov
NMC	8 modems were repaired in addition to other activities related to the center	Nov

From NDPC NORSAR channels have been remotely
monitored, and LP instruments adjusted as
follows:

```
2 Vertical seism. MP adj.  3 times
3 NS            "    "   "   5   "
6 EW            "    "   "   8   "
1 Vertical      "    FP  "   1   "
3 NS            "    "   "   3   "
6 EW            "    "   "   7   "
```

06C	SP seismometer 03 replaced due to constant HF noise	23 Dec
	Otherwise repair and maintenance of equipment at the maintenance center, including re-establishment of the laboratory	Dec
	From NDPC NORSAR channels have been remotely monitored and LP instruments adjusted as follows:	Dec

```
1 Vertical seism. MP adj.  1 times
3 NS            "    "   "   3   "
2 EW            "    "   "   2   "
2 Vertical      "    FP  "   2   "
3 NS            "    "   "   3
2 EW            "    "   "   2   "
```

1986

| NMC | A prototype filter card was designed and 12 SP LTA cards repaired | Jan |
| NORESS St. D7 | Power supply battery replaced | Jan |

Subarray/ area	Task	Date
	From NDPC SP and LP channels have been monitored and LP instruments adjusted as follows:	Jan
	4 Vertical seism. MP adj. 2 times 5 NS " " " 9 " 5 EW " " " 5 " 3 Vertical " FP " 6 " 3 NS " " " 4 " 2 EW " " " 2 "	
NMC	Repaired 1 PDR-2, 4 SLEM test generator cards and 2 ADC MUX cards	Feb
	25 SP LTA were made ready for replacement of original low pass filters	
	Prototype card still tested in February	
	From the NDPC NORSAR SP and LP channels have been monitored and LP instruments adjusted as follows:	Feb
	1 Vertical seism. MP adj. 3 times 1 NS " " " 1 " 1 EW " " " 3 " 3 Vertical " FP " 3 " 1 NS " " " 1 " 1 EW " " " 3 "	
01A-06C	Preventive maintenance/inspection and minor adjustments of SP/LP instruments	10-21 Mar
NORESS	TWT Amplifier checked and cleaned. Replaced HUB-15 card for site D7	26 Mar
NORESS	Replaced DHL-68 card site C4	26 Mar

Subarray/ area	Task	Date
	From NDPC NORSAR SP and LP channels have been monitored and LP instruments adjusted as follows:	Mar
	2 Vertical seism. MP adj. 3 times	
	3 NS " " " 4 "	
	2 Vertical " FP " 2 "	
	1 NS " " " 1 "	

Table V.1 Activities in the field and at the NORSAR maintenance center, including NDPC activities related to the NORSAR array, Oct 1985 - Mar 1986.

V.2   Improvements and modifications

A prototype broadband filter intended to replace the existing filters on all SP LTA cards has been designed at the NMC.

Since January such a filter has been tested out on 06C channel 05.

V.3   Array status

As of 31 March 1986 the following channels deviated from tolerances:

    01A 01   8 Hz filter

         02   8 Hz filter

         04   attenuated 30 dB

    06C 05   Prototype SP LTA card with broadband filter installed
              for test purposes

                              O.A. Hansen

VI.   DOCUMENTATION DEVELOPED

Bungum, H., J. Havskov, B.K. Hokland & R. Newmark: Contemporary
seismicity of Northwest Europe, submitted for publication.

Christoffersson, A., E.S. Husebye & S.F. Ingate: Wavefield
decomposition. A novel approach to 3-component record analysis,
submitted for publication.

Husebye, E.S., J. Hovland, A. Christoffersson, K. Åström, R. Slunga,
& C.-E. Lund: Tomographical mapping of the lithosphere and astheno-
sphere beneath S. Scandia and adjacent areas, submitted for publi-
cation.

Husebye, E.S., B.O. Ruud & A. Christoffersson: Broadband seismometry:
Reliable event locations from single-site 3-component records,
submitted for publication.

Loughran, L.B. (ed.): Final Technical Report, 1 Apr - 30 Sep 1985,
NORSAR, Kjeller.

Pettersen, Ø. & D.J. Doornbos: A comparison of source analysis methods
as applied to earthquakes in Tibet, submitted for publication.

Ringdal, F.: A study of magnitudes, seismicity and earthquake detect-
ability using a global network, submitted for publication.

L.B. Loughran

VII.   SUMMARY OF TECHNICAL REPORTS/PAPERS PREPARED

VII.1   Regional event detection using the NORESS array

Since January 1985 data from the small-aperture array NORESS in Norway
have been processed in real time at the NORSAR data center at Kjeller.
The data used in the detection processing comprise 25 SPZ channels,
deployed over an area 3 km in aperture and sampled at a 40 Hz rate.
The detection algorithm has been described by Mykkeltveit and Bungum
(1984), and briefly consists of

-    Digital narrow-band filtering (six filter)

-    Beamforming (conventional and incoherent)

-    STA/LTA detector applied to each beam

-    Frequency-wavenumber analysis of detected signals

-    Association of regional phases to aid in locating events.

Preliminary results from the NORESS processing have earlier been presented
in NORSAR Semiannual Technical Summaries (SATS). In this paper, we discuss
in particular the automatic detection performance for events at regional
distances, and the spectral characteristics of signal and noise at very
high frequencies.

Regional detectability

An assessment of the NORESS detection capability at regional distances
has been obtained by comparing the automatic NORESS detector output to
the bulletins produced on the basis of local seismic networks in Fen-
noscandia. In particular, we have used as a data base the catalogue of
seismic events in Northern Europe regularly compiled at the University
of Helsinki.

The time period covered by this study is the 6-month interval April-
September 1985, during which the RONAPP processor was operated with a
fixed beam deployment (re. NORSAR SATS 84-85). A total of 477 events
reported in the Helsinki catalogue (Fig. VII.1.1a) with local magni-
tudes in the range 1.7-3.3, were cross-checked with the NORESS detection

list. The epicentral distances from NORESS ranged from 500 to 1500 km. For each event, the expected arrival times at NORESS for P, Sn and Lg were computed, using standard travel time tables, and matched to NORESS detection entries.

Fig. VII.1.1b shows the magnitude-distance distribution of the events in the data base. Events detected at NORESS are shown as crosses, non-detections are indicated as triangles. In this figure, "detection" means that at least one phase (P, Sn or Lg) was reported by NORESS.

A summary of the statistics on automatic detection of primary vs. secondary phases is given in Table VII.1.1. We note that, at low magnitudes, many events are detected only on secondary phases. It is also noteworthy that several events, even in the higher magnitude range, are detected as P-phases only. However, visual inspection of the signal traces shows that in virtually all of these cases an Lg phase may be identified by the analyst. Thus, the lack of secondary phase detections is a problem within the automatic processor that requires improvements in the algorithms in order to extract emergent phases in the coda of a preceding P-phase.

M_L	1.5-2.0	2.1-2.5	2.6-3.0	3.1-3.5
P detection only	13	39	16	0
P + secondary phase*	16	105	30	3
Secondary phase only*	28	88	2	0
No detection	48	87	2	0
Total	105	319	50	3

* "Secondary phase" meaning Sn or Lg (or both) detected.

Table VII.1.1   Summary of automatic NORESS detection statistics for the regional data base.

Fig. VII.1.1 shows that there is only a slight degradation in detec-
tion capability with increasing distance for the range considered. As
an initial estimate of detection thresholds, we have therefore com-
bined the data in the distance range 700-1400 km and estimated detec-
tion thresholds as shown in Fig. VII.1.2 (detection on either P, Sn or
Lg) and Fig. VII.1.3 (P-detection only). The method described by
Ringdal (1975) has been applied.

From Fig. VII.1.2 we observe that the 50 and 90 per cent regional
detection thresholds are close to $M_L = 1.9$ and 2.5, respectively. When
only P phase detections are counted (Fig. VII.1.3), the respective
thresholds are $M_L = 2.3$ and 2.7.

It would clearly be desirable to tie these thresholds to the global m_b
scale. It has, however, not been possible to do this for the present
data set, since all of the 477 reference events are much too small to
have any teleseismic detection. Nevertheless, the local magnitude
scale in question has been developed so as to be consistent with
world-wide m_b, and the differences are not thought to be significant.
This topic will be subject to further study.

As a final note, we remark that the large majority of reference events
are mining explosions, mostly from mines in Western Russia. We have
not yet attempted systematically to compare the detectability of these
explosions to that of the (very few) earthquakes in the data base, but
initial studies do not indicate major differences for the two source
types.

High-frequency studies

The recently installed high-frequency recording system (HFSE) at
NORESS has provided a unique opportunity to study noise and signal
characteristics at frequencies up to at least 50 Hz. These studies

have only begun, but it is already apparent that much important infor-
mation can be extracted from the high frequency part of the spectrum.

An example of a high-frequency recording is shown in Fig. VII.1.4,
corresponding to an M_L = 5.0 earthquake off the west coast of Norway
on February 6, 1986 (distance = 417 km). The unfiltered record shows
the expected amplitude pattern, i.e., Lg as the dominant phase, Pg
much larger than Pn. The picture changes dramatically when considering
the high-frequency part of the record. In the filter band 30-50 Hz,
the Pn and Sn phases dominate the seismogram, and the Pg and Lg phases
are not even visible.

Fig. VII.1.5 shows HFSE spectra from the vertical component for the
same event. We see that Lg exceeds the preceding noise (which in fact
is the Sn coda) only up to about 10 Hz, whereas Pn has large SNR over
the entire frequency band.

A further discussion of recorded HFSE P-wave spectra at various
distances is given in Subsection VII.2.

In conclusion, the NORESS regional detection capability appears to be
M_L = 2.5 or better out to at least 1500 km. Many small events are
detected only on secondary phases, and the further improvement of
automatic detection of such phases is important. At distances up to
500 km, considerable improvements in detection capability are possible
by taking advantage of the high frequencies which propagate very effi-
ciently in this distance range. The high frequency band is also poten-
tially valuable for improved phase identification, especially to
separate Pn from Pg and Sn from Lg.

F. Ringdal

References

Loughran, L.B. (ed.) (1985): NORSAR Semiannual Technical Summary, 1 Oct 84-31 Mar 85.

Loughran, L.B. (ed.) (1985): NORSAR Semiannual Technical Summary, 1 Apr - 30 Sep 1985.

Mykkeltveit, S. & H. Bungum (1984): Processing of regional seismic events using data from small-aperture arrays, BSSA, 74, 2313-2333.

Ringdal, F. (1975): On the estimation of seismic detection thresholds, BSSA, 65, 1631-1642.
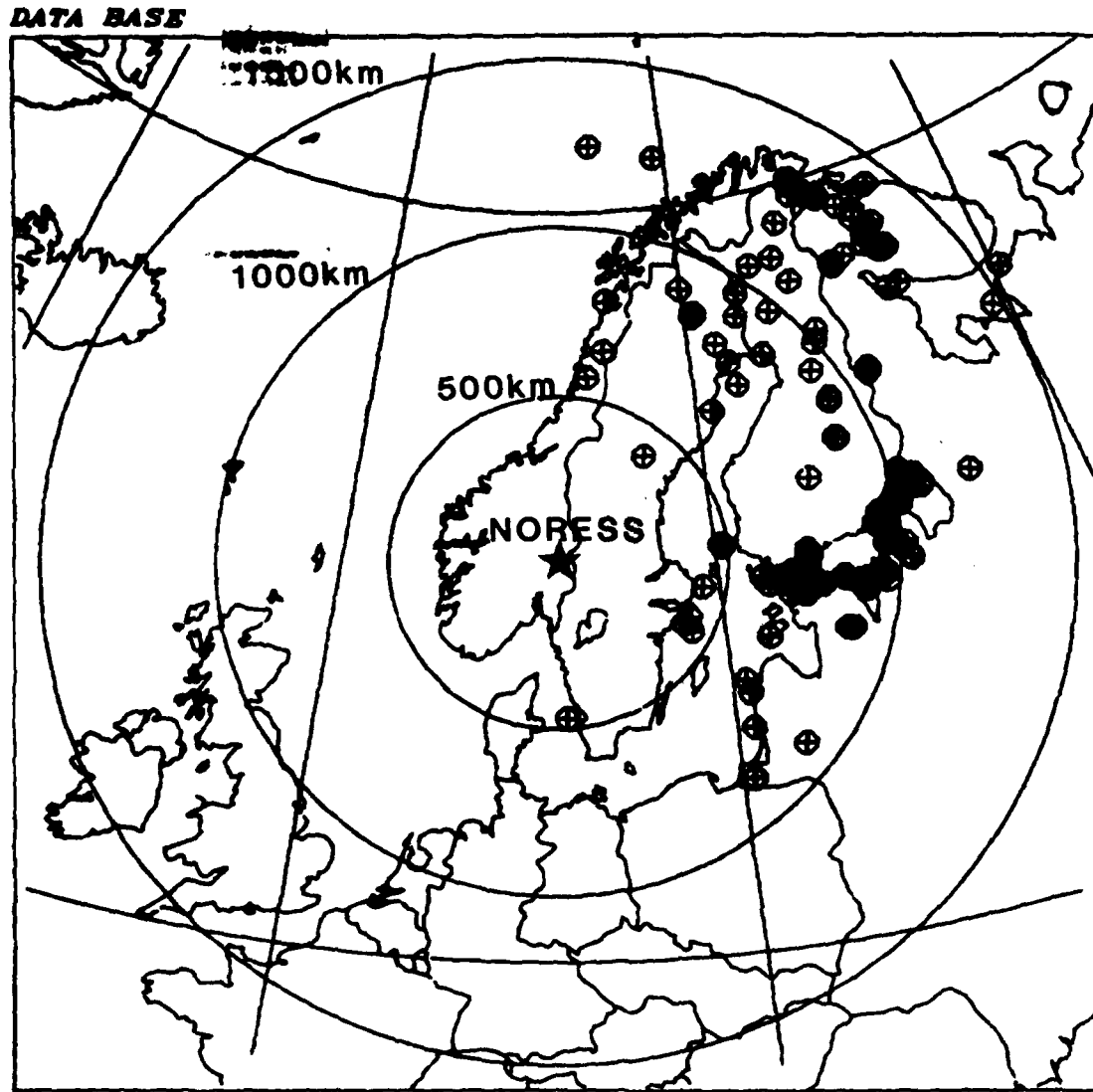
DATA BASE

Fig. VII.1.1a Geographical distribution of 477 reference events used
as a data base for the detectability study in this
paper.

NORESS REGIONAL DETECTION
AZIMUTH RANGE 15-175 DEGREES
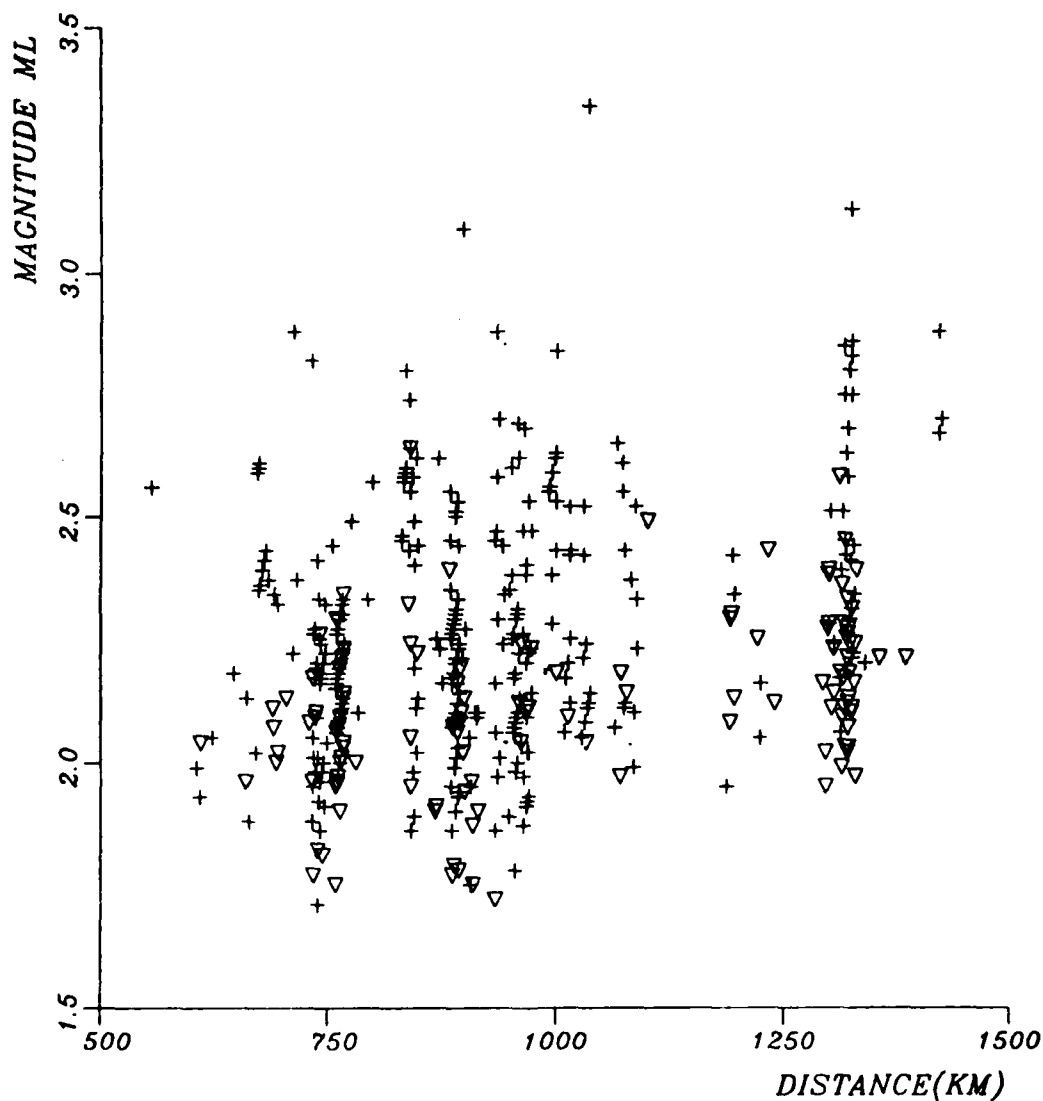
Fig. VII.1.1b Distribution of events in the data base as a function of
epicentral distance from NORESS and local magnitude M_L.
Crosses denote events detected automatically at NORESS
(either P, Sn or Lg phase), whereas non-detected events
are marked as triangles.
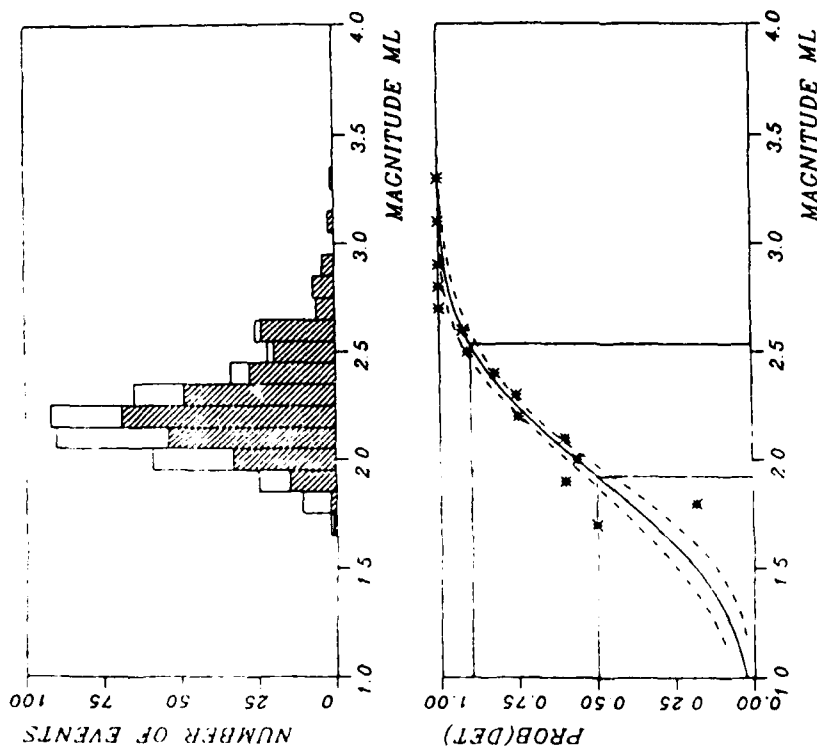
Fig. VII.1.2   Distribution of events by magnitude (upper part), with events detected for at least one phase (P, Sn or Lg) corresponding to the hatched columns. The bottom part of the figure shows the estimated detection probability curve as a function of magnitude, with the observed detection percentages marked as asterisks.
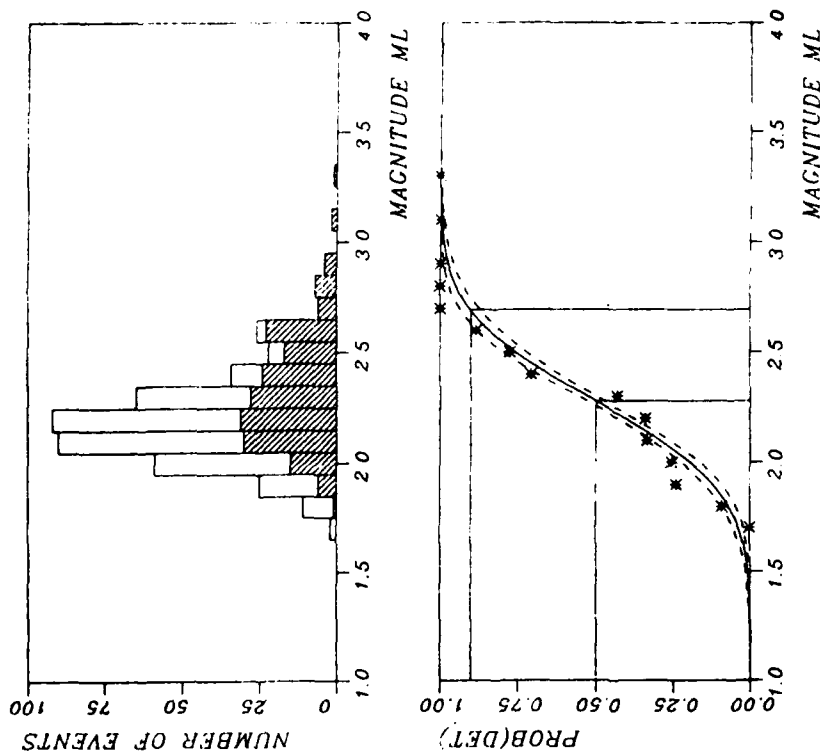
Fig. VII.1.3   Same as Fig. VII.1.2, except that only events with a detected P-phase are counted as detections.

W.NORWAY D=417KM
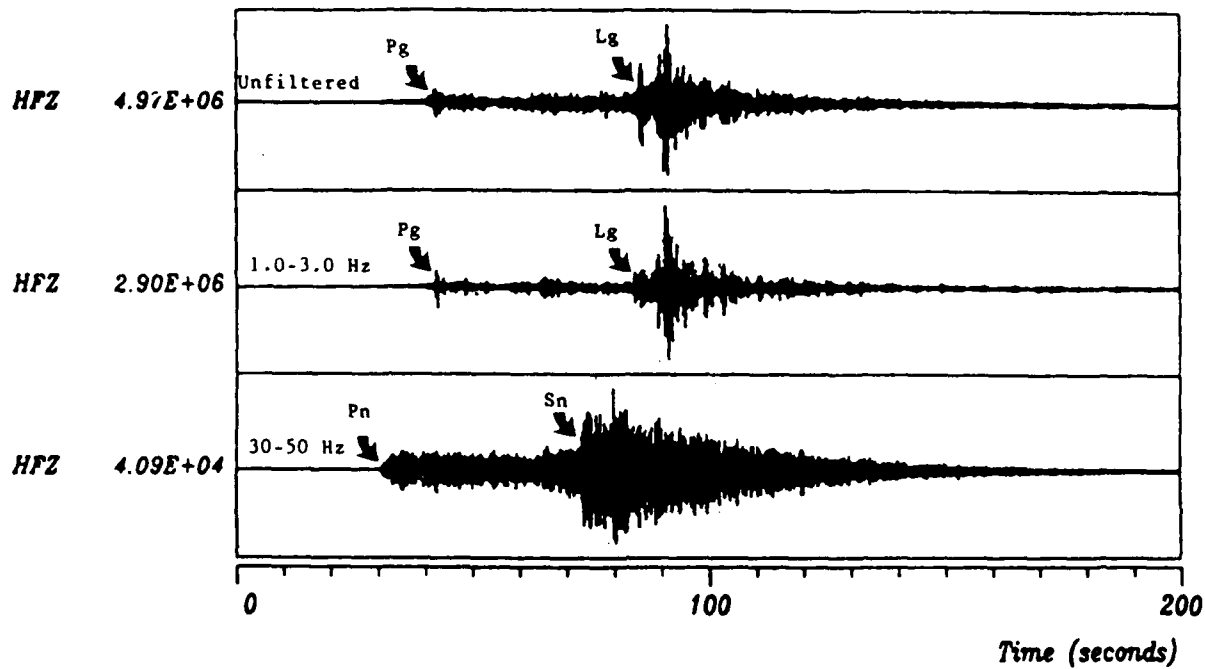
P WINDOW
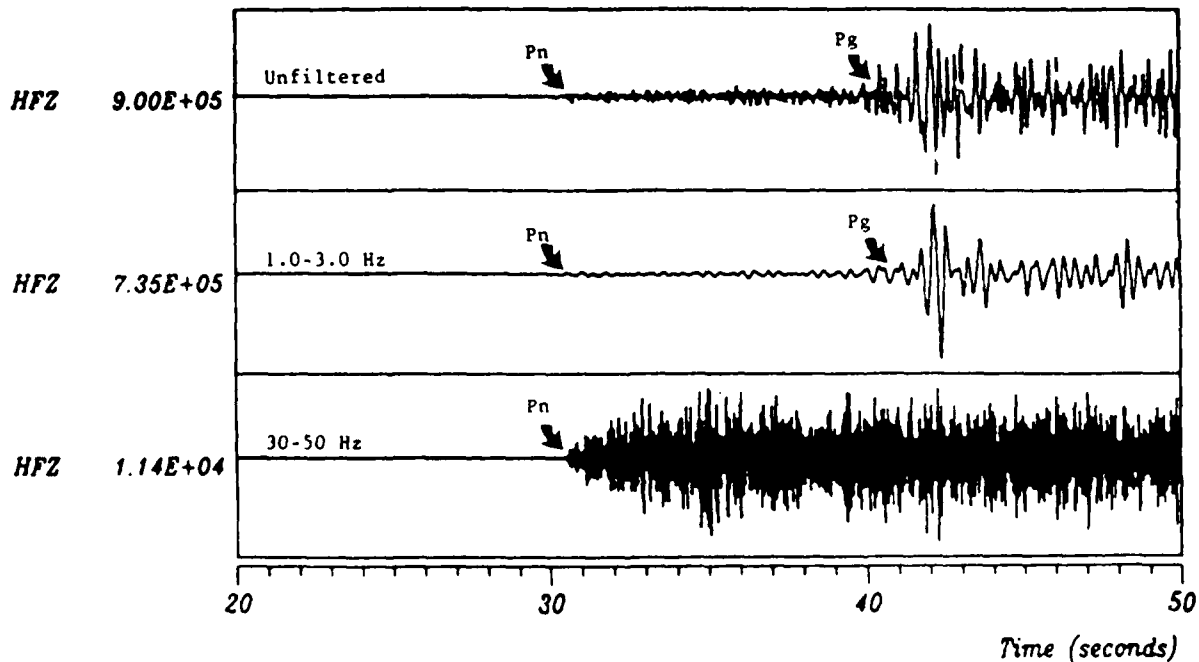
Fig. VII.1.4 Time domain plots of the HFSE recordings on the SPZ channel
at NORESS for an M_L = 5.0 earthquake off the west coast of
Norway (distance = 417 km). The upper part covers the entire
wavetrain (unfiltered and in two filter bands as indicated).
The bottom part is an expanded view of the P window. Note the
prominence of Pn and Sn in the high-frequency band.

HFZ 86036 17.54.30
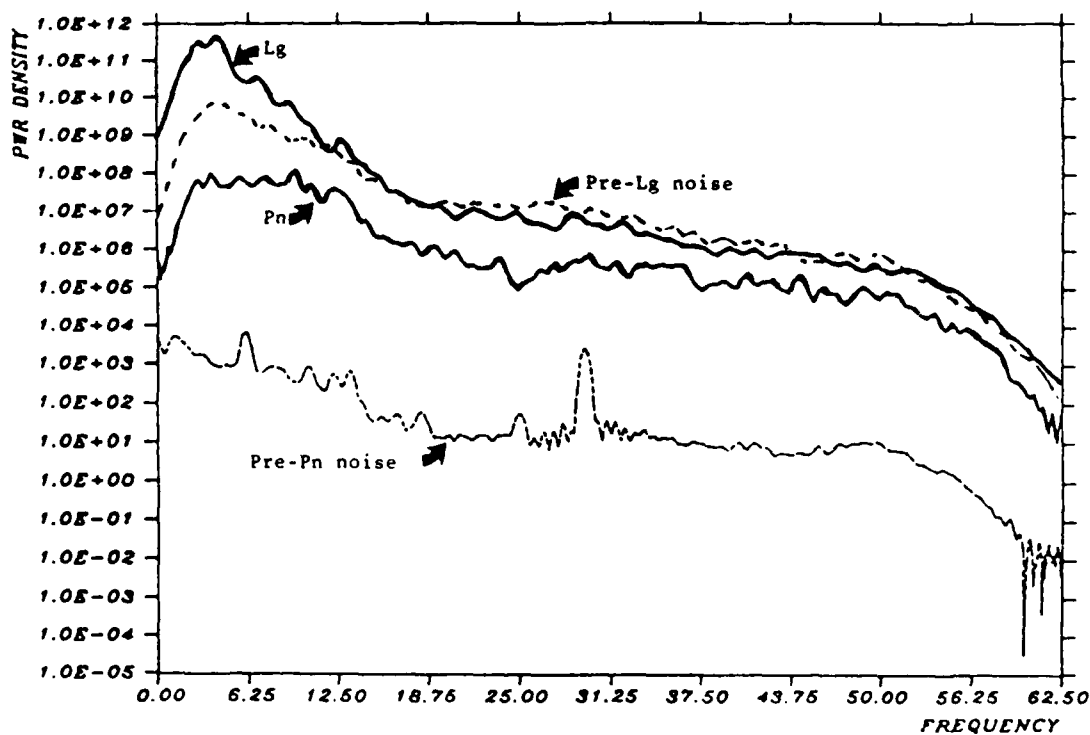
Fig. VII.1.5   Spectral plot of the Pn and Lg phases for the event shown in
Fig. VII.1.4. Note that the Pn SNR remains approximately
constant across the entire high-frequency part of the
spectrum.

VII.2   Initial results from the NORESS High Frequency Seismic Element (HFSE)

The HFSE is an advanced seismic recording system, specially designed to record high frequency energy with high resolution and large dynamic range. The system, which is a self-contained, modular hardware package, has been designed and constructed by Sandia National Laboratories.

The HFSE provides for both single axis and three axis field selectable implementations. The single axis (vertical) configuration has the widest bandwidth and permits studying frequencies to above 100 Hz. The three axis (Z,N,E) configuration permits the studying of vertical-horizontal relational characteristics of frequencies to above 50 Hz. In the initial implementation, the three axis configuration has been chosen.

The digitizer is a Gould Inc. Enhanced Delta Modulation Encoder (EDME). The EDME provides 21 bits of dynamic range (120 dB) in a 24-bit format. The vertical axis EDME is configured as a dual sample rate device; both 125 and 250 Hz sampled data are provided to the system processor. The two horizontal EDMEs are configured as 125 Hz sample rate devices. The 250 Hz sample rate EDME incorporates a digital filter to obtain a usable bandwidth of 3-112 Hz. The 125 Hz sample rate EDME channels have a usable bandwidth of 3-56 Hz. The input voltage ranges are ±10 volts full scale for all channels.

The HFSE has been installed at the center site of the NORESS array, i.e., at 60.735 N, 11.541 E, at an elevation of 247 m above sea level. Data input is from a three-component short period seismometer of type Geotech S-3. The seismometer is emplaced in a 60 m borehole.

We note that the same seismometer is currently being used as one of the three-component sensors in the NORESS array (code F0). Thus, we have a possibility to verify the HFSE response in the frequency band where the two systems overlap (0-20 Hz).

The HFSE installation was conducted during October/November 1985, in cooperation between Sandia and NORSAR personnel. Data have been available at the NORSAR Data Center since late November 1985, and are currently being stored permanently on magnetic tapes.

We are currently conducting a systematic study of the spectral characteristics of HFSE-recorded seismic phases, and in this section we present a few representative examples, together with brief comments summarizing the most important features. For further detail, referer ͻ is made to Ringdal (1986).

The noise spectra shown in the following represent the noise prior to the P phase of each event, and have been estimated using the indirect covariance method. We first estimate the correlation function by splitting a long data record into many windows, calculating a sample correlation function for each window, then averaging the sample correlation functions. Typically, we use 20 windows, each of which is 5 seconds long. Because the earth noise has such a large dynamic range, we prewhiten it prior to estimating the correlation function with a low-order prediction-error filter. The spectrum is then estimated by windowing the correlation function with a 3-second Hamming window, then computing the Fourier transform. The spectral estimate obtained this way is compensated then for the effects of prewhitening and normalized to a 1-second window length.

Signal spectra have been estimated using the same technique, but with 4 overlapping windows, each of 7 seconds length. Start times of these windows are 3, 2, 1 and 0 seconds before signal onset, respectively. Thus we achieve a smoothing of the signal spectra while retaining compatibility with the noise spectra.

Fig. VII.2.1 shows, as an example, uncorrected P-wave spectra for 4 regional P-phases, together with spectra of the preceding noise. A noteworthy feature is distinct noise peaks at selected frequencies. The strong peak around 30 Hz apparently reflects noise interferences caused by mechanical equipment installed in the NORESS hub (fans, etc.), and is not thought to represent any malfunctioning of the HFSE, nor actual earth noise. The peaks occasionally seen at 6 and 12 Hz are typical of daytime hours, and seem to be generated by a sawmill located about 15 km from the site. With regard to the signal spectra shown, the most noteworthy feature is the considerable high frequency P-energy, across the entire HFSE bandwidth, for the two closest events.

Fig. VII.2.2 shows, schematically, a suite of smoothed P-wave spectra representing typical regional events, at various distances, recorded at the HFSE. The figure has been compiled on the basis of about 100 regional events, and represent average spectra over all azimuths, scaled to magnitude M_L = 3.0.

The figure illustrates the strong distance-dependence of high frequency signal energy. Of particular interest is the observation that the signal and noise spectra are approximately parallel across the entire frequency band for distances out to about 500 km. Thus, within this distance range, the possibility of utilizing high frequencies for event characterization are excellent even at very low magnitudes. At further distances, the signal spectra start to merge with the noise

(the crossover point being dependent on distance as well as magnitude). E.g., at 900-1000 km, there seems to be significant SNR at $M_L = 3$ for frequencies up to about 25 Hz.

It must be noted that we have observed considerable spectral variability with source type and location, even within limited distance ranges. Thus Fig. VII.2.2 must be interpreted accordingly. We are currently in the process of studying further these spectral variations, and the results reported here are of preliminary nature.

F. Ringdal
B.Kr. Hokland
T. Kværna

Reference

Ringdal, F. (1986): Quarterly Technical Report, High Frequency Signal Propagation Studies, NORSAR, Kjeller, Norway.
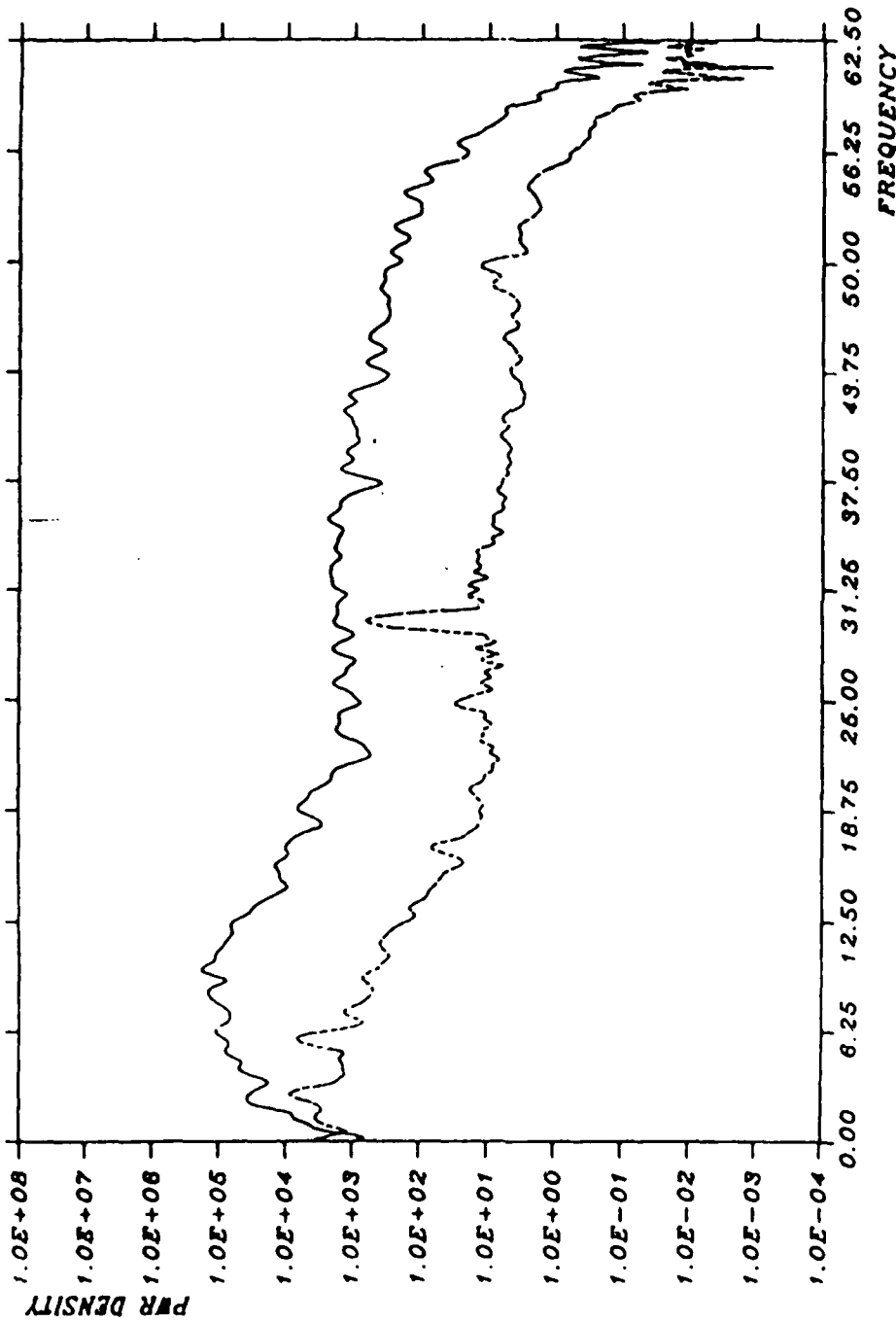
Fig. VII.2.1a-d   HFSE uncorrected P-wave and noise spectra (SPZ component) for four regional events. Event parameters (data date, time, distance, azimuth, M_L, source type, if known) are given in each case. Note the gradual decline of high frequency signal energy with increasing distance.
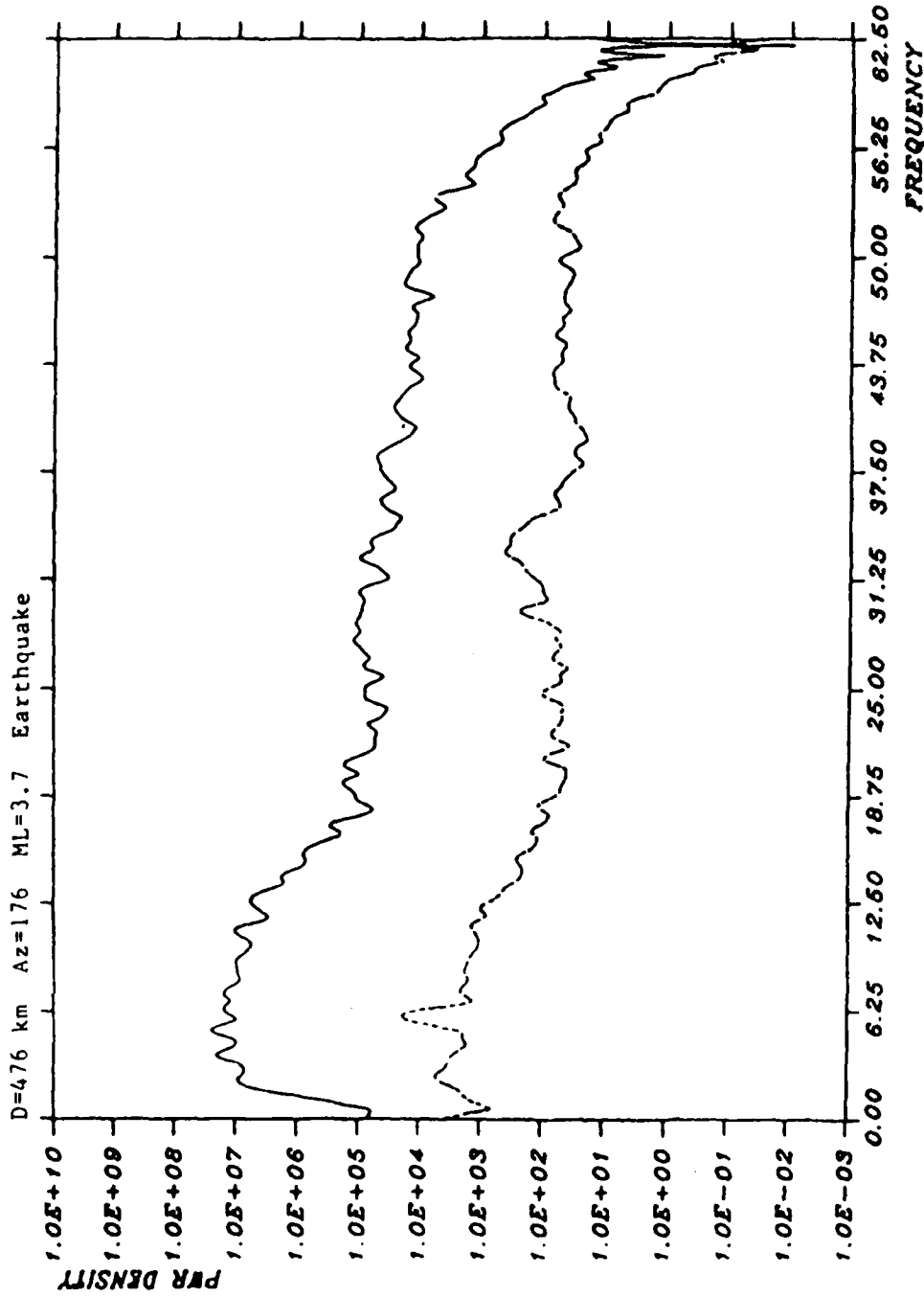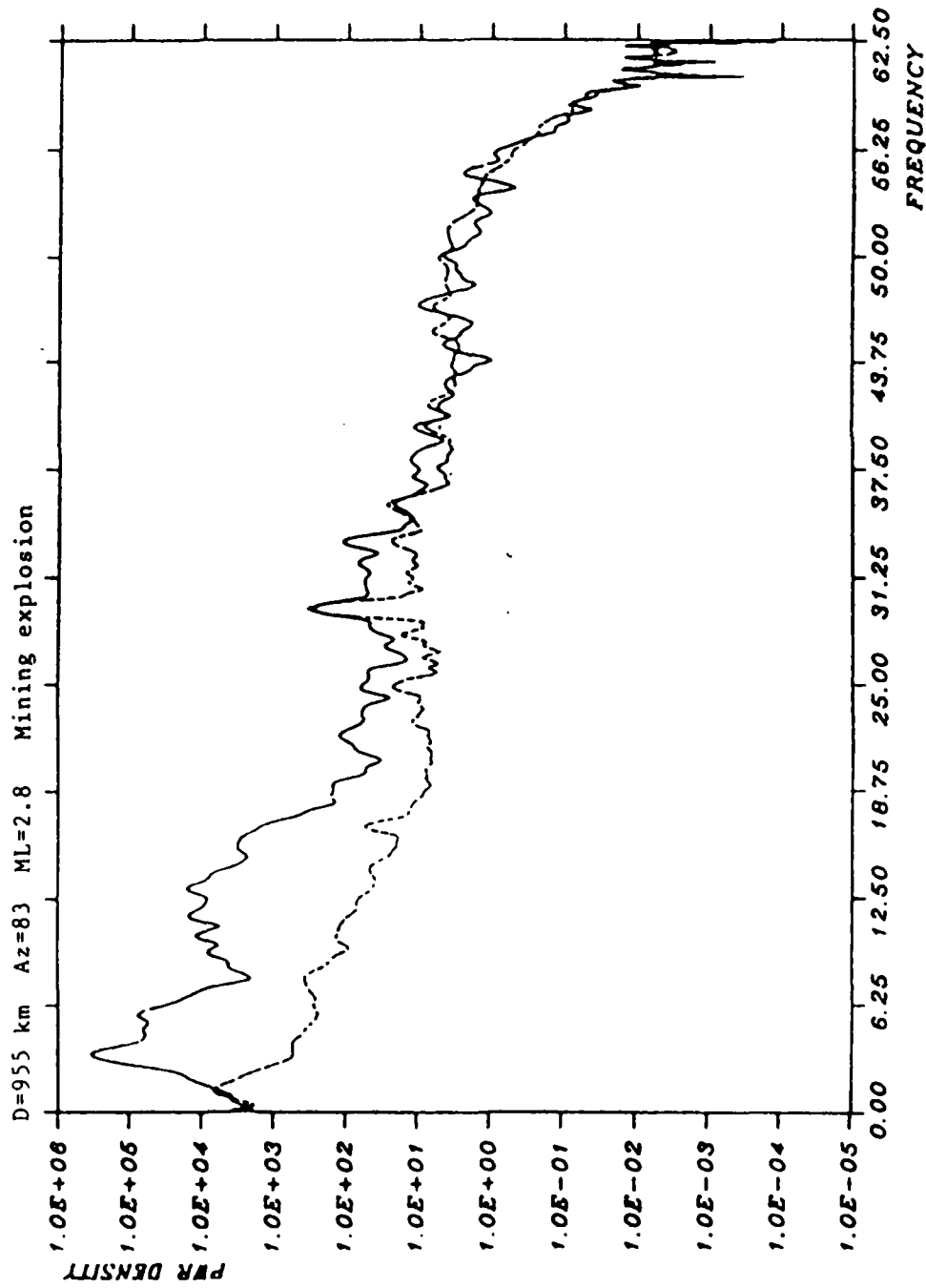
Fig. VII.2.1b

HFZ 85360 13.09.15 PN - NOISE

D=955 km Az=83 ML=2.8 Mining explosion
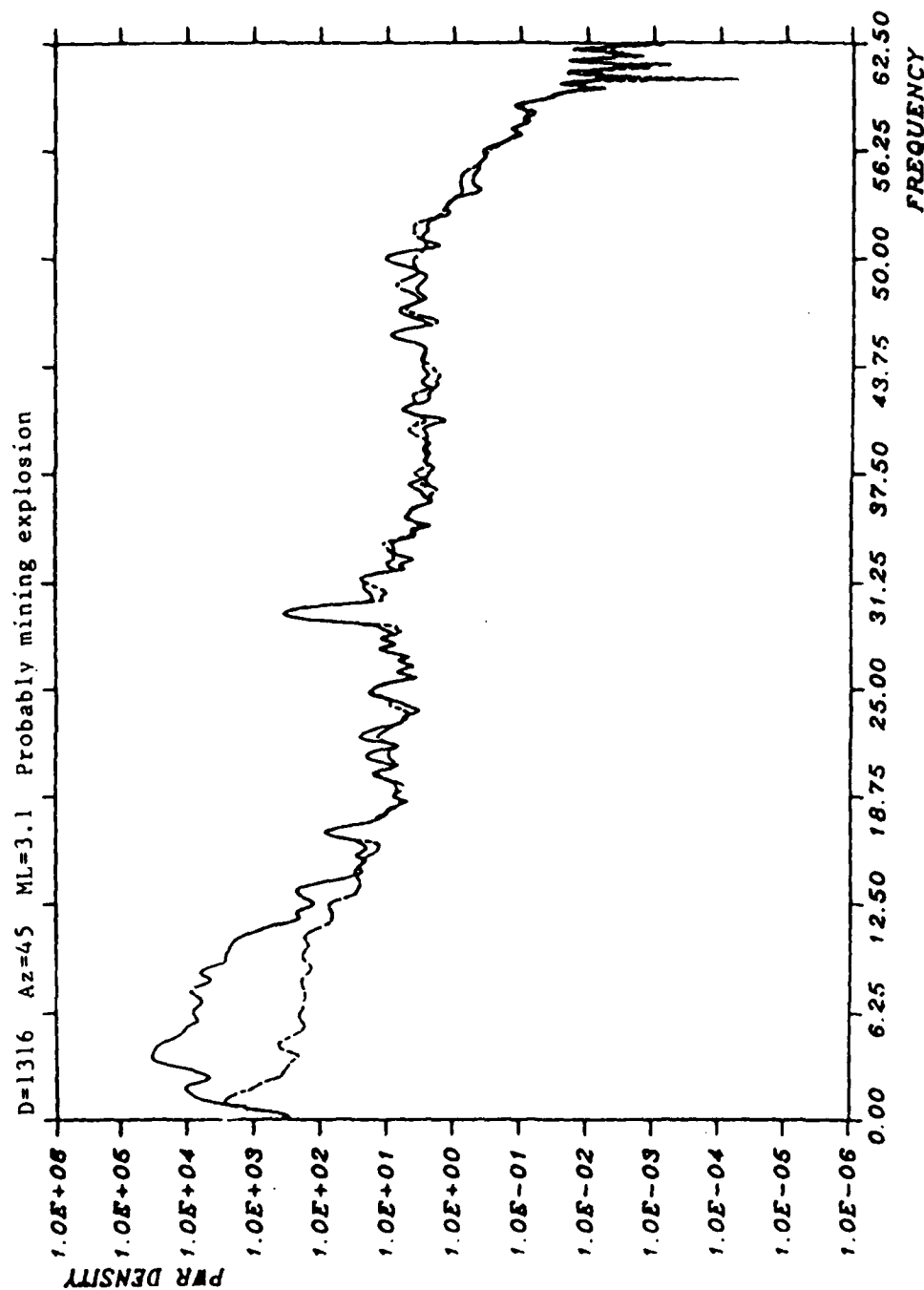
Fig. VII.2.1c

Fig. VII.2.1d

NORESS HIGH FREQUENCY RECORDINGS
SIGNALS SCALED TO MAGNITUDE 3.0
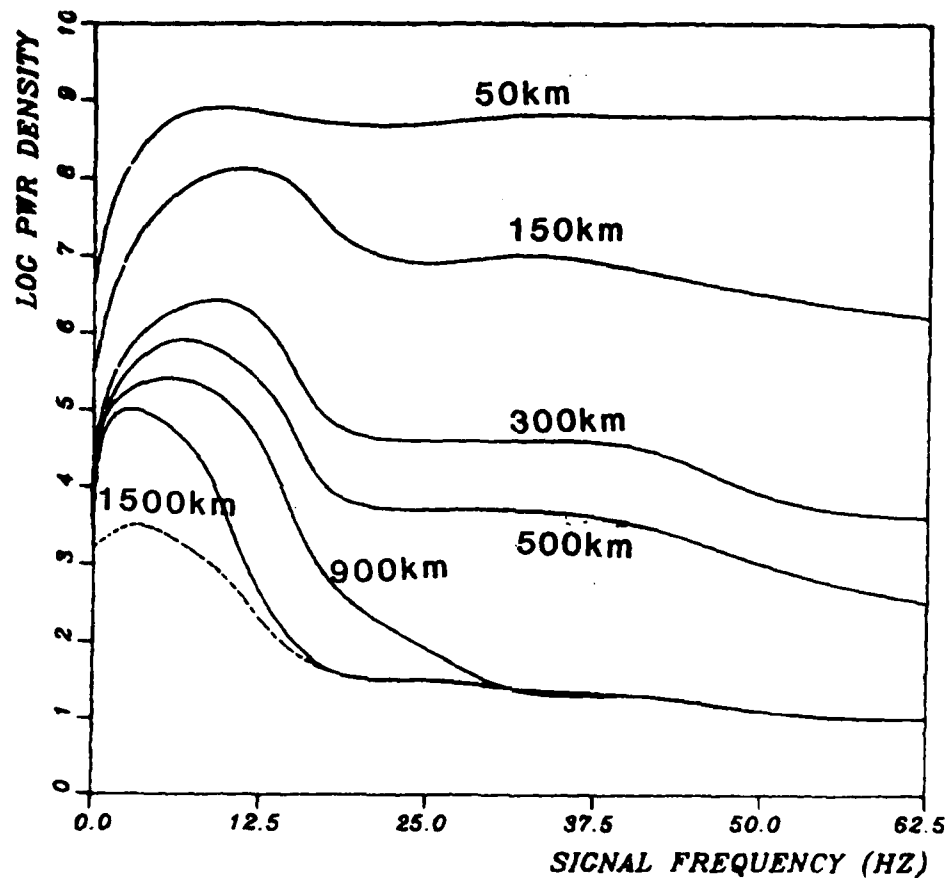
Fig. VII.2.2 Schematic illustration of high frequency P-wave spectra
recorded at the HFSE, at various regional distances. The
figure represents average features of about 100 regional
events at various distances and azimuths, all scaled to
M_L = 3.0. A typical noise spectrum is shown as a dotted
line. Note that a considerable smoothing has been
applied to the spectra, and that there are significant
variations between individual events, even within
limited epicentral areas.

VII.3 NORESS real time processing performance for events in Western Norway and the North Sea

Our previous semiannual report contained a contribution (Mykkeltveit, 1985) on the performance of NORESS real time processing for events in Western Norway and the North Sea. The data base under consideration consisted of 132 events automatically located by the NORESS online processing package (RONAPP) and also reported independently by the University of Bergen, based on their network of six seismic stations located on the west coast of Norway. In the present study, we have extended our previous investigation by taking a different approach: The bulletin of events reported by the network was used as the starting point for a search in the RONAPP automatic detection log for all detections that could be associated with these events.

The events reported by the network are explosions and earthquakes within or near the network, in addition to events in the North Sea. The distance range to NORESS for these events was 250-700 km. Since the goal of our investigation was an evaluation of the performance of RONAPP with respect to locating regional events, it was necessary to carefully check the quality of the network locations. As a result of this process, all reported events within the network were accepted. In addition, the quality of the locations of all events outside the network but within 100 km of the nearest station was considered satisfactory. The British Geological Survey (BGS) publishes a bulletin for the North Sea region based on arrival times reported for stations in Norway, Shetland and Scotland. Events in this region for which the locations were constrained by station readings from both sides of the North Sea and reported by BGS were also added to our event list, which contains 251 events for the period April-September 1985.

The RONAPP detection log for the period April-September 1985 contains
approximately 14,000 entries, each with information on detection
time, phase velocity and direction of arrival, as well as other
parameters. For the events in the list based on the network bulletin,
expected arrival times at NORESS for the phases Pn, Sn and Lg were
computed and compared with actual detection times in our detection
log. The velocity-depth model used to generate these arrival times at
NORESS is the one used in the RONAPP location algorithm: a three-
layered crust of thickness 40 km overlying a half-space.

Fig. VII.3.1 shows the detection capability of NORESS/RONAPP for the
events in our data base. The criterion for declaring a detection for a
P- or S-phase for these events is the existence of an entry in the
RONAPP detection log that can be associated with such arrivals. The
requirement for accepting a P-phase association is a phase velocity
exceeding 6 km/s, an arrival time deviating by less than 10 sec from
the expected arrival time for Pn, and an estimated direction of arri-
val within 30° of the "true" direction, determined from the reported
location. Acceptance of an S-phase association results from a phase
velocity less than 6 km/s, deviation from the expected arrival time
for Sn or Lg less than 10 sec, and an estimated direction of arrival
within 30° of the true direction. The reported magnitudes M_D are dura-
tion magnitudes and are found to correspond well to the local magni-
tudes M_L automatically determined by RONAPP and included in the NORESS
event bulletins. The epicentral distances for the events included in
Fig. VII.3.1 range from 250 km to 700 km. The distribution within the
data base is such that the detection probabilities inferred from this
figure are representative for events at a range of approximately
400 km. At this range a detection probability of 50% is achieved at
magnitude M_L of about 1.8. If the requirement is relaxed to detection
of one phase (P or S) only, the detection probability increases to
approximately 70% at magnitude 1.8.

Fig. VII.3.2 shows deviations from expected arrival times (based on the network locations) for _all_ detections from RONAPP that can be associated with the 251 events (the criterion is again that the azimuth estimated for the detected phase must be within 30° of the azimuth from the network location). These detections are classified as P detections if the estimated phase velocity exceeds 6 km/s, and as either Sn or Lg if the phase velocity is below this value. The detections are classified as Sn if the signal arrives before a time corresponding to the mid-point between the expected arrival times for Sn and Lg, otherwise it is classified as Lg. Fig. VII.3.2 indicates that the class of P detections is composed of slightly early Pn detections and Pg arrivals typically 4 seconds after Pn. A closer examination of the RONAPP plots for these events showed that the P detections at 27 seconds and later correspond to true Sn and Lg arrivals, for which the f-k analysis resulted in a wrong phase velocity. Similarly, the Sn detections that are early by 20 seconds or more correspond to true P arrivals, for which the f-k analysis gave wrong velocities.

Fig. VII.3.3 includes one arrival only for each phase type, namely, the earliest detection of type P, Sn and Lg, for each of the events in the date base. This figure shows that the Pn arrivals are typically a few seconds early relative to our model, that frequently Pn is missed and the first detected P is Pg, that Sn detection times are fairly close to expected ones, and that Lg onset detections are typically early by about 3 seconds. These observations suggest changes in the velocity-depth function embedded in our automatic location procedure, for events in this region. For example, the group velocity of 3.50 km/s used by RONAPP for the Lg onset in the range estimation should be changed to approximately 3.60 km/s.

Fig. VII.3.4 shows average phase velocities for all arrivals in Fig. VII.3.2, for which there are three or more detections within each one second interval, for each of the phases. All events have been "normalized" to an epicentral distance of 400 km, in the sense that expected arrival times of Sn and Lg have been set at 41 and 58 seconds after Pn, respectively, but the observed deviations from the expected arrival times of Sn and Lg have been retained. We see a fairly sharp drop in the phase velocity at travel time zero seconds, corresponding to the transition from Pn to Pg arrivals. It is also seen that on the average, Sn phase velocities are higher than those for Lg. The Lg phase velocities appear remarkably stable at about 4.1 km/s.

In conclusion, this study has shown that the RONAPP performance for events at a distance of 400 km from NORESS is very satisfactory for magnitude 2 and above for RONAPP's current beam deployment. The study has also provided statistics on the rate of failure of the f-k analysis in determining the phase type. Finally, the study has provided a basis for changes in the travel-time model that will lead to better precision in the automatically determined locations.

S. Mykkeltveit

References

Mykkeltveit, S. (1985): Evaluation of NORESS real time processing performance: Case study for 132 Western Norway/North Sea events. Semiannual Technical Summary, (ed. L.B. Loughran), 1 April - 30 September 1985, NORSAR, Kjeller, Norway.
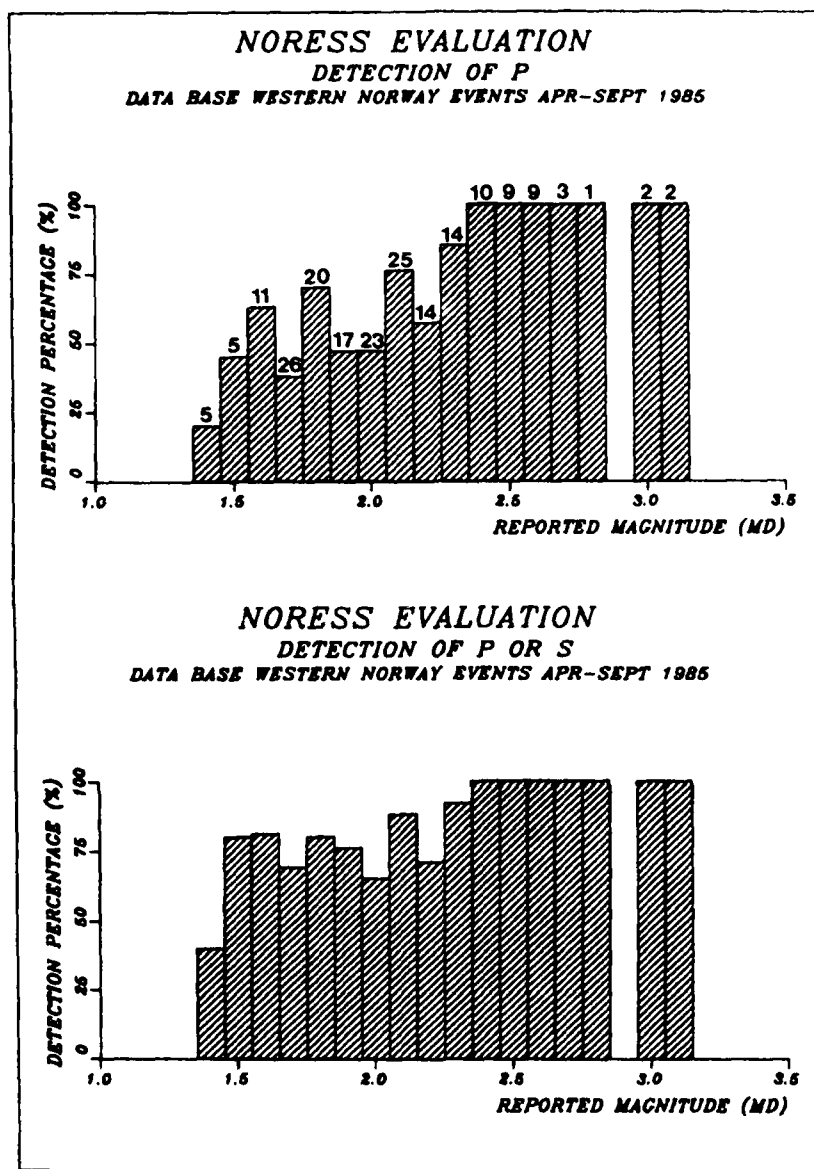
Fig. VII.3.1   NORESS detection probabilities for the events in our
              data base. The top figure shows probabilities for detec-
              tion of a P-phase, while the bottom histogram shows pro-
              babilities of detection of a P- or S-phase. The numbers
              on top of the columns (top figure) give the number of
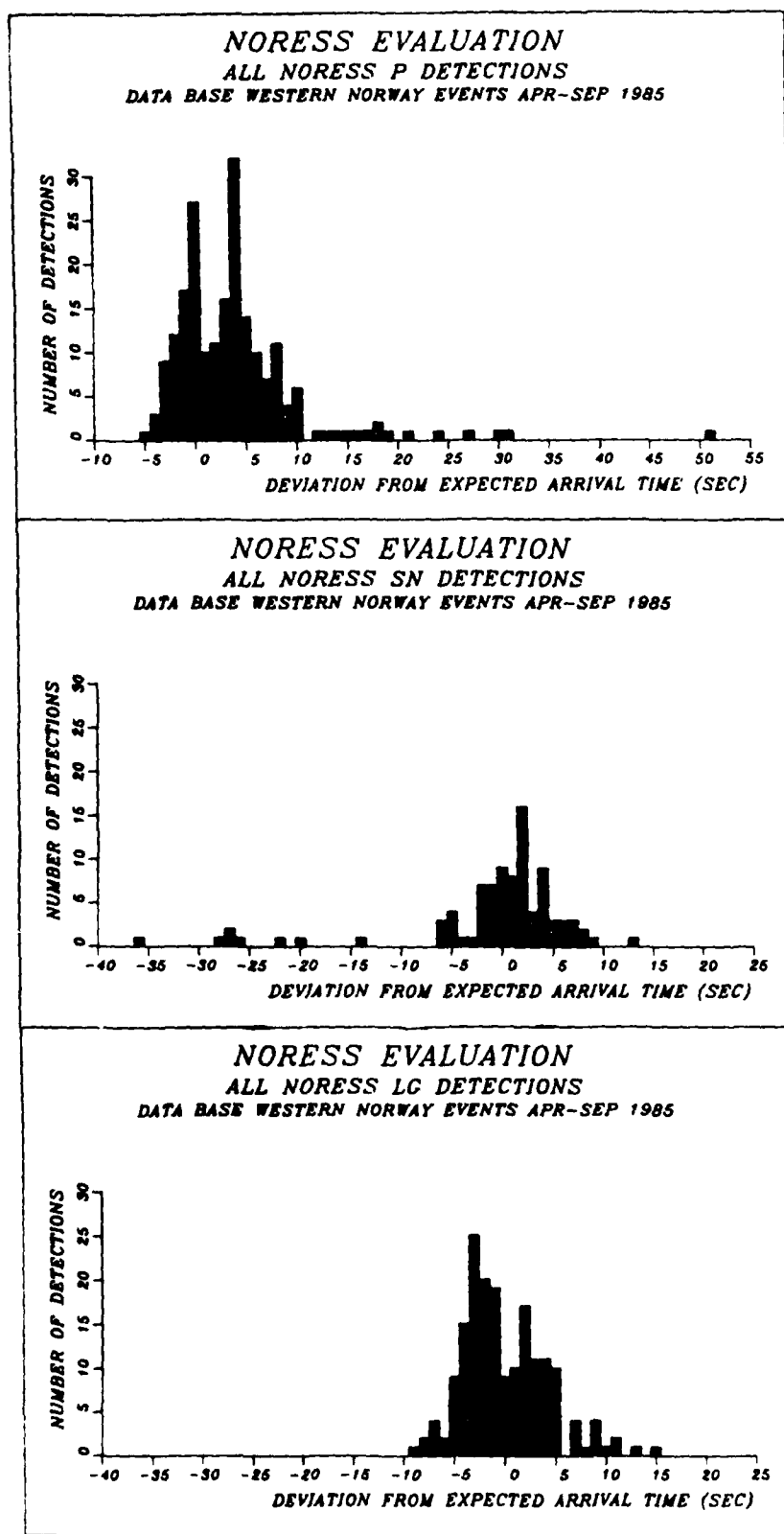   events reported for each magnitude.

NORESS EVALUATION
ALL NORESS P DETECTIONS
DATA BASE WESTERN NORWAY EVENTS APR–SEP 1985

NORESS EVALUATION
ALL NORESS SN DETECTIONS
DATA BASE WESTERN NORWAY EVENTS APR–SEP 1985

NORESS EVALUATION
ALL NORESS LG DETECTIONS
DATA BASE WESTERN NORWAY EVENTS APR–SEP 1985

Fig. VII.3.2   Deviations from expected arrival times for P (top), Sn
(middle) and Lg (bottom) for NORESS detections
corresponding to the 251 Western Norway events.

NORESS EVALUATION
NORESS FIRST P DETECTIONS
DATA BASE WESTERN NORWAY EVENTS APR–SEP 1985

NORESS EVALUATION
ALL NORESS FIRST SN DETECTIONS
DATA BASE WESTERN NORWAY EVENTS APR–SEP 1985

NORESS EVALUATION
ALL NORESS FIRST LG DETECTIONS
DATA BASE WESTERN NORWAY EVENTS APR–SEP 1985
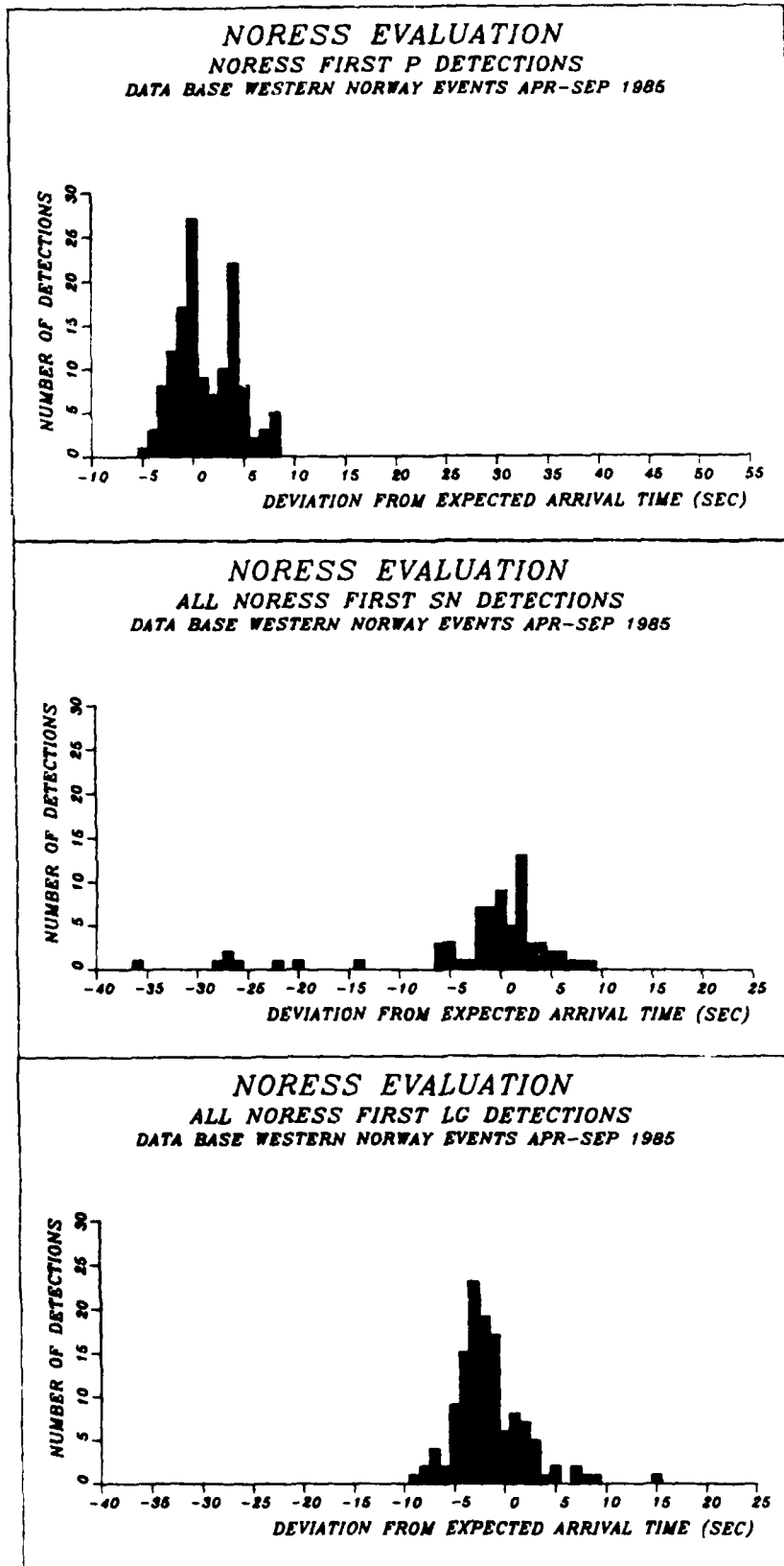
Fig. VII.3.3   Same as VII.3.2, but now only the first detection is
included for each phase type.
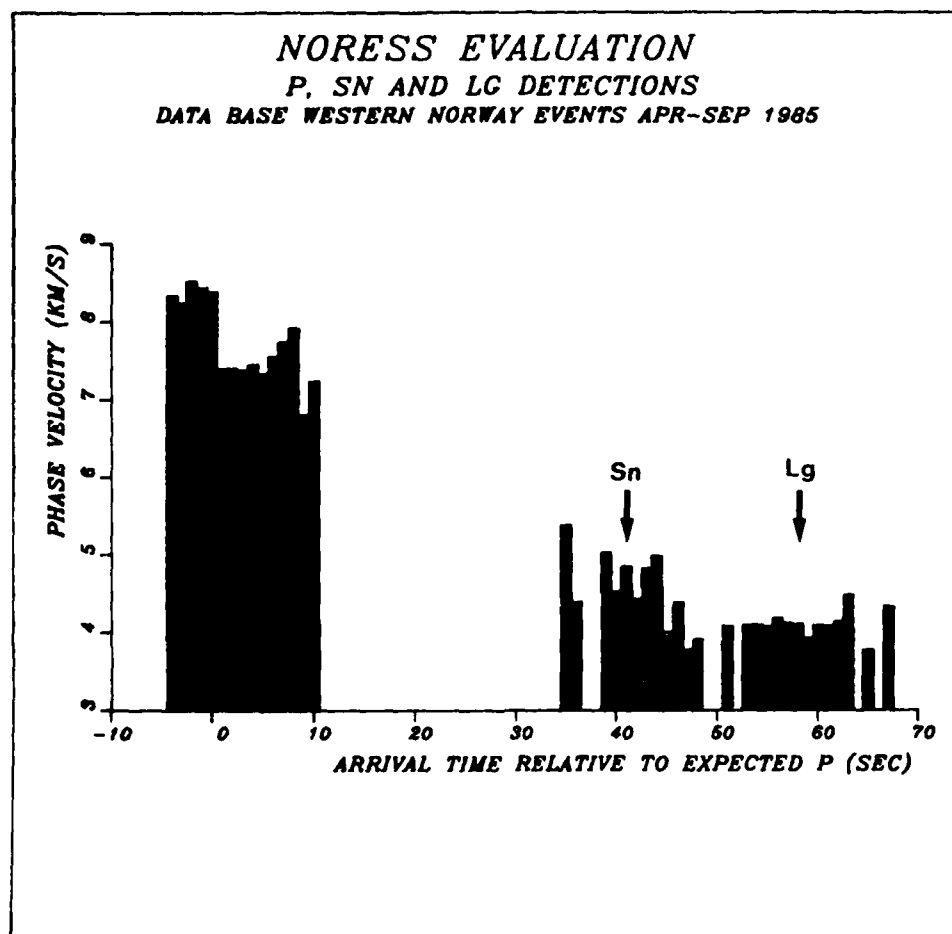
Fig. VII.3.4 Average phase velocities for the detections in
Fig. VII.3.2. All events have been "normalized" to an
epicentral distance of 400 km, with expected arrival
times for Sn and Lg as indicated by the arrows.

VII.4   NORESS noise spectral studies, preliminary report

A project has been started to investigate NORESS noise recordings on a
regular basis, and the objective is to find noise characteristics that
are relevant to detection algorithms. The first task has been to
determine how the noise varies with respect to frequency, time of day
and array geometry. To obtain this an automatic procedure to compute
hourly noise spectra for selected beams and single channels has been
implemented.

It is important to note in this regard that many model studies earlier
conducted on projected seismic monitoring capabilities have been based
on estimates of seismic noise levels that have been measured during
"quiet" conditions. Even though a standard deviation usually is asso-
ciated with these levels, it is clear that a much more reliable
assessment can be obtained if actual noise measurements over extended
time periods are available.

Procedure

The method that has been adopted for the power spectrum estimates is
described by T. Kværna and coauthors in the NORSAR Scientific Reports
nos. 2-84/85 and 1-85/86. Their method gives smoother spectrum at all
frequencies as compared to the direct FFT-spectrum, i.e., we see no
large variations in the power estimates at the various frequencies,
which is clearly demonstrated in Fig. VII.4.1. The computed beam
spectra are based on three different configurations:

Configuration 1 consists of FOZ plus A-ring, plus B-ring, named BRING;
Configuration 2 consists of FOZ plus B-ring, plus C-ring, named CRING;
Configuration 3 consists of FOZ plus C-ring, plus D-ring, named DRING.

The number of instruments are 9 (BRING), 13 (CRING), and 17 (DRING).
Beams are formed using infinite velocity, i.e., straight summing of
the traces is performed. In addition, we calculate average noise
spectrum from the individual Z-component spectra.

The power spectra are computed hourly, using 60 seconds of data, and the procedure runs automatically on the NORESS online computer, (IBM 4341) concurrently with NORESS online recording and RONAPP processing. Care has been taken to avoid any irregularities in the data, and the various checks that are performed are as follows.

A data analysis time window is first selected (starting at the hour). If NORESS has reported any detection within 2 minutes of the hour, the time is adjusted so as to avoid such signals. Various data quality indicators are also inspected, and time is adjusted as necessary to avoid possible bad data segments.

When an acceptable data time interval has been found, RMS is computed for each of the SPZ components. We mask any instrument that has an RMS which differs by more than a predetermined factor from the average RMS for the other Z-components.

Using this procedure we get a set of functions $P(f,t,i)$ where P is the power measured in squared quantum units, f is frequency (512 points), and i is channel number (beam or single sensor; currently 36 total). The variable t is time, sampled each hour, with possible slight adjustments as described above.

Results

Preliminary results from this study are presented in Figs. VII.4.2 through VII.4.7. All of these figures show _relative_ variations in noise power levels (measured in dB), and are based on data uncorrected for instrument response.

Fig. VII.4.2 is a contour plot showing average noise power as a function of time for all NORESS SPZ channels during a typical workday (Monday 7 April 1986). The most significant feature is a sharp increase

during day time in the noise power around 6 Hz frequency, and, to a lesser extent, around 12 Hz. These spectral peaks are clearly tied to a localized noise source in the vicinity of the NORESS array (a sawmill located 15 km away), and is repeatedly observed in the data analyzed so far.

Fig. VII.4.3 presented results for the same day as covered by Fig. VII.4.2 as time-domain plots based on a subset of frequencies. We see again that the noise level for frequencies below 2.0 Hz have no significant variations versus the time of day, whereas all higher frequencies are strongly affected by cultural noise. For the 6.0 Hz band we see a 15 dB increase in noise level. However, at the highest frequency shown (16 Hz), the diurnal variations are again relatively modest.

Fig. VII.4.4 and VII.4.5 are similar to Fig. VII.4.3, but cover 1 week of data, respectively.

These figures show clearly the differences in diurnal variations on workdays and holidays, thus confirming that the main source of such variation at frequencies above 2 Hz is cultural activity. An interesting observation is that the noise level at 4 Hz appears to be lower during holidays than at nighttime on workdays, but the significance of this is currently unclear.

These two figures also show that the noise level variation in the 1 Hz band is independent of time of day, but still shows significant fluctuations on more long-term basis. The explanation is that low frequency microseisms generated by, e.g., storm activity in the North Sea have a significant influence at this frequency, but not at frequencies exceeding 2 Hz.

Fig. VII.4.6 shows a comparison between borehole and surface noise power at the NORESS central site. The borehole instrument clearly shows a consistent noise reduction, especially at higher frequencies. However, preliminary investigations have also shown that the P signal level is suppressed in the borehole recordings; thus the actual SNR gain may be quite modest.

Fig. VII.4.7 illustrates the beamforming noise suppression at NORESS using different subgeometries. The data shown correspond to average SPZ noise (MEANZ) and the three geometries BRING, CRING and DRING. The upper figure contains averages within the 3.9 - 4.4 Hz band. In the lower figure there are two parts: The upper part of the figure covering the 0.9 - 1.1 Hz band and the lower part 11.9 - 12.1 Hz. Observations are as follows:

At 1 Hz frequency, the noise is correlated for the innermost part of the array, and only the DRING geometry shows significant noise suppression (about 10 dB).

At 4 Hz, all three geometries show significant noise suppression; in particular the C-ring is effective, averaging almost 15 dB suppresion ($\sqrt{N}$ corresponds to 11 dB). This better than $\sqrt{N}$ suppression is a feature which has been earlier observed, and is tied to extracting "optimum" subgeometries for given frequencies, thus taking advantage of "destructive" noise correlation.

At 12 Hz, the noise is uncorrelated, and the three geometries give each approximately $\sqrt{N}$ noise suppression.

In summary, these preliminary investigations have already provided important insight into the noise characteristics observed at NORESS. While many of the features (e.g., the strong 6 Hz peak) are clearly

tied to the actual local conditions particular to the NORESS site, other characteristics (such as the better than $\sqrt{N}$ beam noise reduction in some cases) could well have more general application. We plan in future studies to compile more comprehensive statistics in order to fully evaluate the noise characteristics at NORESS, and will in particular study the correlation between noise level and local wind conditions. We will also incorporate noise spectra from the NORESS High Frequency Seismic Element in order to expand the studies to include higher frequencies.

J. Fyen

D9Z 113-07.42.21
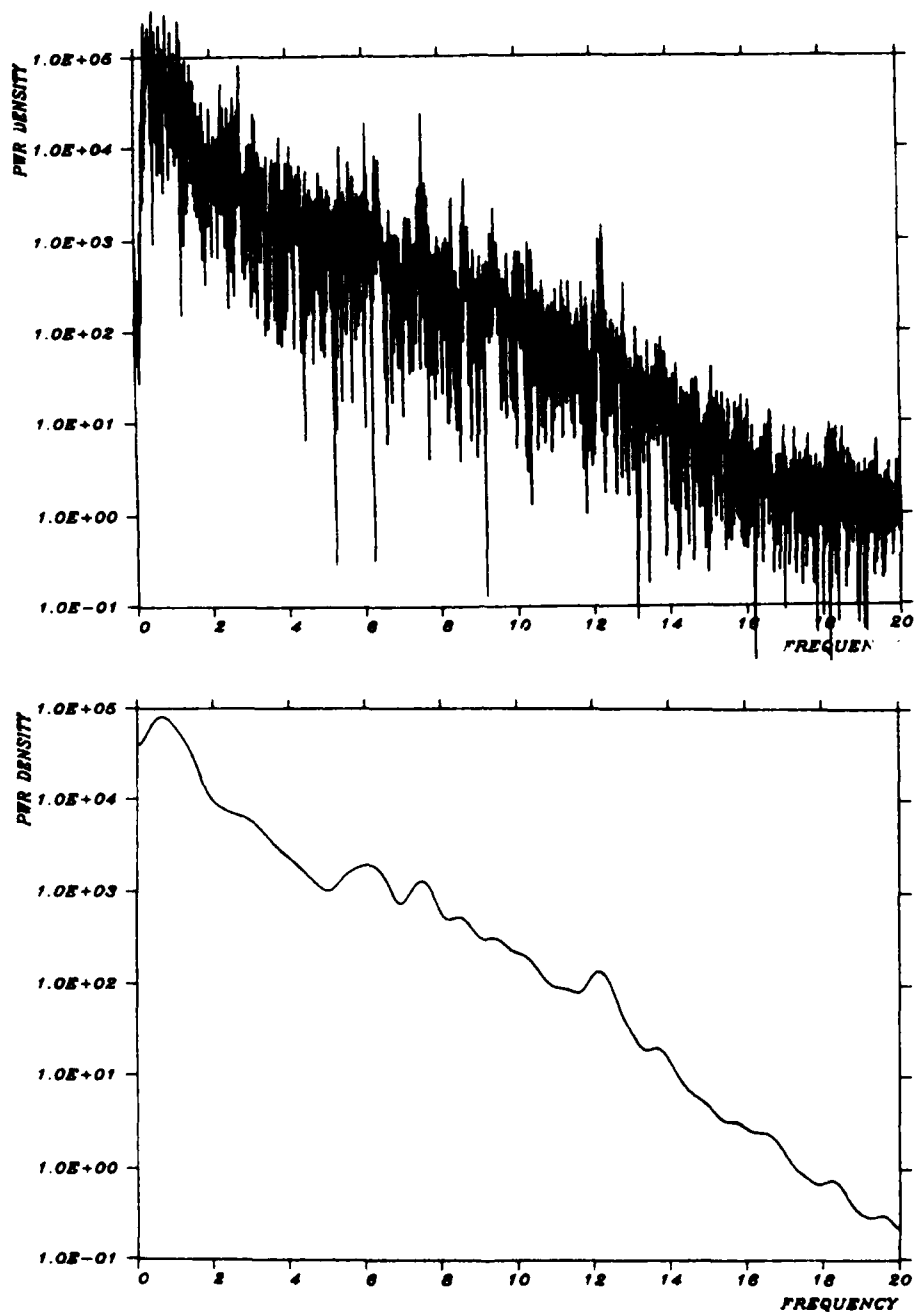
Fig. VII.4.1   The upper figure shows power spectrum for D9Z, using
               60 sec of data and direct FFT. The lower spectrum is
               obtained by a prewhitening of the data, windowing the
               autocorrelation and then transforming this function. The
               resulting spectrum is then compensated for the pre-
               whitening and is shown to be very smooth.

MEANZ 97- 0 - 98- 0
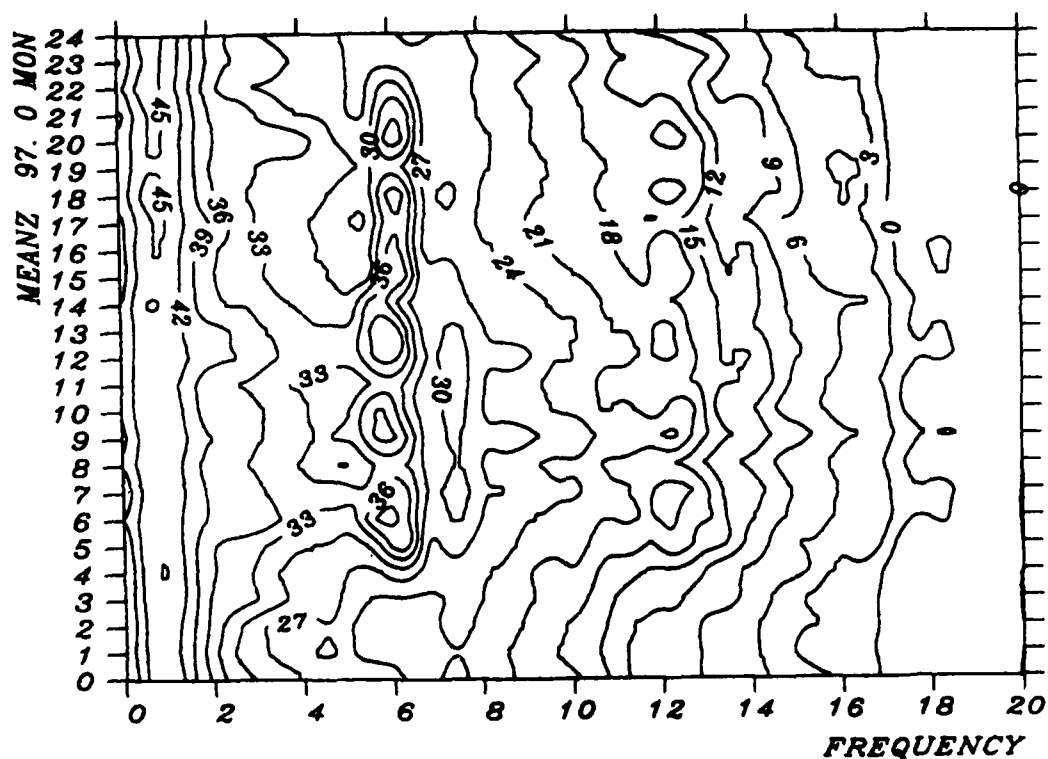
Fig. VII.4.2 This figure shows average power for all NORESS SPZ chan-
nels plotted versus time (00-24) and frequency. There
are 25 points (hours) in time axis, and 512 points in
frequency. We can see a clear peak in the power distri-
bution starting at time 0400 GMT and frequency 6.0 Hz.
This peak is due to activities in a saw-mill located
approximately 15 km from the array. It is seen that the
noise power increases during day time, to a lesser
extent, also at other frequencies, except in the lowest
frequency band (below 2 Hz).

MEANZ SPC860970000000
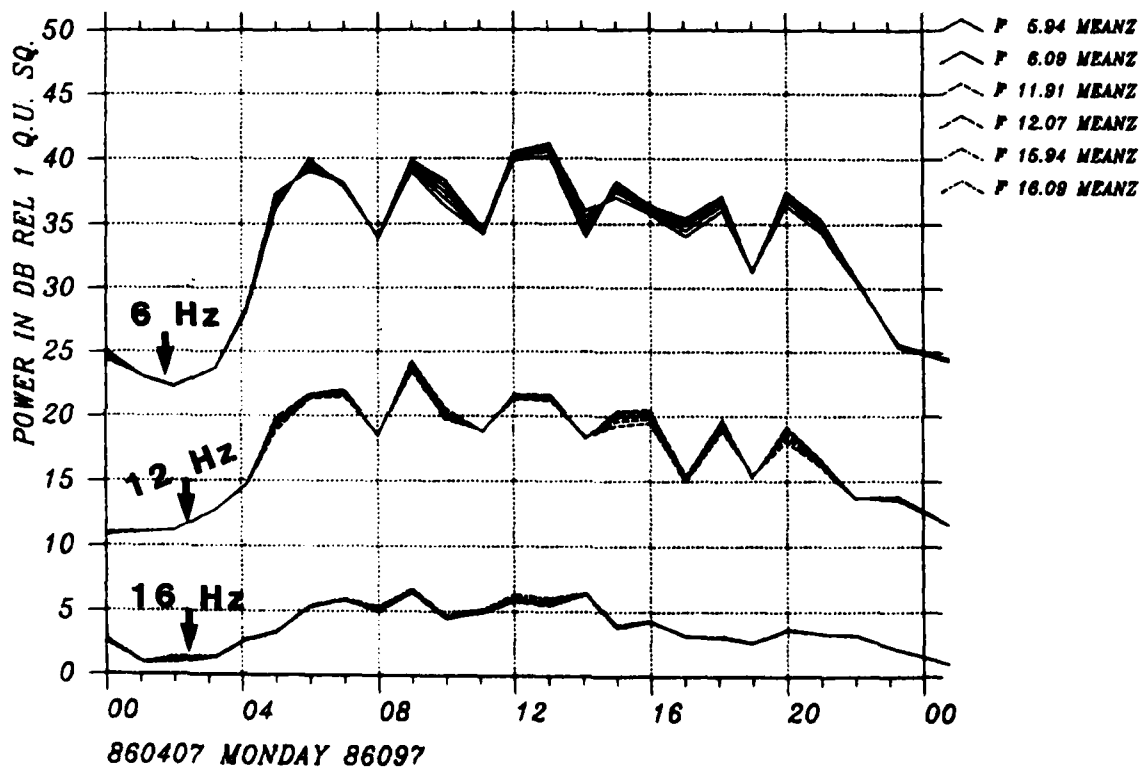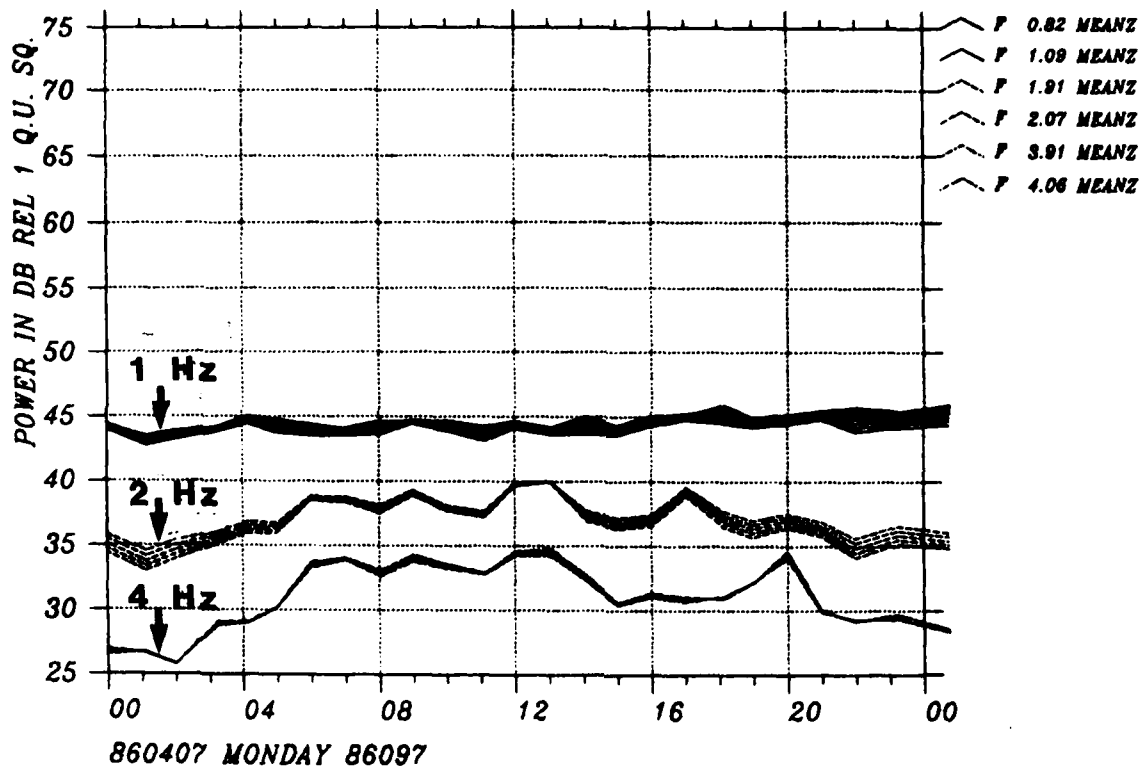
Fig. VII.4.3 Average NORESS SPZ spectral levels as a function of time of
day for a typical workday (Monday, 7 April 1986). The plot
shows a sequence of narrow bands (±0.1 Hz) around the indi-
cated frequencies. Note the relative stability of the
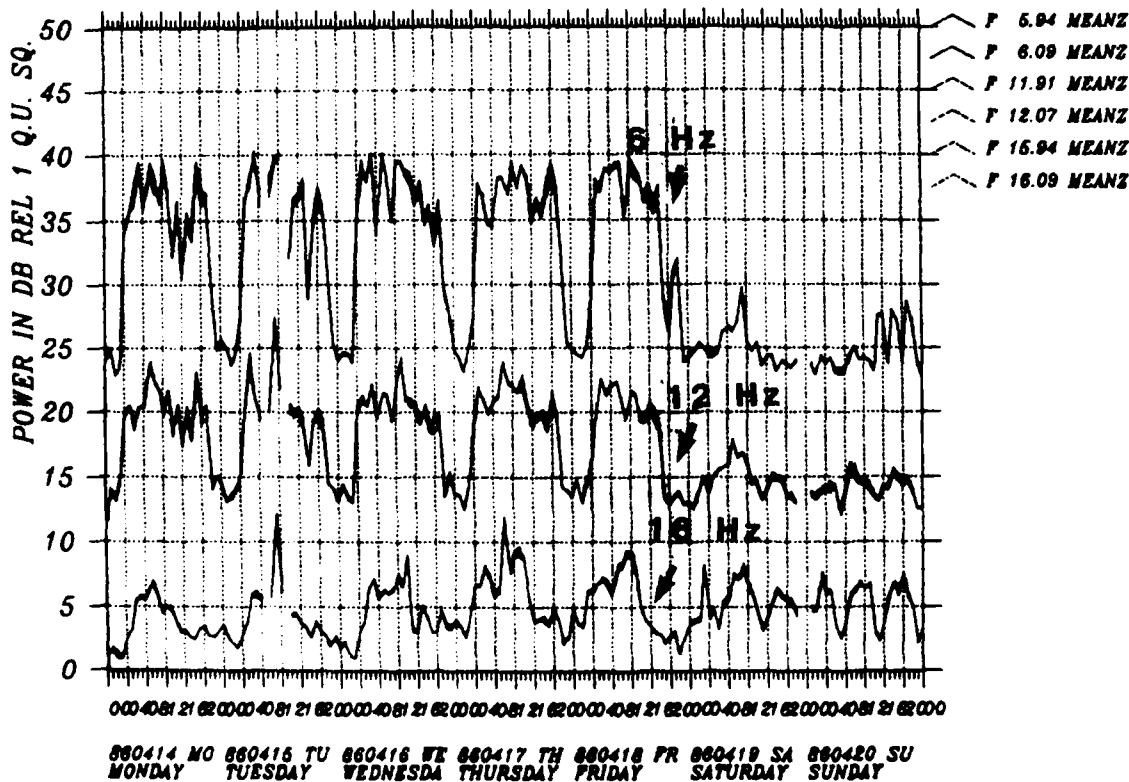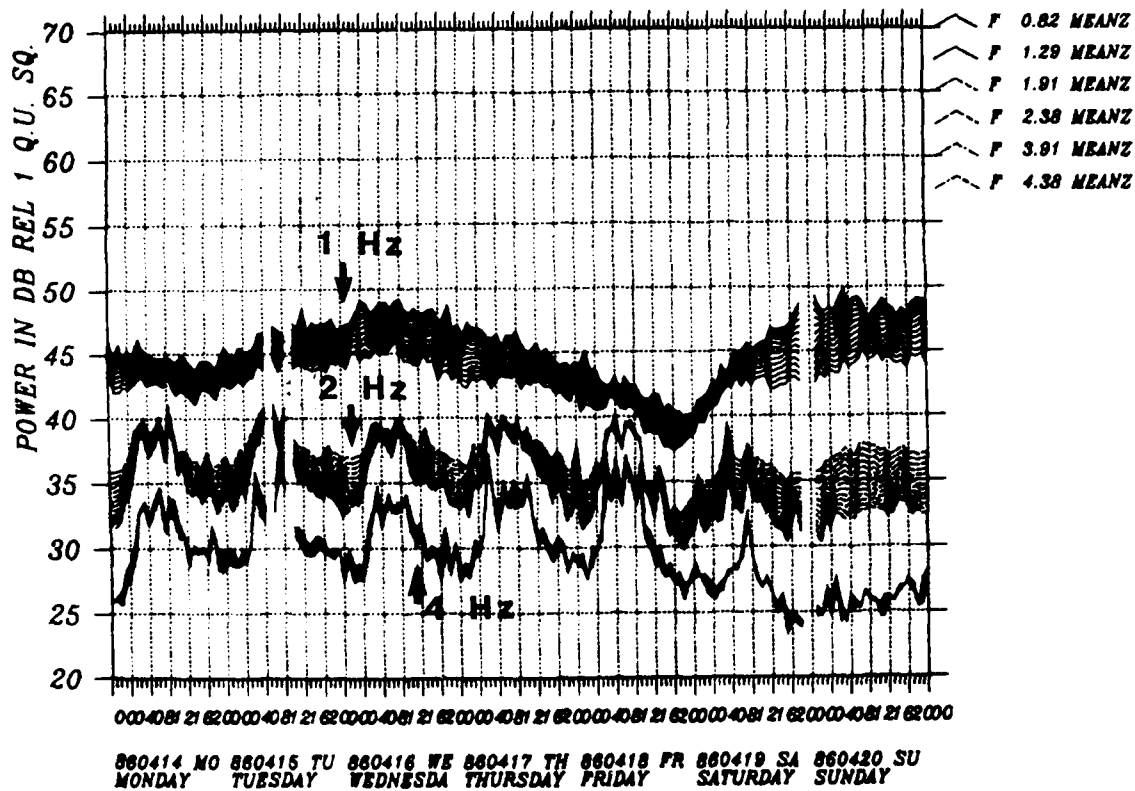spectral levels except at 6 and 12 Hz, as explained in the
text.

MEANZ SPC861040009030

Fig. VII.4.4   Average NORESS SPZ spectral levels for the week Monday
14 April through Sunday 20 April 1986 (cf. Fig. VII.4.3).
Note the lack of diurnal variations during the weekend.
Also note the slow variations in the band around 1 Hz.
This is due to low frequency microseisms, and is not seen
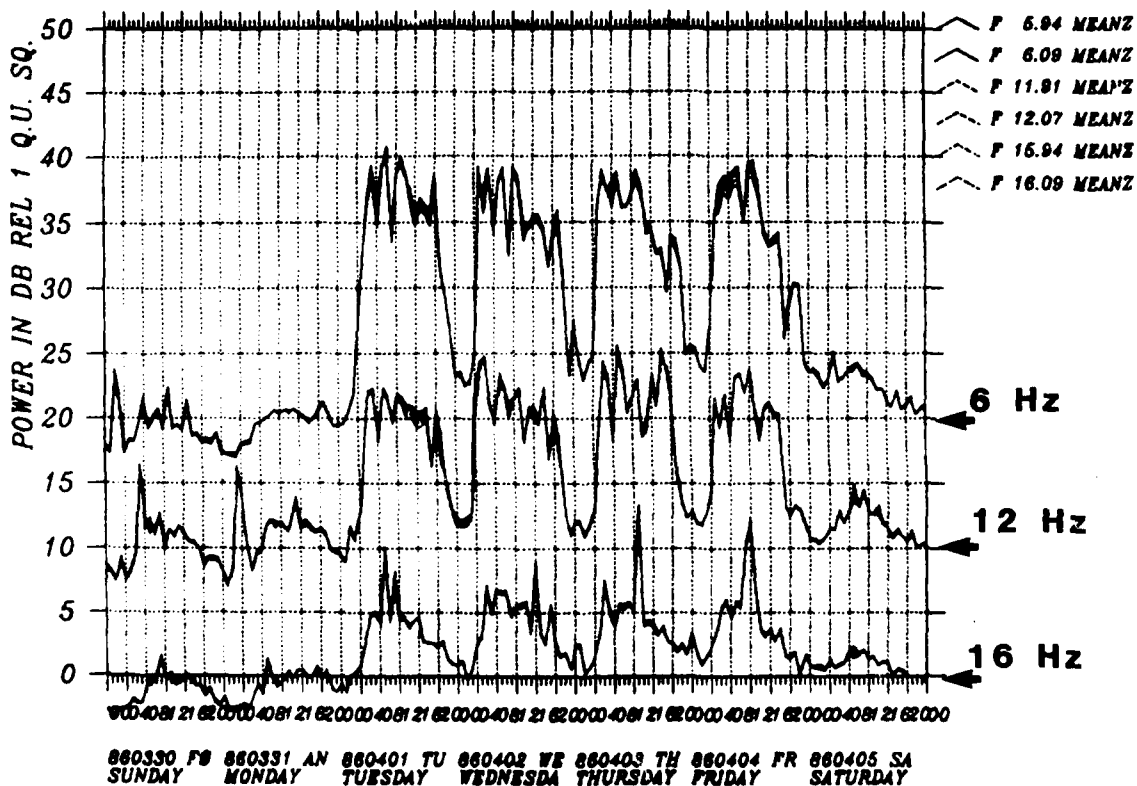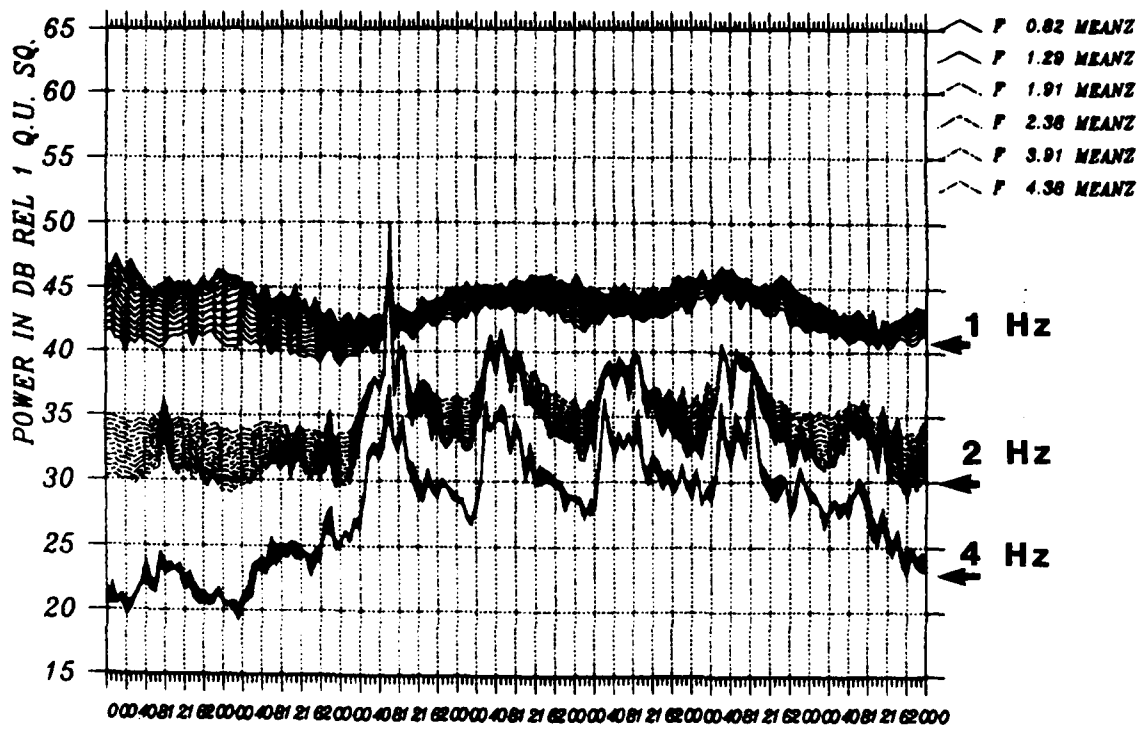at higher frequencies.

MEANZ SPC860890000000

Fig. VII.4.5   Same as Fig. VII.4.4, but for the week starting Sunday,
Easter day. Note that Sunday, Monday and Saturday of
this week are holidays. See the comments for Fig.
VII.4.4.

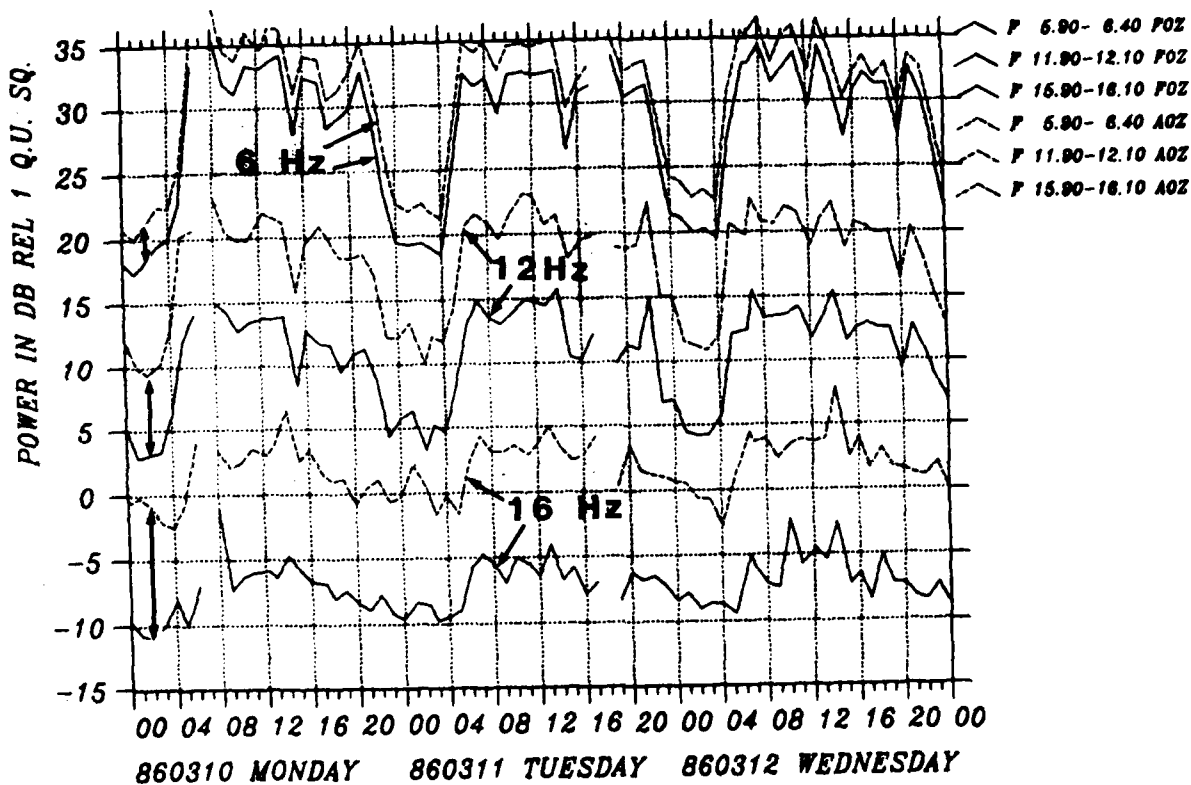FOZ   AOZ   SPC860690003220   5.90-16.10

Fig. VII.4.6   Three-day comparison of surface noise level (AOZ,
              stippled lines) and borehole noise level (FOZ, solid
              lines) at three frequencies. Note the larger borehole
              noise suppression at higher frequencies.
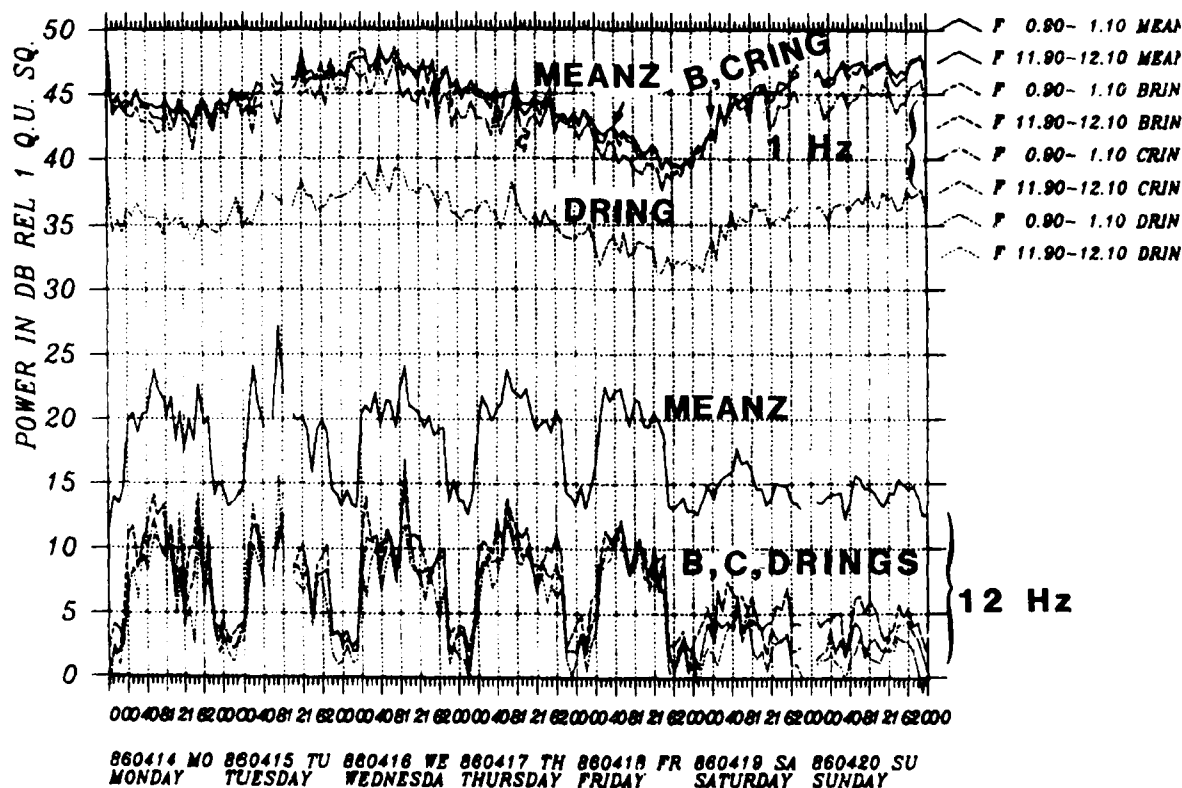
MEANZ BRING CRING DRING SPC861040009030

Fig. VII.4.7 Comparison of average SPZ noise with beam noise for
three beam configurations (see text). Note that at 1 Hz
only the D-ring provides significant noise suppression.
At 4 Hz, the C and D rings are most effective. At 12 Hz,
the three beams are similar.

VII.5   An integrated approach to slowness analysis with arrays and three-component stations

In the past an online array detection, location and phase association procedure termed RONAPP has been developed, and it has been in routine use to analyze regional data from the NORESS array. More than one year of experience with this algorithm has shown that in some cases the azimuth estimate for P and secondary phases from the same event may differ by more than 30 degrees and therefore are not correctly associated. Fig. VII.5.1 shows a typical data set of P-Lg azimuth differences from 23 events recorded within an arbitrary three-day interval. The RONAPP results (along the vertical axis) show a considerable spread with a median value of 6.3 degrees. Whereas part of these azimuth differences may be an effect of earth structure, it should also be noted that the methods in routine use do not fully exploit the redundancy in the data. We have therefore begun a program to extend standard frequency-wavenumber analysis by incorporating a priori information applicable to three-component and possibly wide-band data. We consider the matched filter as an extension of standard frequency-wavenumber analysis, and the maximum likelihood filter as an extension of "high-resolution" analysis.

As in other work, slowness solutions are inferred from a covariance matrix $\underline{C}$. Here we introduce $\underline{C}$ as a function of slowness $\underline{s}$ by phase shifting the signals. $\underline{C}(\underline{s})$ has the components

$$C_{nm}(\underline{s}) = \int F_n(\omega,\underline{s}) \, F_m^*(\omega,\underline{s}) \, d\omega/2\pi \qquad (1)$$

where

$$F_n(\omega,\underline{s}) = F_n(\omega) \, \exp(i\omega\underline{s}\cdot\underline{x}_n)$$

and $F_n(\omega)$ is the Fourier spectrum at channel n.

Beamforming or matched filtering can be expressed by the normalized response

$$P(\underline{s}) = \underline{g}^+\underline{\underline{C}}\underline{g}/\{|\underline{g}|^2 \text{ tr } \underline{\underline{C}}\} \qquad (2)$$

The normalized response by the maxim likelihood method (M.L.M.) is

$$P'(\underline{s}) = \{\underline{g}^+\underline{\underline{C}}^{-1}\underline{g}\}^{-1} \cdot |\underline{g}|^2/\text{tr } \underline{\underline{C}} \qquad (3)$$

The vector $\underline{g}$ in equations (2) and (3) can take on different forms:

(a)   1-component array : $\underline{g}^T = (1, \ldots\ldots, 1)$

(b)   3-component sensor: $\underline{g}^T = (q_x, q_y, q_z) = $ displacement vector

(c)   3-component array : $g_n = q_j$, $j = x, y$ or z.

In (a) and (c), the $\underline{\underline{C}}$ matrix is a function of slowness $\underline{s}$. In (b) and (c), the $\underline{g}$ vector is a function of slowness $\underline{s}$. In the latter case the surface interaction must be taken into account. As a consequence, 3-component results for the P phase depend on the S-velocity in an isotropic model, and results for SV depend on both the P and S velocity. Equations (2) and (3) are similar to the results of Esmersoy et al (1986), and they represent a generalization of earlier results.

Because equations (2) and (3) accomodate both array and 3-component data, they form a suitable basis for evaluating the relative perfor-mance of different methods. For the P phase we have compared wide-band to single frequency processing, array to 3-component processing, and beamforming or matched filtering to the high resolution or maximum likelihood method. NORESS records from five events at the same loca-tion in the Leningrad region provide a suitable data base for this

purpose. A typical example of 3-component records from one of these events is shown in Fig. VII.5.2. Results are summarized in Figs. VII.5.3, VII.5.4 and VII.5.5. An additional result, obtained with a different data set, is given in Fig. VII.5.1.

One inference to be drawn from Fig. VII.5.1 is that, when applying beamforming or some other phase adjusting operation, more stable results are obtained by employing a wider frequency band, provided the signal-to-noise ratio is adequate over the band and the phase shifts are introduced consistently (i.e., frequency dependent). Based on the results of Figs. VII.5.3, VII.5.4 and VII.5.5, a summary concerning the relative performance of a 1-component array and a 3-component sensor is given in Table VII.5.1. It should be noted here that, whereas M.L.M. gives an apparently higher resolution for all configurations considered, for location purposes the stability of the solution is more important. Fig. VII.5.5 demonstrates that the best results for P are obtained by conventional (wide-band) beamforming of a vertical component array. Fig. VII.5.5 also shows that not only are the 3-component solutions less stable, they are also site dependent.

Our conclusions at this moment are based only on P data. Equations (2) and (3) are equally applicable to S, Lg and other phase types, but the signal model is more complicated. Fig. VII.5.6 shows preliminary results when applying S models to a section with Lg records of a four-element array of 3-component stations. The results are consistent with the NORESS solution. However, several aspects require further investigation.

T. Kværna
D.J. Doornbos

Reference

Esmersoy, C., V.F. Cormier and M.N. Toksöz (1986): Three component array processing. In: The VELA Program, Ed. A.U. Kerr, DARPA.

1-comp. array	3-comp. sensor

Principle:

1-comp. array	3-comp. sensor
Employs phase differences	Employs amplitude ratios
Resolution increases with frequency	Resolution frequency independent
Solution averaged over array plane	Solution for one site
Solution model independent	Solution model dependent

Practice:

1-comp. array	3-comp. sensor
Good coherence on same component	Less coherence between different components
Solutions consistent	Solutions less consistent
M.L.M. less efficient	M.L.M. more efficient

Table VII.5.1

3 days with 23 events
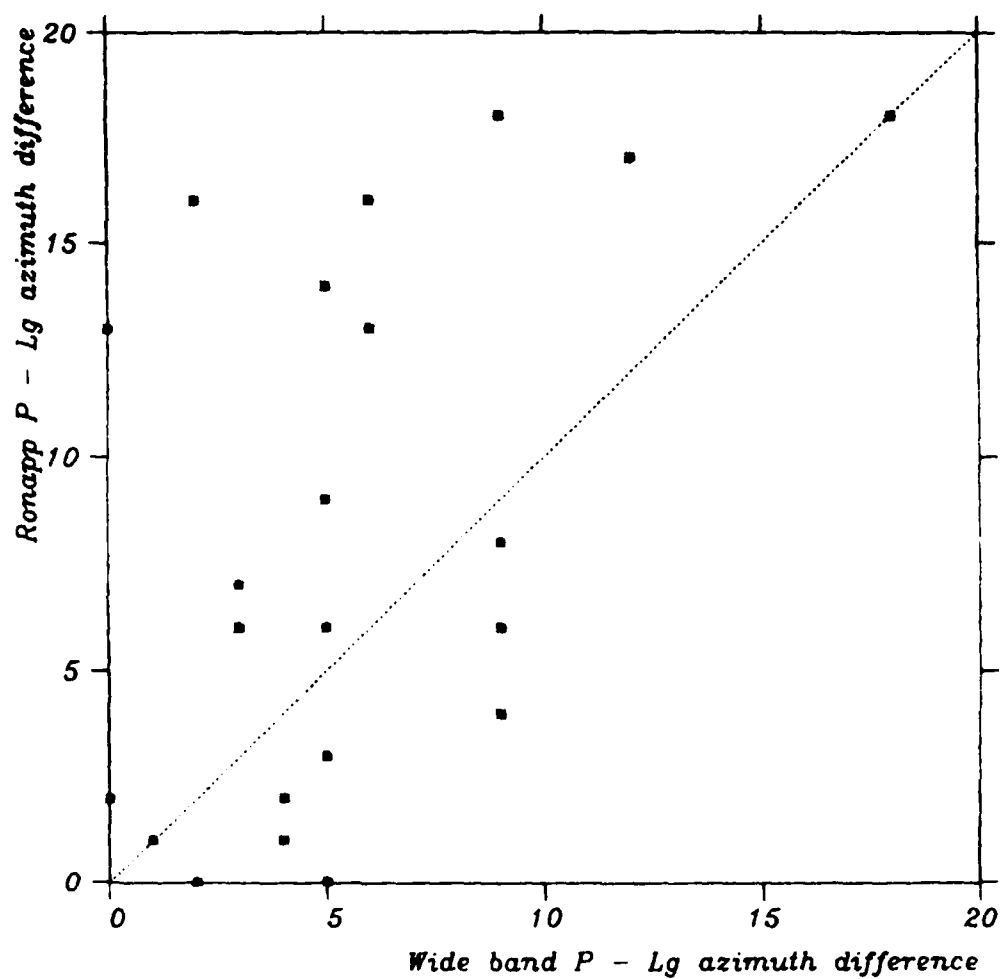
Median (Wide Band) – 4.3

Median (Ronapp) – 6.3

Fig. VII.5.1 P-Lg azimuth difference measured by two different
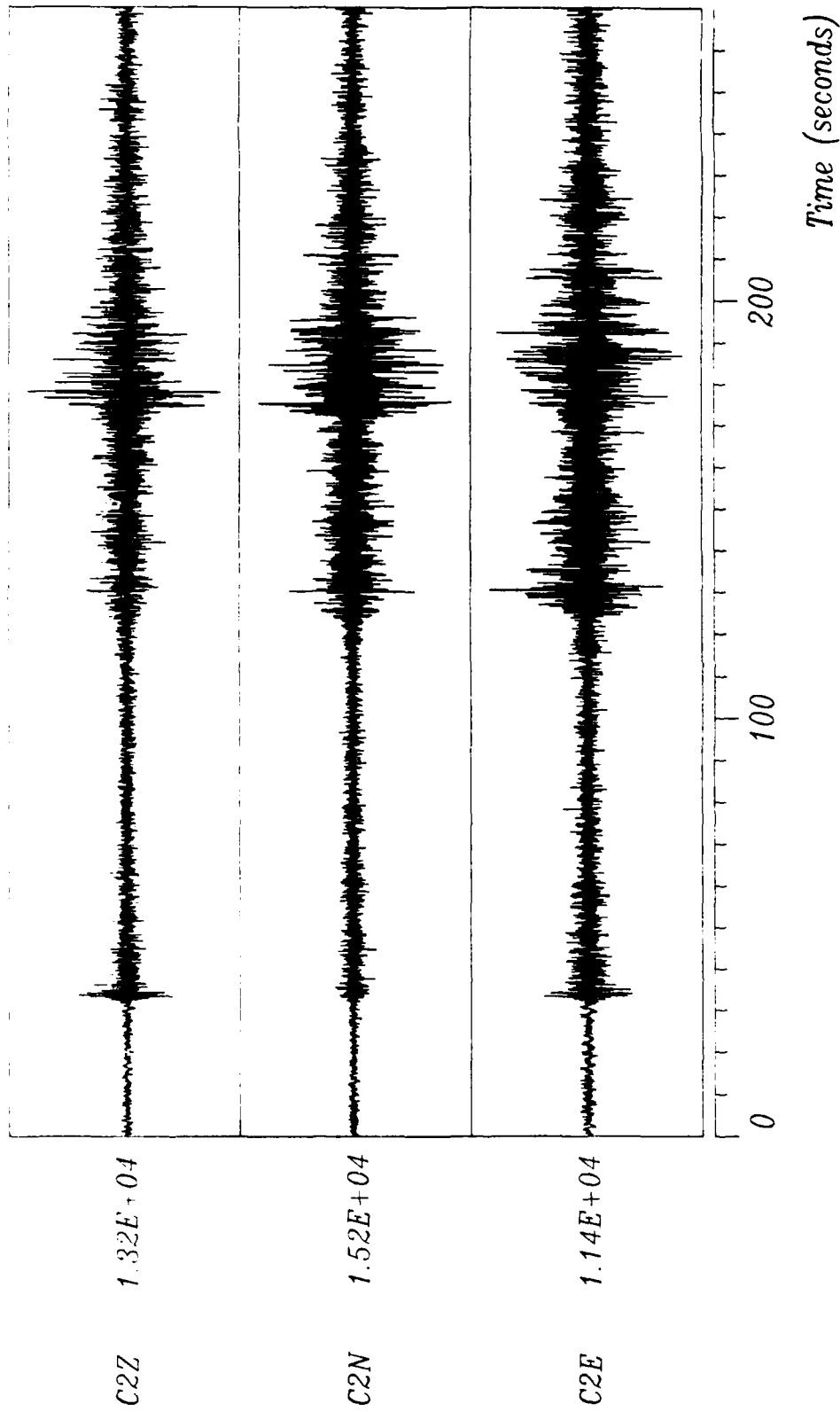methods: The wide-band method versus the RONAPP
procedure.

PST 85065 12.24.10.00

C2Z   1.32E+04

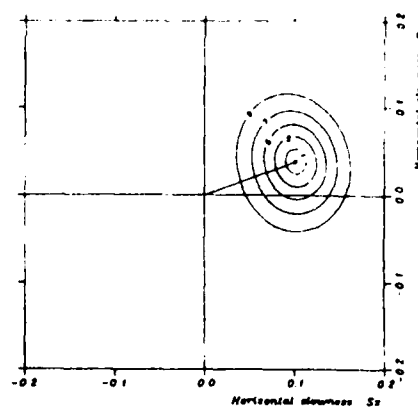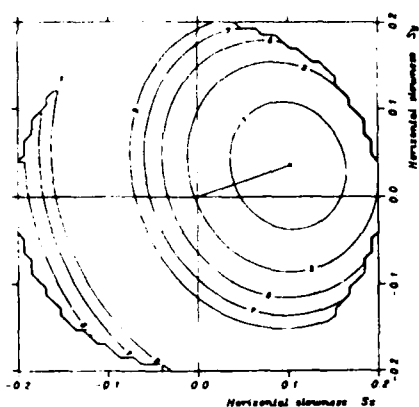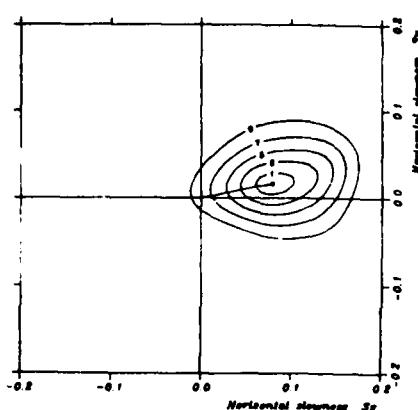C2N   1.52E+04
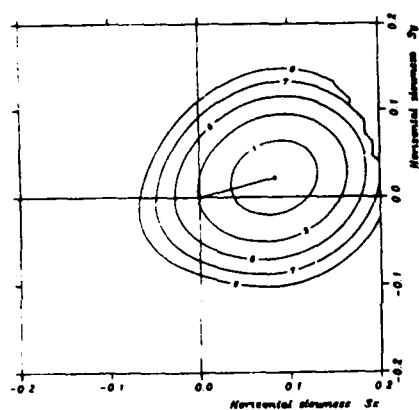
C2E   1.14E+04

Time (seconds)

Fig. VII.5.2 Typical three-component records from event in Leningrad region. Scaling factors of different components are shown to the left.
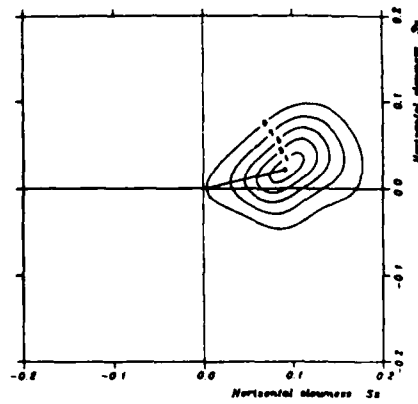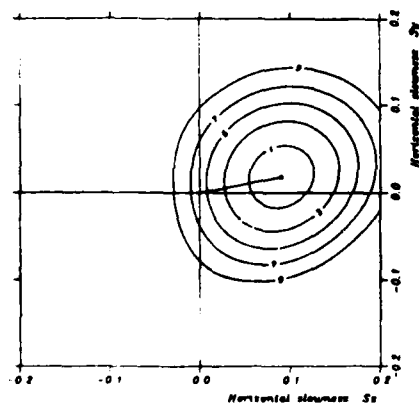
CONVENTIONAL   MLM

One 3-comp. station

Array of four 3-comp. stations

Array of 25 vertical instruments

Fig. VII.5.3 Slowness response of P phase from Leningrad event pro-
              cessed by conventional wide-band method, and by maximum
              likelihood method (MLM). Results for one 3-component
              station, for an array of four 3-component stations, and
              for an array of 25 vertical component stations (the
              NORESS array). Slowness in s/km.
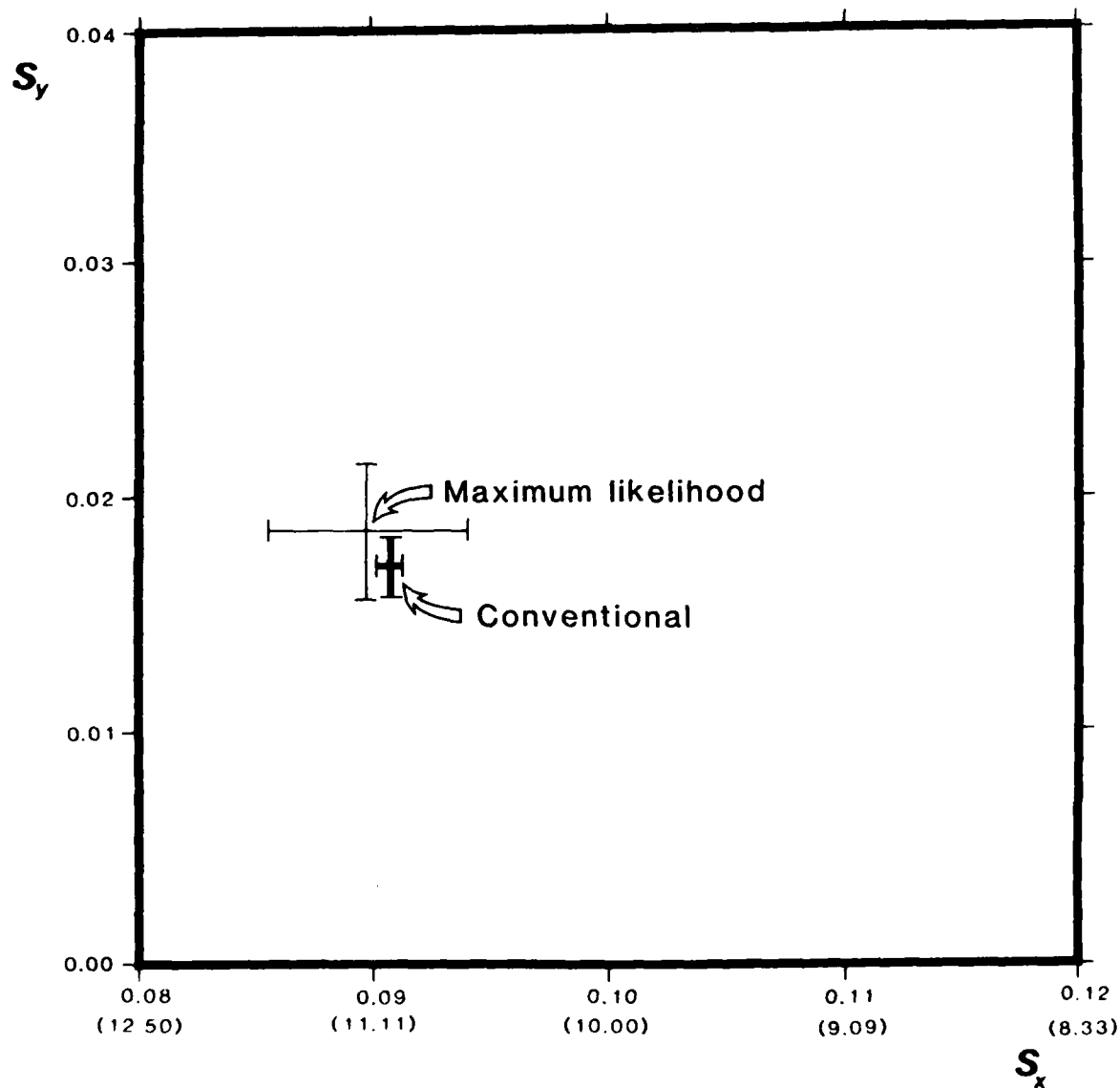
Array of 25 vertical instruments

Fig. VII.5.4 Slowness results for P phase from 5 events in the same
location (Leningrad region). Bars denote standard
deviations. Solutions by conventional wide-band method
and by maximum likelihood method.
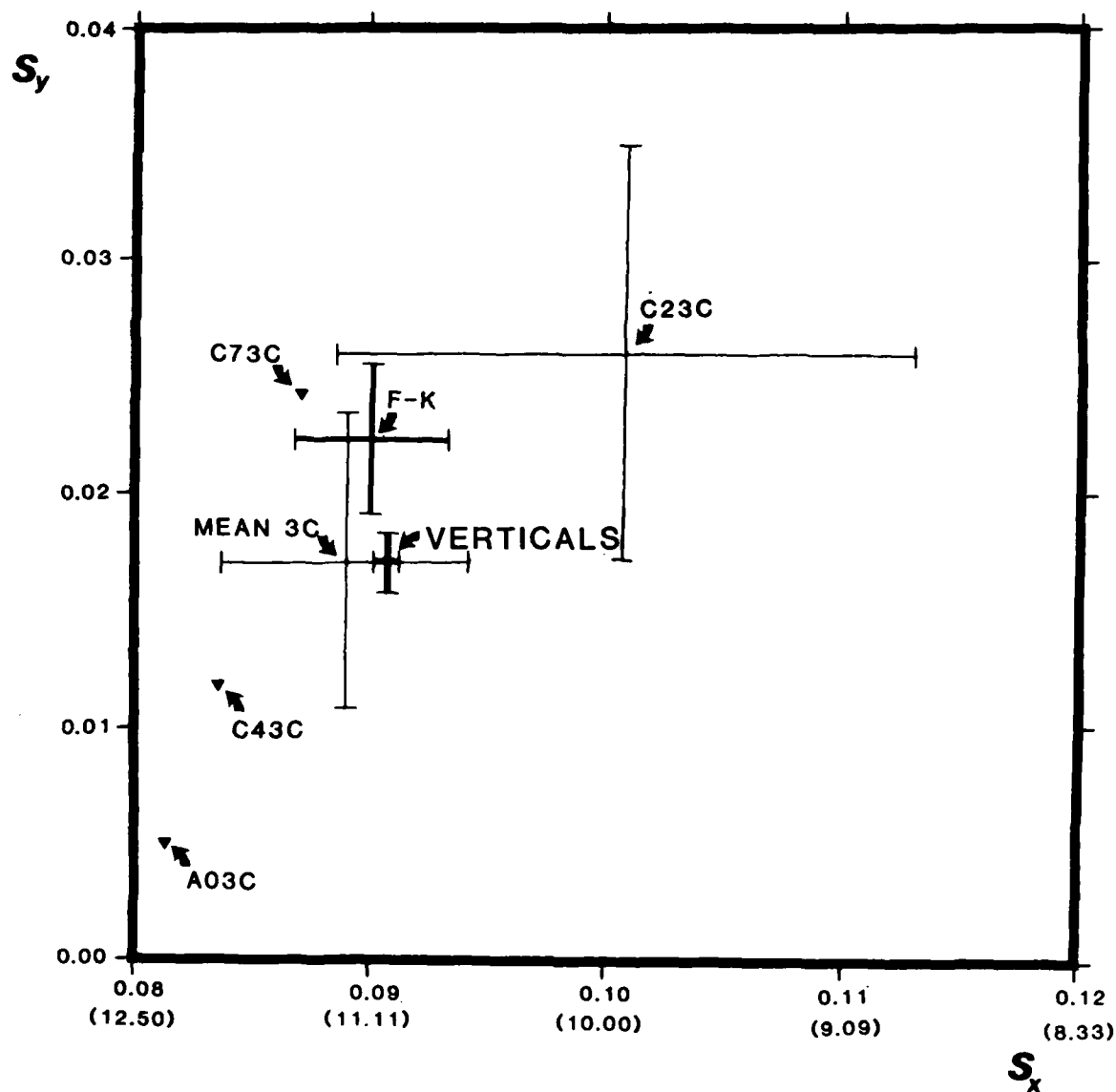
Fig. VII.5.5 Slowness results for P phase from 5 events in the same
location (Leningrad region). Bars denote standard
deviations. VERTICALS: wide-band solution with vertical
component NORESS array. F-K: RONAPP solution with same
array. A03C, C23C, C43C, C73C: 3-component solution for
individual sites: st. dev. is given only for C23C, but
results for the other sites are comparable. MEAN3C: mean
of 3-component solutions for the 4 individual sites.

Array of four 3-component stations
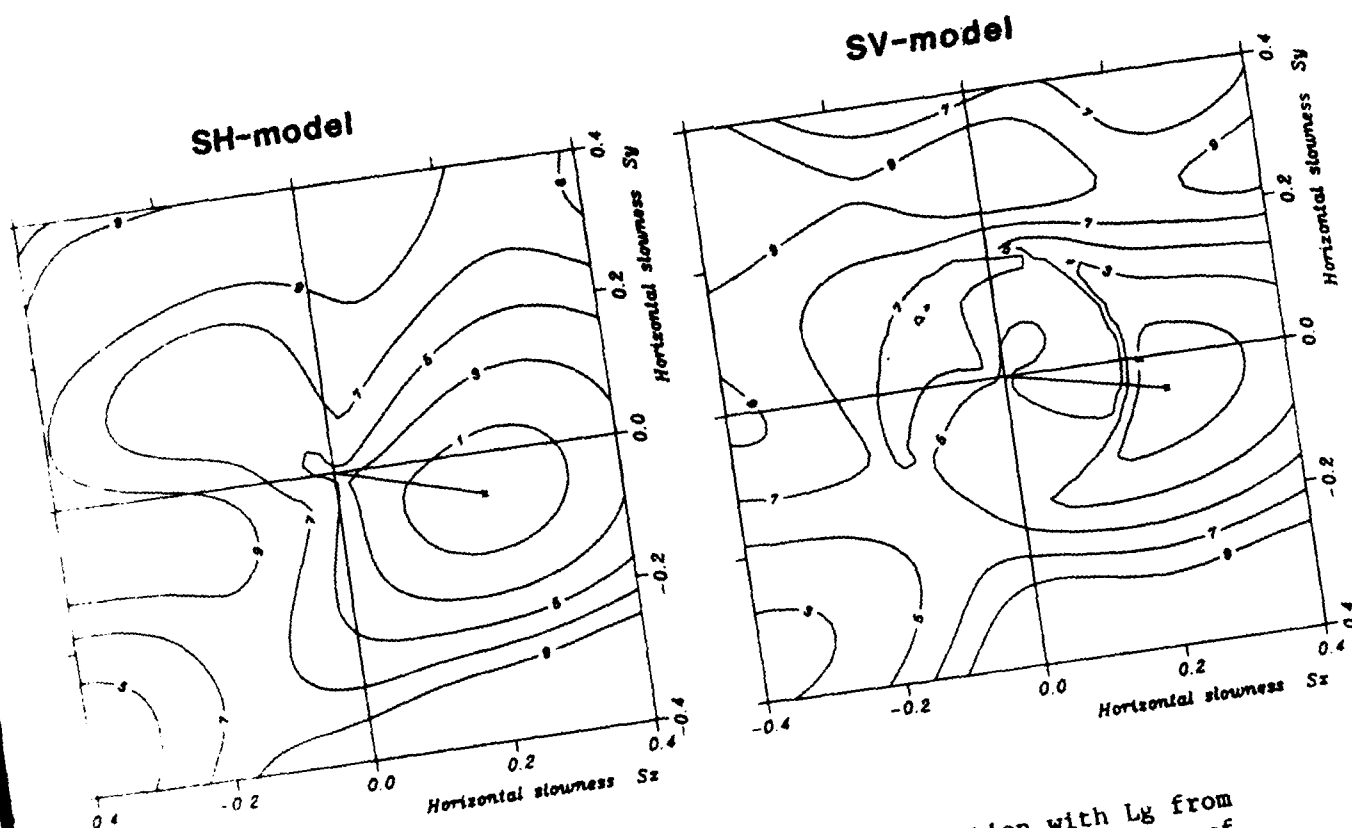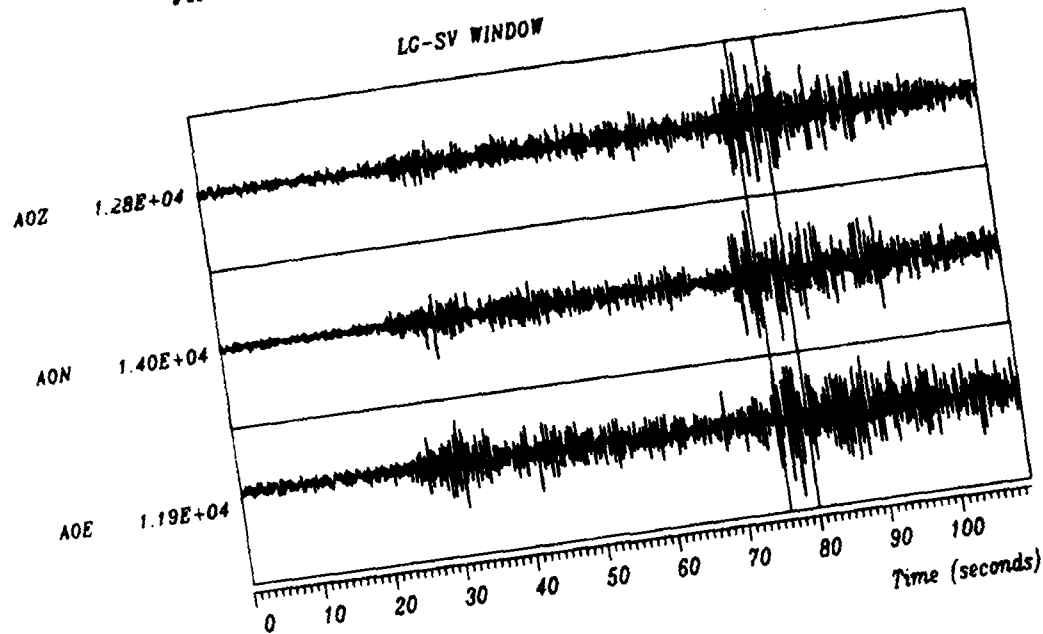
LG-SV WINDOW

SH-model   SV-model

Fig. VII.5.6 Slowness response for given time section with Lg from Leningrad event. Wide-band method applied to array of four 3-component stations. Separate solutions for SH and SV type motion.

VII.6 Wavefield decomposition using ML-probabilities in modelling single-site 3-component records

This topic was dealt with in the previous NORSAR Semiannual Technical Summary, and a comprehensive write-up of the theoretical framework for this approach has now been completed (e.g., see Christoffersson et al, 1986). In this section, we will discuss some principal features of this novel analyzing technique, particularly those of importance for practical applications which will be demonstrated in subsequent sections.

Time vis-à-vis frequency domain analysis

So far our preference has been for time domain analysis, as good time resolution is achievable (window length 1-2 cycles), while the relative bandwidth is sufficiently broad to dampen the adverse effects of unstable narrow-band spectral estimates, particularly when short time windows are used. We have in fact not explored frequency domain analysis, although a practical advantage here is that the observational degrees of freedom would be 6 + 6 (amplitude and phase), while in the time domain we have only 6 (amplitude). Olson and Samson (1979) have demonstrated potential advantages of frequency domain operation for event detection.

Particle motion modelling

With only 6 observational degrees of freedom available (symmetric covariance matrix), particle motion modelling for P, SV, SH, L (Love) and R (Rayleigh) must be simple, and in this respect we follow standard approaches. The crucial question is naturally whether these models are adequate in practice, particularly in view of the well-documented wave propagation complexities for crustal phases (e.g., see Kennett, 1983). On the basis of extensive 3-component analysis of real data (NORESS records), the following comments apply.

P-waves: Few problems are encountered here. P-wavelets are easily
identified as such, and very good slowness estimates are obtainable.
Azimuth estimates are within ± 5 deg of true ones (for LP data often
within ± 2 deg), and apparent velocity within ± 2 km s^{-1}. For small
events, say for SNRs less than 2, larger estimation errors may ensue,
although a suite of slownesses for several wavelets often provide good
average estimates.

Shear waves: These waves are very important for locating events
because P-S differential travel times provide reliable estimates of
epicentral distances for broadband recordings and short period recor-
dings at regional distances. However, S-waves are far more complex
than P because mode conversions, reflections beyond critical angles,
etc., produce non-linear particle motions. This is not incorporated in
the model, so χ^2-tests on S-wave presence often fail. Two strategies
here are under consideration: i) more complex models entailing use of
arrays of three-component stations and ii) simplifying the model from
3 to 2 dimensions, as triggering failures mainly reflect correlations
between radial and transverse components. Regarding the first we have
only experimented with simple stacking of the four 3-component sta-
tions with NORESS; besides improved SNR, this does not solve the
"problem". In the second case, reliable S-wave identification occurs,
but the penalty is loss of azimuth resolution. For calculating dif-
ferential travel times (and epicentral distances), this is not a
severe drawback.

R- and L-waves: We have relatively little experience in analysis
(mostly of the Sg/Lg-wavetrain) and the problems encountered for S-
waves appear to prevail here as well -- 2-D modelling is under
consideration.

False alarms -- noise directionality

It is well known from array operations that the false alarm rate
(noise wavelet triggering) to some extent reflects the structure of
the noise field. Such phenomena are well known for NORSAR, that is,
the false alarm rate increases for relatively monochromatic noise, as
is the case during periods of strong coastal surfs (e.g., see Steinert
et al, 1975). Such phenomena are seen in the NORESS detection log, but
for this array such problems are more interesting. For example, Ingate
et al (1985) found that the noise correlation (as a function of sensor
separation) is somewhat different for horizontal and vertical travel-
ling waves, which was attributed to the so-called "whispering" mantle
effect or P-wave reverberations in the mantle. Also, the large dynamic
range (120 dB) in the NORESS recording system implies that local
operations like hevy machinery, hydroelectric power stations, etc.,
may temporarily constitute localized noise sources. An example here is
given in Fig. VII.6.1, where semblance analysis implies a sort of beat
phenomenon at 100 deg azimuth and velocity 2.8 km s^{-1}. We associated
this with the Braskereid power station in the river Glomma and coin-
ciding with the spring flooding. In 3-component analysis we see parts
of the Rayleigh waves as vertical travelling P-waves, apparently
because the horizontal part of R is lost in the noise. The Hunder-
fossen power station ($\Delta \sim 67$ km, Az = 330 deg) also seems to act as a
noise source; in the 3-component analysis we see it is as Pg-
travelling waves in the azimuth section 300-360 deg. The Hunderfossen
"noise source" has also been seen in NORSAR analysis (e.g., see
Nikolaev and Troitskiy, 1986).

Structural complexities beneath NORESS

The essence of wavefield decomposition analysis is simply to identify
wavelets of a specific type, and then provide estimates of the asso-
ciated slowness vector. Apparent velocity applies only to P- and
SV-waves. There is naturally an important problem in separating random

and deterministic scattering sources, but a puzzling feature at NORESS
is that transverse (SH) motion occasionally is seen in the middle of
the teleseismic P-wavetrains as illustrated in Fig. VII.6.2, but never
at all four 3-component stations at the same time. This implies the
existence of an anomalous body just beneath NORESS at a depth of
around 15-20 km on the basis of P-S move-out times.

The traditional way of locating heterogeneous bodies beneath an array
or network is that of inverting P travel time anomalies (e.g., see Aki
et al, 1977, and Section VII.8). We are conducting this kind of
experiments for NORESS, and preliminary results on the basis of travel
time residuals for P waves are shown in Fig. VII.6.3. A 3-layered
reference model was used; layer thicknesses of 1, 1.5 and 2.5 km,
respectively, layer velocities were 5.8, 6.0 and 6.2 km s^{-1}, respec-
tively, while the corresponding block sizes were 0.8, 1.0 and 1.2 km,
respectively. The obtained velocity anomalies have a minimum range of
± 1.0 km s^{-1}, which in turn explained 60% of the variance in the
observations. In this kind of experiment resolutin decreases rapidly
when layer depth greatly exceeds that of array aperture.

The next steps in our efforts to map heterogeneities beneath NORESS is
that of amplitude inversion, and also to synthesize amplitude anoma-
lies on the basis of derived velocity anomalies.

3-component analysis results — displays in easily interpretable manner

A common problem for the many techniques developed for analysis of
3-component records, that is, exploiting the wavefield structure, is
that the results are not displayed in an easily interpretable manner.
Often rather messy particle motion plots, records distorted by non-
linear rectinlinear filtering, etc., apparently is no answer to this
kind of problem. In our approach results are displayed in terms of
χ^2-probabilities (or apparent velocity for P when relevant), as a
function of time and azimuth as illustrated in Fig VII.6.4. In the

upper part, the original and filter records are displayed (Z, Trans-
verse, Radial components for a given azimuth), together with their
filtered versions. The filtering is a simple weighting operation using
the estimated probabilities (peak values) within a given azimuth band.
Further refinements are feasible, that is, by only accepting probabi-
lities associated with a given velocity range. For example, in this
way we may exclude crustal reverberations (Pg-contributions) when ana-
lyzing teleseismic events.

Typical window lengths are one/two cycles, time increment 1/3 or 1/2
of this, azimuth increment 0.5-2.0 deg, and the records themselves are
bandpass filtered (zero phase shift) prior to analysis when needed.
Parameterized analysis results are easily extractable using interac-
tive graphics (IBM PC/AT) combined with cursor usage. So far, this is
restricted to wavelet onset time and corresponding azimuth, velocity
and probability, the essential parameters for epicenter locations.

The last question to be addressed in this section is how well does our
novel 3-component analysis technique work for poor SNRs. It is dif-
ficult to give a simple answer to this problem, but in a number of
cases 3-component analysis of stacked records (the 4 stations A0, C2,
C4 and C7) provide phase identification of weak signals not seen or
not easily seen in the NORESS beam records. In other cases the array
would detect events which are probably not detectable by 3-component
analysis.

Practical applications of 3-component analysis

Besides the scattering study described previously (Dainty and Husebye,
1986), our main application of our 3-component analysis technique has
been in parameter extraction for epicenter locations at local,

regional and teleseismic distances. These topics are dealt with in Section VII.7.

E.S. Husebye
B.O. Ruud
A. Christoffersson, Univ. of
   Uppsala

References

Aki, K., A. Christoffersson & E.S. Husebye (1977): Determination of the 3-dimensional seismic structure of the lithosphere. J. Geophys. Res., 82, 277-296.

Christoffersson, A., E.S. Husebye & S.F. Ingate (1986): Wavefield decomposition using ML-probabilities in modelling single-site 3-component records, Geophys. J. R. astr. Soc., submitted for publication.

Ingate, S.F., E.S. Husebye & A. Christoffersson (1985): Regional arrays and optimum data processing schemes. Bull. Seism. Soc. Am., 75, 1155-1177.

Kennett, B.L.N. (1983): Seismic Wave Propagation in Stratified Media. Cambridge Univ. Press.

Nikolaev, A.V. & P.A. Troitskiy (1986): The earth structure study by means of seismic noise: Method, results and prospects. Phys. Earth Planet. Inter., in press.

Olson, J.V. & J.C. Samson (1979): On the detection of the polarization states of Pc micropulsations. Geophys. Res. Lett., 6, 413-416.

Steinert, O., E.S. Husebye & H. Gjøystdal (1975): Event detection false alarm rate and noise stability at NORSAR. J. Geophys. Res., 41, 289-302.
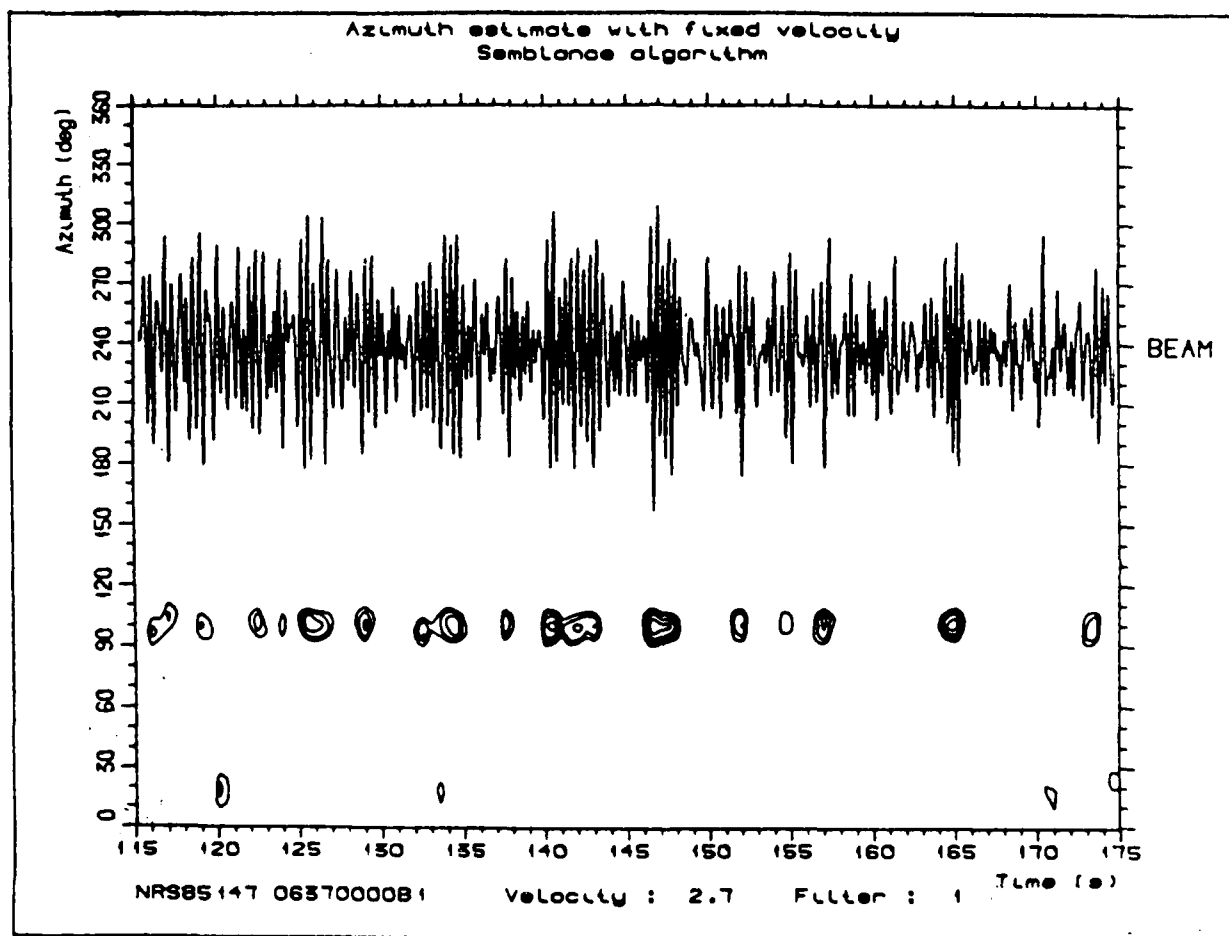
Fig. VI.6.1   Noise directionality as illustrated from presumed vibra-
tions at Braskereidfoss power station at 06.47, 27 May
1985 (spring flooding in river Glomma). Semblance ana-
lyzed used with vel = 2.7 km s^{-1}; triggering occurred
only at az $\approx$ 100 deg. The associated beam wavelets are
also displayed. Such effects are also manifested in the
NORESS detection log, and naturally generate Pg-
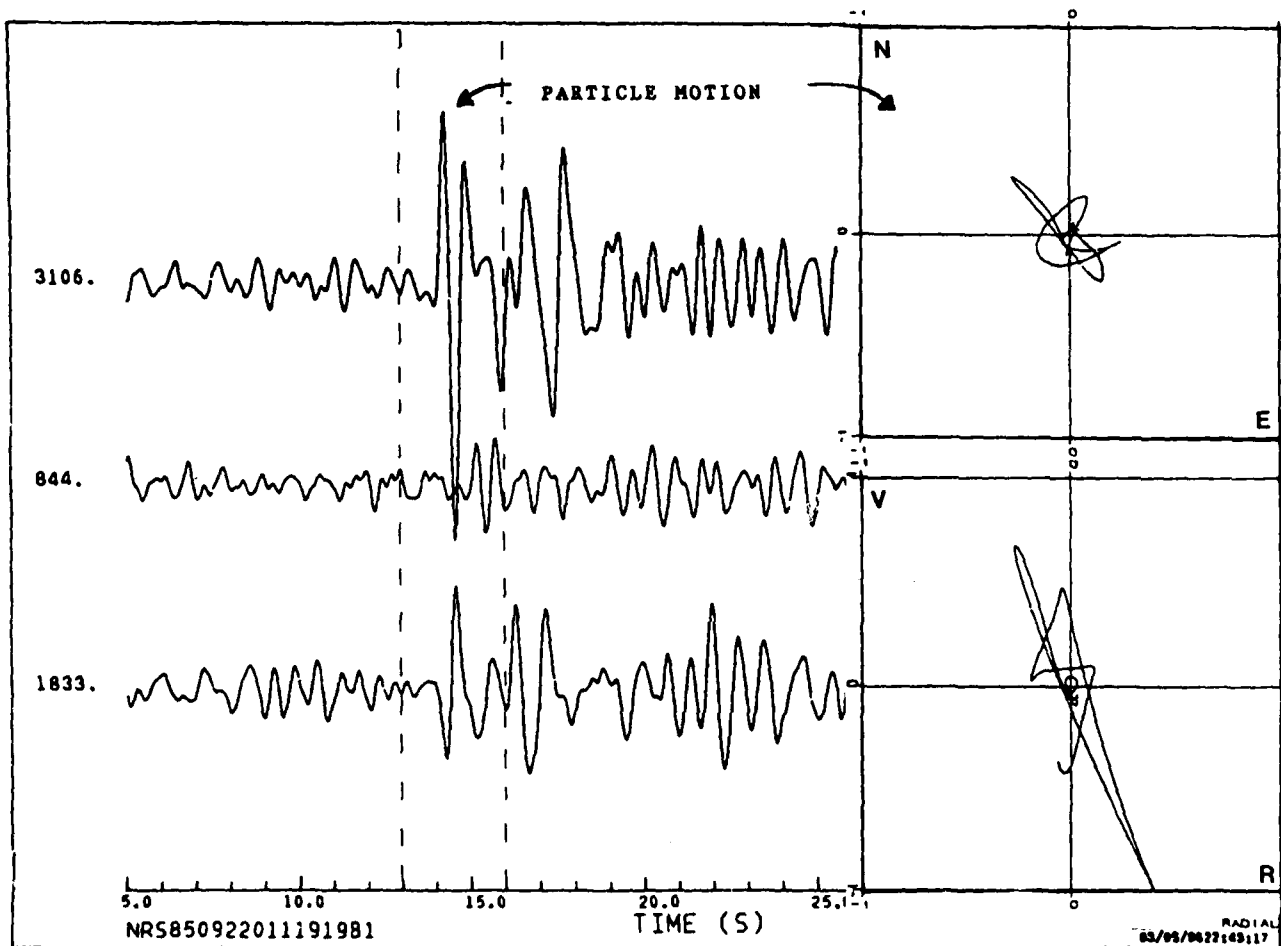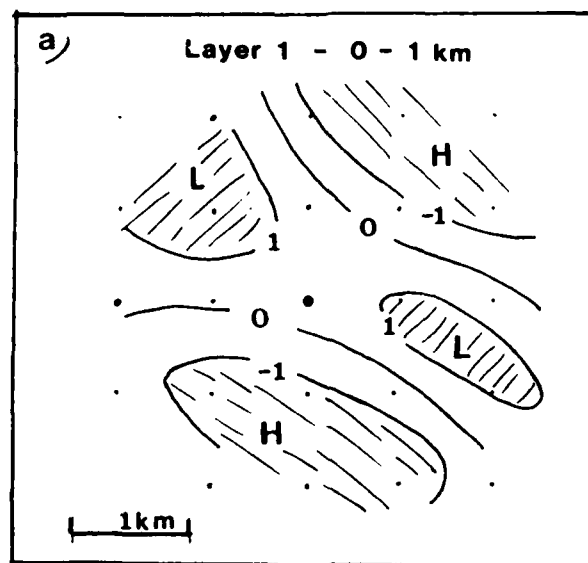triggering in 3-component analysis.

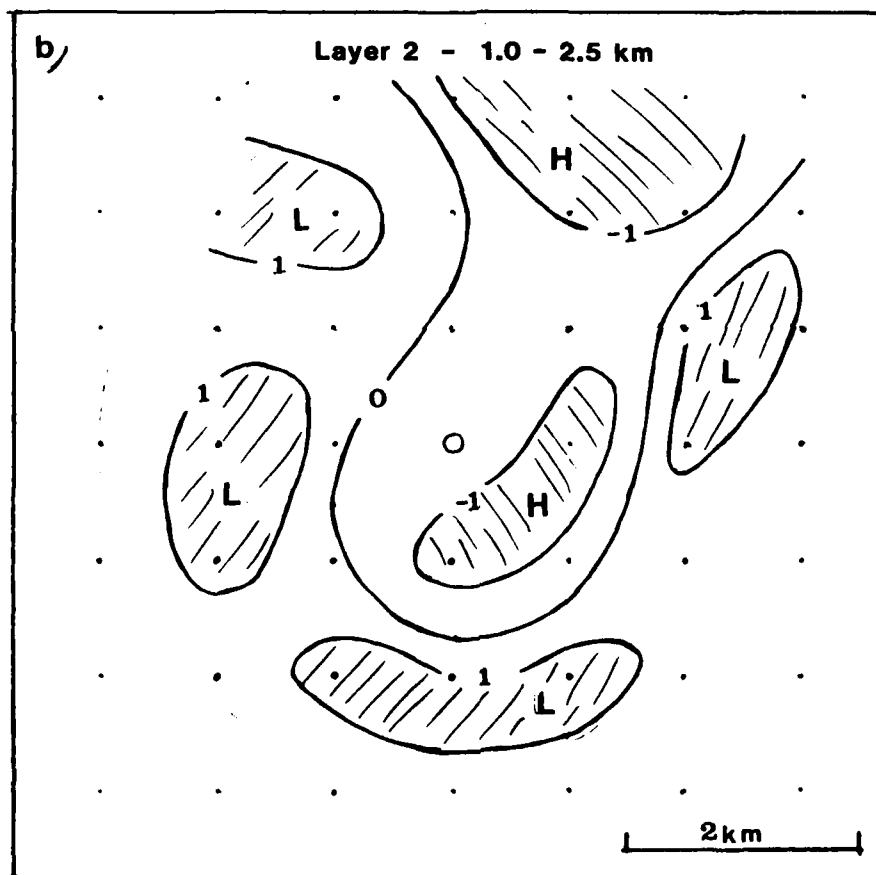Fig. VII.6.2   Nevada explosion 2 April 1985. SV-presence in the P
signal.

Fig. VII.6.3 Tomographic mapping of NORESS upper crustal structure.
Estimated velocity perturbations are of the order of ±1
per cent; the model "explains" 60% of the variance in
the "original" travel time residuals (e.g., see Aki
et al, 1977). Interestingly, crustal anomalies beneath
NORESS cause significant biases in the estimation of P-
wave slowness vectors which are not seen in
corresponding estimates using 3-component records.
Fig. a) velocity anomalies in layer 1; 0-1 km, block
size 0.8 km; H=high and L= low velocities (in per cent)
re the average of 5.8 km s^{-1}.
Fig. b) velocity anomalies in layer 2; 1.0-2.5 km; block
size 1.0 km and average velocity of 6.0 km s^{-1}.
Fig. c) velocity anomalies in layer 3; 2.5-5.0 km; block
size 1.2 km and average velocity of 6.3 km s-1.
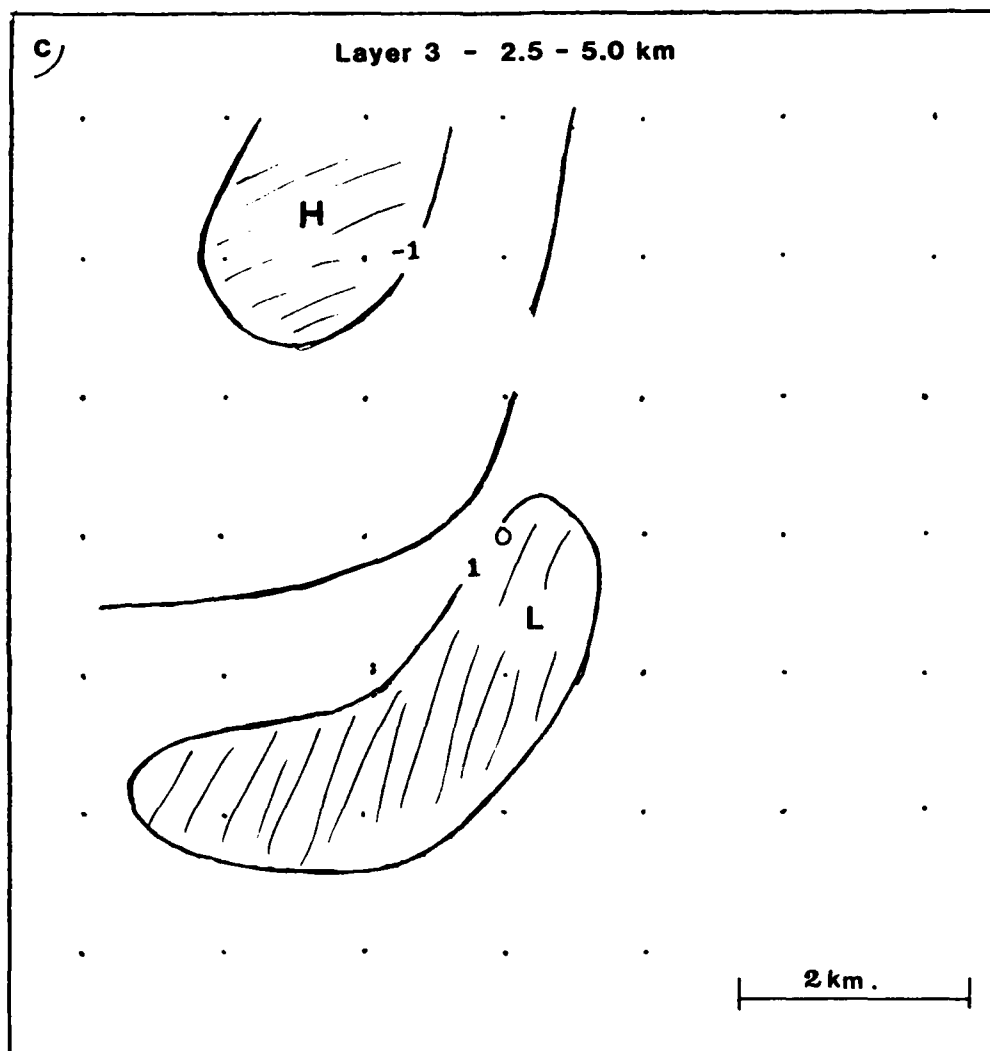
Fig. VII.6.3 (cont.)
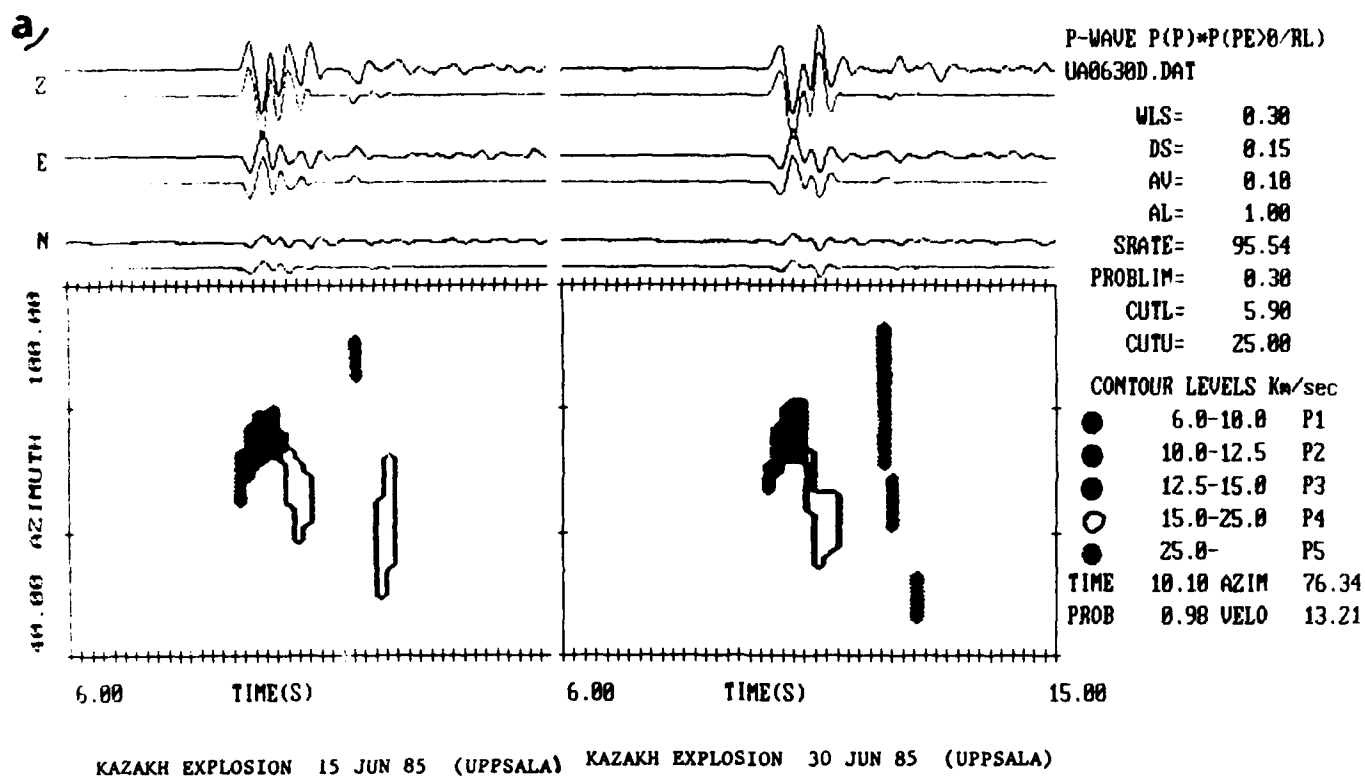
Fig. VII.6.4 Output from 3-component record analysis. Upper traces are
original while lower are weight filtered on the basis of
estiamted P-presence probabilities in the velocity windows of
5.9-25.0 km s^{-1}. Instead of plotting χ^2-probabilities the
corresponding apparent velocities are contoured as a function
of time and azimuth. The lower right parameter printouts were
"read" from the graphic screen via cursor crosses as indi-
cated. Fig. a) Two nuclear explosions as recorded in Uppsala,
Sweden (note similarities in pattern). Fig. b) Hindu Kush
earthquake of 4 September 85 (for details, see Table
VII.7.2).

Fig. VII.6.4 (cont.)

VII.7   Event locations using small arrays and single-site
3-component records

There are in principle 3 approaches to the problem of accurately
locating seismic events, which in turn reflects parameter extraction,
namely:

i)   P-arrival times from a network of stations

ii)   For arrays and 3-component stations - the slowness vector
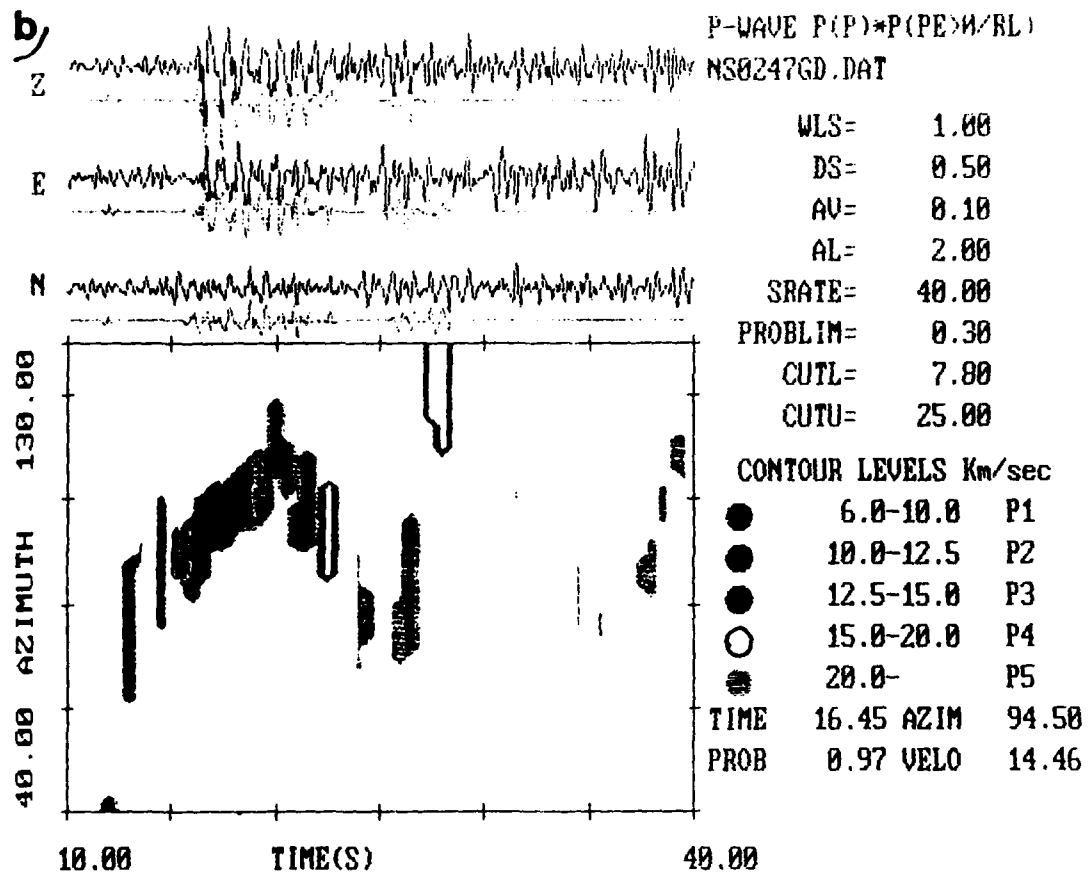   or distances estimates from differential travel times

iii)   Waveform parameterization in combination with pattern
         recognition technique, available seismicity information, etc.

In this section we will address mainly point ii), exemplified by ana-
lysis of NORESS data, and discuss point iii) in terms of 3-component
and semblance parameterization of the whole event record.

Single-site epicenter location principles

Single-site estimates of epicenter coordinates are tied to the
geometry of a triangle (station, North Pole, epicenter) on a sphere.
Parameters needed here are azimuth and epicentral distance. The latter
can be obtained from an estimate of apparent velocity, which is then
converted to epicentral distance via standard tables like the J.B.
Very accurate distance estimates can be achieved if more than one
phase can be identified in the records - with a corresponding conver-
sion of differential travel time to distance via J.B. Note that for
local and regional events two identified phases are normally required
since the associated velocity gradients vs distance are zero or at
best very small. Another problem for local and regional phases is that
specific travel time curves have to be generated, and this is also
addressed below.

Event locations using NORESS broadband records

This is the simplest case of single-site event location because low
frequency body waves are generally transparent to crustal hetero-

geneities and in generally prominent secondary phases like PP, PPP, S, etc., are easy to identify.

An example of 3-component analysis of NORESS broadband records is shown in including times, velocity and azimuth for all phases identified. Note that the given apparent velocities were derived using an upper crustal P velocity of 7 km s^{-1} when correcting for the actually measured apparent angle of incidence (P to S interference on the surface). In other words, low frequency waves "see" a relatively large portion of the lithosphere.

In our event location experiment here, 6 earthquakes with good SNR were analyzed as indicated above, and the ensuing event locations are tabulated in Table VII.7.1. The average mislocation error is only 1 deg ($43^\circ < \Delta < 154^\circ$), which is rather impressive as no sort of corrections have been introduced.

Teleseismic event locations - short period records

This is the most difficult case when single-site 3-component records are used, the reason being that the distance estimate in most cases can only be derived from the measured apparent velocity. For example, at 60° an error of 1 deg in the angle of incidence corresponds to 4 deg in distance. Nevertheless, single-site 3-component record analysis can provide a first rough estimate of epicenter locations as illustrated in Table VII.7.2, where the outcome of an experiment in locating a number of Central Asia (Hindu Kush) events is given. Additional constraints on epicenter locations now under consideration are thos of incorporating seismicity information and/or probabilities from 3-component analysis patterns. For example, in the case of the Aleutian Islands events, incorporating seismicity information implies that distances are "locked" to the epicenter distribution in the said region, while at the same time retaining the original azimuth estimate.

Occasionally an event location may be very wrong, but a properly
trained analyst should on the basis of past experience (access to pro-
cessed 3-component records of previously occurring events in the same
general area) be able to handle such cases in a decent manner.

Event locations at local and regional distances

As mentioned, travel time curves for crustal phases have constant gra-
dients, so apparent velocity estimates mainly serve as a diagnostic
for phase identification but hardly provide an acceptable distance
estimate. Exceptional cases may be repeated quarry blasting, etc.,
where signal spectral content (spectograms) may suffice for recogni-
tion of event location. In this section we treat the more conventional
approach to event locations, that is, in principle similar to the
approach used in analysis of NORESS broadband event records described
above. There is one minor but significant difference here: standard
travel time curves like J.B. are not very representative for Fenno-
scandia, so local travel time curves have to be generated. A reason-
able approach here is outlined below:

The standard approach here is to generate travel time curves on the
basis of seismic profiling results in terms of layer thicknesses and
associated velocity distributions. Besides considerable local
variations in these parameters, the extent of velocity gradients in
the crust is not well known. Anyway, our approach to this problem is
to combine NORESS observed travel times for crustal phases with epi-
center solutions as reported by local seismological agencies. Con-
sidering such a data set to be equivalent to that from a refraction
profiling survey, we have used inversion techniques (e.g., see
Braille, 1973; Ruud, 1986) to estimate velocities and crustal thick-
ness. The outcome of such an experiment, on the basis of "3-component"
arrival time pickings for Pg, Sg, Pn and Sn for 11 local events, are
shown in Table VII.7.3. We take such a model and associated travel
time curves to be representative for NORESS per se. We note in passing

that the crustal thickness estimate of about 34 km obtained here com-
pares favorably with that of Berteussen (1976) of 33 km on the basis
of spectral ratio analysis of NORSAR long periodic records. For loca-
lizing travel time curves, we may restrict the observational data to
events in a small area. The resolution of the estimated parameters
becomes poorer, but the travel time curves would be more accurate.

In the case of estimating epicenter coordinates plus focal depth, the
above procedure is reversed, that is, now distance, origin time and
depth are taken as unknowns, and the outcome of an experiment of
locating 13 local and regional events is presented in Table VII.7.4.
For the depth parameter estimation, the Sn is most informative and
this phase is occasionally prominent on transverse records.

Summary

The examples given above demonstrate clearly that using 3-component
event records, good to very good event locations are feasible at any
distance. Further refinements in analysis like using seismicity infor-
mation and/or wavefield decomposition patterns should make further
improvements realistic. It would be most interesting to check the
event location performance for a combination of two 3-component sta-
tions being a few hundred kilometers away from each other.

B.O. Ruud
E.S. Husebye

References

Berteussen, K.-A. (1977): Moho depth determinations based on spectral
    ratio analysis of NORSAR long period P-waves. Phys. Earth Planet.
    Inter., 15, 13-27.

Braille, L.W. (1973): Inversion of crustal seismic refraction
    and reflection data, J. Geophy. Res., 78, 7738-7744.

Ruud, B.O. (1986): Inversion methods in seismic prospecting.
    Semesteroppgave, Inst. for Geology, Univ. of Oslo.

Event	Origin Time h m s	Lat. (deg)	Long. (deg)	H (km)	m_b/err. (deg)	Dist. (deg)	Azi (deg)	Vel. (km/s)	Region
6/6-85 (1)	02.40.12.8 (02.40.05)	0.95N (0.20N)	28.43W (28.70W)	10 (33)	6.3 (0.80)	67.10 (67.90)	224.21 (224.20)	17.4 (19.65)	Central Mid-Atlantic Ridge
29/7-85 (2)	07.54.44.3 (07.54.42)	36.19N (37.54N)	70.89E (71.54E)	101 (33)	6.7 (1.45)	42.10 (43.50)	93.30 (94.0)	13.60 (13.55)	Hindu Kush Region
23/8-85 (3)	12.41.59.7 (12.42.02)	39.42N (39.31N)	75.27E (75.39E)	33 (33)	6.4 (0.14)	43.9 (44.0)	89.0 (89.0)	13.80 (13.44)	Southern Xinjang, China
21/9-85 (4)	01.37.13.8 (01.37.15)	17.82N (16.94N)	101.67W (102.61W)	33 (33)	6.3 (1.26)	85.21 (86.40)	298.59 (299.0)	22.4 (22.55)	Near coast of Guerrero, Mexico
5/10-85 (5)	15.24.02.2 (15.23.57)	62.26N (61.29N)	124.31W (124.94W)	10 (33)	6.5 (1.01)	52.49 (53.50)	335.88 (335.10)	15.0 (15.10)	Northwest Territories, Canada
7/11-85 (6)	19.12.29.8 (19.12.08)	35.20S (35.18S)	179.36W (178.16W)	33 (33)	6.2 (0.98)	153.5 (153.7)	20.3 (18.1)	32.0 (55.1))	East of North Island, New Zealand

Table VII.7.1 Focal parameters, taken from the PDE listings of USGS, for the events used in analysis. Parameters in parentheses are those estimated from the single-site 3-component broadband recordings (NORESS). The distance differences between the two sets of event location estimates are listed in the m_b-column.

Event	Origin Time h m s	Lat. (deg)	Long. (deg)	H (km)	mb/err. (deg)	Dist. (deg)	Azi (deg)	Vel. (km/s)	Region
18/7-85 (1)	17.40.12.9 (17.38.45)	30.36N (11.10N)	94.84E (90.70E)	33	4.9 (19.6)	60.70 (75.0)	79.50 (94.0)	16.3 (19.0)	Hindu Kush
29/7-85 (2)	07.54.44.3 (07.54.42)	36.19N (37.5N)	70.89E (71.5E)	101	6.7 (1.5)	42.10 (43.5)	93.30 (94.0)	13.60 (13.60)	Hindu Kush (BB)
7/8-85 (3)	15.43.22.7 (15.46.41)	27.88N (46.60N)	53.05E (38.40E)	15	5.4 (22.0)	43.0 (21.0)	120.8 (120.0)	13.70 (10.1)	Hindu Kush
13/8-85 (4)	03.42.40.8 (03.41.45)	36.30N (28.90N)	71.12E (72.50E)	75	5.1 (7.5)	44.30 (51.00)	95.50 (100.0)	13.90 (14.80)	Hindu Kush
23/8-85 (5)	08.32.56.9 (08.32.49)	39.36N (37.70N)	75.37E (74.80E)	66	5.0 (1.7)	43.90 (45.00)	89.0 (91.0)	13.80 (13.90)	Hindu Kush
23/8-85 (6)	12.41.59.7 (12.49.09)	39.42N (38.40N)	75.27E (71.80E)	33	6.4 (2.9)	43.90 (43.0)	89.0 (93.0)	13.80 (13.7)	Hindu Kush
23/8-85 (7)	14.11.41.8 (14.10.44)	39.56N (31.10N)	75.22E (76.20E)	33	4.9 (6.5)	43.90 (51.0)	89.0 (95.0)	13.80 (14.80)	Hindu Kush
23/8-85 (8)	16.25.32.2 (16.25.32)	39.45N (41.50N)	74.83E (78.90E)	33	4.9 (3.7)	43.90 (44.0)	89.0 (84.0)	13.80 (13.8)	Hindu Kush
23/8-85 (9)	20.33.48.2 (20.34.29)	39.27N (42.20N)	73.01E (67.60E)	33	4.8 (5.0)	42.90 (38.0)	91.90 (93.0)	13.60 (13.1)	Hindu Kush
4/9-85 (10)	08.32.25.8 (08.31.45)	36.23N (32.9N)	71.02E (75.2E)	66	4.9 (3.7)	44.30 (49.0)	95.60 (94.5)	13.90 (14.50)	Hindu Kush
11/9-85 (11)	01.57.20.9 (01.56.24)	40.36N (33.10N)	63.10E (65.10E)	33	4.7 (7.4)	37.20 (44.0)	99.0 (104.0)	13.10 (13.8)	Hindu Kush

Table VII.7.2 Focal parameters, taken from the PDE listings of USGS, for the events used in analysis. Paremeters in parentheses are those estimated from the single-site 3-component recordings (NORESS). The distance differences between the two sets of event locations are listed in the mb-column.

Layer (km)	P-velocity (km s^{-1})	S-velocity (km s^{-1})
33.5	6.50	3.67
Moho	8.20	4.67

Table VII.7.3 Best-fitting crustal model on the basis of 11 local and regional events recorded by NORESS.

Event	Origin Time h m s	Lat. (deg)	Long. (deg)	H (km)	ML/err.	Azi. (deg)	Dist. (km)	Agency	Region
29/1-85 (1)	11.59.47 (11.59.45.5)	59.3N (61.08N)	28.10E (29.18E)	0 (15)	- (207)	92.6 (80.0)	931 (951)	FIN	Leningrad, USSR
2/4-85 (2)	19.29.40 (19.29.41.1)	66.9N (68.05N)	23.3E (18.81E)	- (15)	- (230)	34.9 (20.0)	893 (883)	UPP	Norbotten, Sweden
23/4-85 (3)	- (13.16.27.5)	58.34N (58.43N)	6.43E (6.34E)	0 (7)	- (11)	229.5 (231.0)	392 (389)	-	Titania exp.
15/6-85 (4)	00.40.21 (00.40.20.9)	56.50N (56.48N)	12.10E (12.21E)	- (13)	- (7)	175.8 (175.0)	471 (474)	UPP	Offcoast Halland, Sweden
27/6-85 (5)	- (08.45.32.4)	59.31N (59.51N)	6.95E (6.73E)	0 (4)	- (51)	240.1 (250.0)	300 (301)	-	Blåsjø
28/6-85 (6)	- (15.42.11.8)	59.31N (59.51N)	6.95E (6.73E)	0 (1)	- (26)	240.1 (245.0)	300 (299)	-	Blåsjø
30/8-85 (7)	07.40.46.9 (07.40.47.4)	61.89N (61.92N)	2.19E (2.29E)	15 (15)	- (7)	288.5 (289.0)	515 (510)	BER	Offcoast W. Norway
8/9-85 (8)	12.31.57.4 (12.31.56.5)	61.24N (61.32N)	3.37E (3.34E)	15 (15)	- (9)	280.8 (282.0)	443 (446)	BER	Offcoast W. Norway
12/9-85 (9)	19.17.43.4 (19.17.44.9)	61.27N (60.95N)	8.10E (7.54E)	15 (13)	- (47)	289.3 (278.0)	195 (218)	BER	Tyin/Lærdal
31/10-85 (10)	02.55.52 (02.55.52.9)	62.8N (63.53N)	18.0E (17.01E)	- (12)	- (95)	53.1 (40.0)	410 (421)	UPP	Angermanland, Sweden
19/1-86 (11)	04.59.24 (04.59.21.4)	65.25N (65.42N)	12.50 (12.53)	- (5)	- (19)	5.1 (5.0)	505 (523)	UPP	Coast of Central Norway
25/1-86 (12)	23.13.25 (23.13.25.5)	61.80N (61.73N)	16.90E (17.04E)	- (19)	- (11)	65.2 (67.0)	310 (314)	UPP	Hälsingland, Sweden
5/2-86 (13)	17.53.35.5 (17.53.35.5)	62.74N (62.66N)	4.63E (5.08E)	15 (18)	- (24)	304.5 (305.0)	426 (405)	BER	Offcoast, NW Norway

Table VII.7.4 Single-site 3-component records used for estimating focal parameters for local and regional events. Note the high accuracy in epicenter distance estimates, and also that zero depths are obtained for known explosions.

VII.8   3-D ray tracing and structural heterogeneities in Fennoscandia

It is well known that array estimates of the P-wave slowness vectors deviate significantly from that expected on the basis of homogeneous earth structures and the corresponding velocity distribution as implied by the J.B. travel time tables. The reason for this is obviously that the "homogeneous" earth assumption is not strictly valid, but still there is some controversy as regards which part of the wave path contributes most significantly to the observed slowness anomalies. In this respect we have undertaken a 3-D imaging of the upper mantle velocity structure beneath the southern part of Fenno-scandia on the basis of P-wave travel time residuals as observed across local seismograph networks (Fig. VII.8.1) in the mentioned area. The results here are displayed in Fig. VII.8.2, and the necessary details on this experiment are given by Husebye et al (1986). Using a 3-D ray tracing approach, we have calculated the range of slowness (azimuth and apparent velocity) anomalies for the NORESS/ NORSAR siting area on the basis of the velocity anomaly structure in Fig. VII.8.1. In extreme cases, that is, with the largest lateral velocity gradients, the corresponding azimuth anomaly was only 3 deg, while apparent velocity anomalies amount to about $\pm$ 0.5 km s^{-1}. Note that in the latter case the choice of top or average crustal veloci-ties would introduce a bias. The above "synthetic" findings have been confirmed from analysis of NORESS broadband records in which cases azimuth anomalies were found to be less than 2 deg and apparent velo-cities less than $\pm$ 1 km s^{-1}. Further details here are given in Section VII.7.

Past analysis of short period P-wave NORSAR recordings gave that the observed slowness vector anomalies could be attributed to structural heterogeneities in the lithosphere just beneath NORSAR (e.g., see Aki
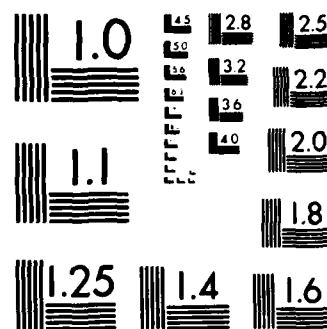
et al, 1977; Christoffersson and Husebye, 1979). Interestingly, analysis of 3-component short period NORESS records provide very good azimuth estimates, while apparent velocity estimates fluctuate considerably (for details, see Section VII.7). The latter seems predominantly to reflect interference phenomena rather than direct structural effects.

E.S. Husebye
J. Hovland, Univ. of Oslo
A. Christoffersson, Univ. of Uppsala
K. Åström, Univ. of Uppsala
R. Slunga, National Def. Res. Establishment, Sweden
C.-E. Lund, Univ. of Uppsala

References

Aki, K., A. Christoffersson & E.S. Husebye (1977): Determination of the three-dimensional seismic structure of the lithosphere. J. Geophys. Res., 82, 277-296.

Christoffersson, A. & E.S. Husebye (1979): On 3-D inversion of P-wave time residuals: option for geological modeling. J. Geophys. Res., 84, 6168-6176.

Husebye, E.S., J. Hovland, A. Christoffersson, K. Åström, R. Slunga, and C.-E. Lund (1986): Tomographical mapping of the lithosphere and asthenosphere beneath S. Scandia and adjacent areas. Tectonophysics, in press.
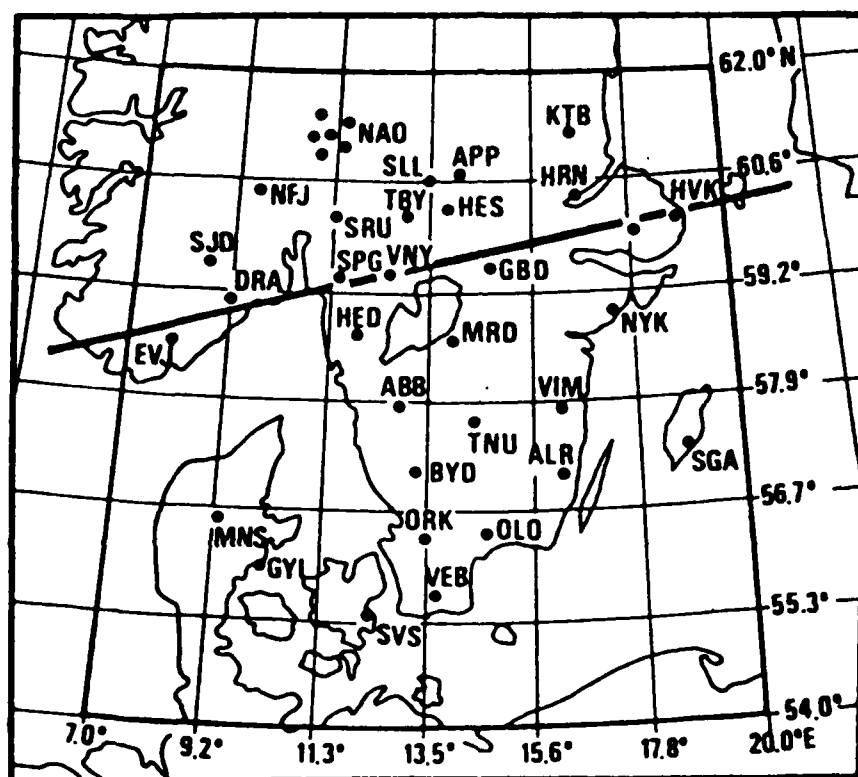
Fig. VII.8.1 The short-period seismograph network of southern Scan-
dinavia from which the P-wave recordings have been used
in analysis. This network consists of the south Swedish
and the southern Norwegian (suspended from operation in
May 1983) networks, plus the NORSAR array and a few
Danish stations (part of the S. Swedish network).
Regarding Sweden, stations HED, MRD, BYD, TNU and ABB
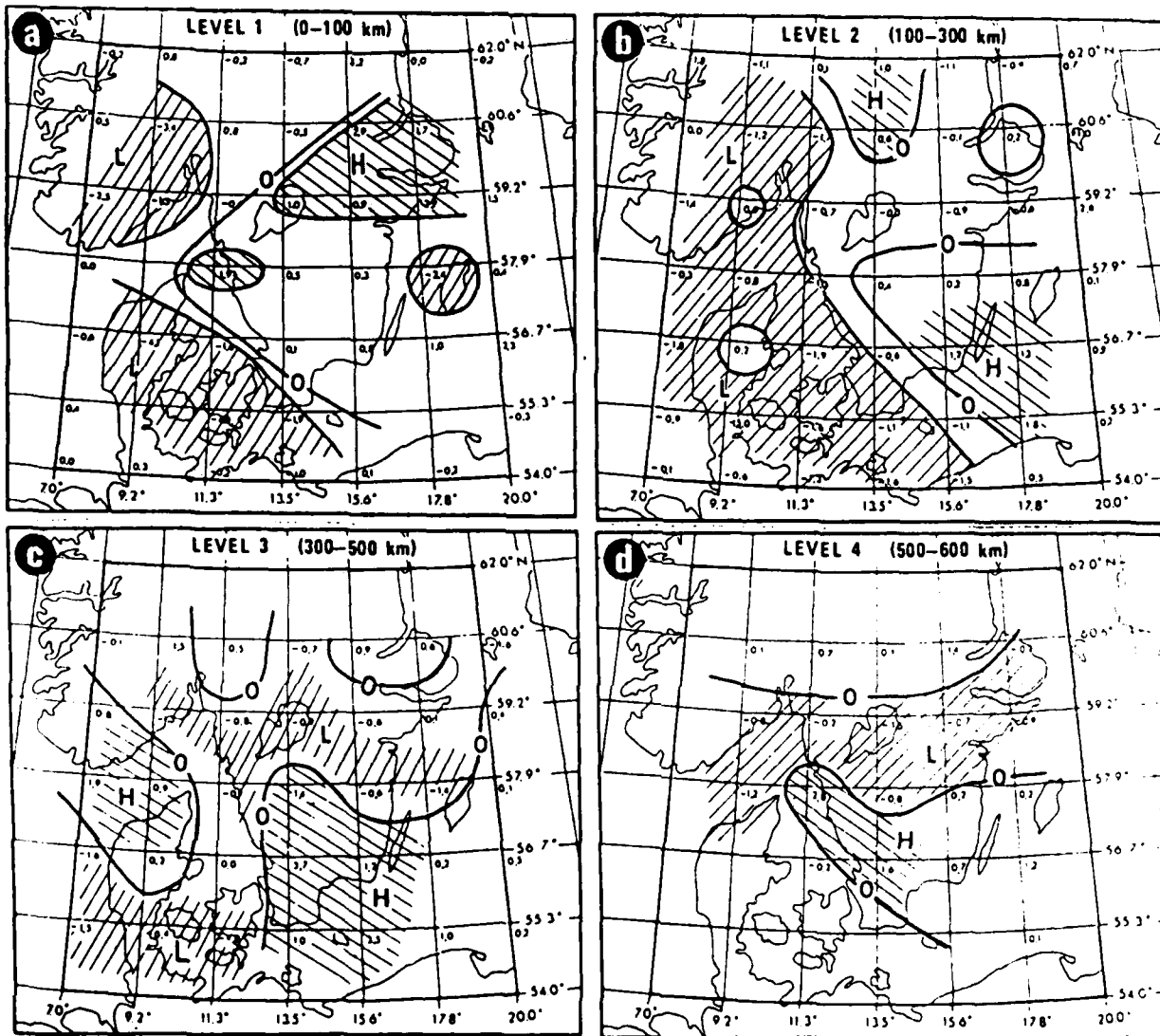are now suspended from operation.

Fig. VII.8.2   3-D seismological images of the S. Scandinavian lithosphere/
              asthenosphere. Here is used a 7 x 7 knot layout on four
              levels (cubic spline velocity interpolation). The given
              seismic velocity perturbations are in per cent; the letters L
              and H denote areas with respectively low and high velocities.
              Knots with resolution less than 0.5 were not used in con-
              touring the velocity anomalies.

END
10-86
DTIC